POLITECNICO DI TORINO

Collegio di Ingegneria Chimica e dei Materiali

Corso di Laurea Magistrale
in Ingegneria Chimica e dei Processi Sostenibili

Tesi di Laurea Magistrale

Synthesis of Silver Nanoparticle-loaded Polymeric Capsules via Aerosol Photopolymerization

Relatore
Marco Sangermano

Candidato
Carlo Trentalange

Marzo 2021

Contents

Abstract **i**
0.1 Obiettivo della tesi . . . i
0.2 Introduzione . . . i
0.3 Risultati . . . ii
0.3.1 Produzione di nanocapsule . . . ii
0.3.2 Produzione di nanocapsule ibride . . . v
0.3.3 Coniugazione con maleimide . . . ix
0.4 Conclusioni . . . xi

1 Introduction **1**
1.1 Overview on Polymeric Nanoparticles . . . 1
1.2 Aerosol Photopolymerization (APP) . . . 2
1.3 Production of Nanospheres and Nanocapsules . . . 3
1.4 Mechanisms of Polymerization . . . 7
1.4.1 Thiol-ene Mechanism . . . 8
1.4.2 Mixed Thiol-Acrylic Polymerization . . . 10
1.5 Conjugation . . . 11

2 Experimental section **13**
2.1 Materials . . . 13
2.2 Equipment and Instrumentation . . . 16
2.3 Analysis Techniques . . . 17

3 Results and Discussion **19**
3.1 Production of Capsules . . . 19
3.1.1 Effect of Thiol-ene monomer relative ratio . . . 19
3.1.2 Using different monomer combinations . . . 22
3.1.3 Effect of glycerol . . . 25
3.2 Production of Hybrids . . . 27
3.2.1 Ag-PVP with ALA and MUL . . . 27
3.2.2 Ag-Ink with ALA and MUL . . . 30
3.2.3 Effect of 1-propanol on increasing loads of silver . . . 32
3.2.4 Effect of Other Stabilizers . . . 39
3.2.5 Changing monomer to solvent (M/S) ratio . . . 40
3.3 Thiol Groups Analysis . . . 43
3.3.1 Ellman's reaction . . . 43
3.3.2 Maleimide conjugation . . . 44

4 Conclusions **49**

List of Figures **52**

List of Tables **53**

Acronyms **55**

Bibliography **57**

Acknowledgments **61**

Abstract

0.1 Obiettivo della tesi

L'obiettivo di questo lavoro è quello di studiare la produzione di nanoparticelle polimeriche attraverso il processo di fotopolimerizzazione in aerosol con meccanismo tiolenico e misto tiolenico-acrilico. Una particolare attenzione è stata rivolta alla produzione di nanocapsule e ibridi polimero-argento per applicazioni future nel campo farmacologico e nell'ambito biomedicale grazie alle eccellenti proprietà ottiche delle nanoparticelle di argento. Uno studio finale sulla funzionalizzazione tramite la biomolecola maleimide è stato effettuato ai fini di confermare la biocompatibilità delle nanoparticelle prodotte.

0.2 Introduzione

Oggigiorno, l'interesse nelle nanoparticelle (NPs) e nelle nanoparticelle ibride (HNPs) è in rapida crescita per via delle numerose potenziali applicazioni nel campo della nanomedicina: somministrazione mirata di farmaci (Farokhzad and Langer, 2009), diagnosi di malattie e bioimaging (Wang et al., 2008). Tra le nanoparticelle, quelle polimeriche sono considerate un promettente sistema di somministrazione per via delle eccellenti proprietà di modifica superficiale, alta capacità di carico e controllo farmacocinetico (Faraji and Wipf, 2009). A seconda della loro struttura interna, le nanoparticelle polimeriche possono essere classificate in nanosfere e nanocapsule. Le prime con una matrice piena regolare, mentre le seconde caratterizzate da un nucleo solido o liquido rivestito da un guscio polimerico (Deng et al., 2020). L'uso di nanocapsule per la somministrazione mirata di farmaci consente di aumentarne l'effettiva efficienza di trasporto nell'organismo e ridurre le perdite dovute al rilascio in prossimità di cellule e tessuti dove l'effetto dell'agente attivo non è richiesto (Calzoni et al., 2019). In aggiunta, le nanoparticelle ibride possono essere prodotte combinando in un'unica struttura le caratteristiche dei polimeri con le proprietà ottiche uniche dei metalli nobili quali oro e argento. Questi ultimi sono da tempo impiegati nel campo della diagnostica, come mezzi di contrasto per risonanza magnetica (MRI) e per le loro proprietà di assorbimento della radiazione UV. Tramite la combinazione di questi metalli con nanoparticelle polimeriche è possibile ottenere sistemi innovativi che ricadono nella definizione di dispositivi "teranostici" in cui le funzioni terapeutica e diagnostica possono essere somministrate in una unica dose (Sailor and Park, 2012).

La produzione di nanosfere e nanocapsule polimeriche è da tempo effettuata tramite tecniche di fotopolimerizzazione. Tra tutte, la fotopolimerizzazione in aerosol (APP) è un processo innovativo, che permette di ottenere particelle con diametro minimo inferiore a 100 nm. Inoltre, permette di lavorare in assenza di tensioattivi, evita l'impiego di grandi volumi di liquido, consente una più facile raccolta del materiale prodotto, un controllo migliore delle dimensioni finali delle particelle e permette la produzione di particelle ibride tramite semplice aggiunta dei metalli alla formulazione iniziale (Widmann and Davis, 1996; Gao et al., 2007: Esen and Shweiger, 1996).

Figure 1: Strumentazione completa: atomizzatore e fotoreattore con filtro di raccolta.

Una volta preparata, la formulazione spray viene atomizzata attraverso un ugello con un meccanismo basato sull'effetto venturi. Le gocce prodotte vengono trasportate attraverso una corrente di azoto nel fotoreattore, all'interno del quale vengono polimerizzate. Il fotoreattore utilizzato in questo studio consiste in 4 tubi in FEP (Etilene Propilene Fluorurato) posti tra due set di 3 lampade UV con potenza di 15 W in grado di emettere radiazioni con lunghezza d'onda compresa tra 270 e 360 nm, con un picco massimo di 312 nm. Il tempo di permanenza delle gocce all'interno del reattore è stimato essere dell'ordine di 15 secondi e risulta sufficiente alla completa polimerizzazione delle gocce. La pressione, mantenuta costante per tutti gli esperimenti è di 1 bar. Una volta fuori dal reattore, le particelle prodotte vengono raccolte in filtri e lasciate ad essiccare per diversi giorni. La durata di ogni esperimento varia tra i 90 e i 120 minuti a seconda della resa e dell'efficienza di polimerizzazione.

0.3 Risultati

Il lavoro sperimentale può essere suddiviso in tre parti principali, nelle quali l'attenzione viene focalizzata su differenti aspetti della produzione e caratterizzazione delle nanoparticelle. La prima parte riguarda la ricerca di formulazioni per la produzione di nanocapsule con meccanismo tiolenico puro o misto. Nella seconda, ci si concentra sulla produzione di nanocapsule ibride contenenti nanoparticelle di argento. Infine, la terza parte riguarda la ricerca dei gruppi sulfidrilici nei campioni di nanoparticelle prodotte nelle sezioni precedenti e la loro bioconiugazione tramite la biomolecola maleimide.

0.3.1 Produzione di nanocapsule

Come formulazione di partenza per la produzione di nanocapsule è stata scelta una combinazione di TRIS/TMPTA in rapporto molare 1:1 già impiegata in studi precedenti (Longo, 2019; Zappitelli, 2017). Le formulazioni di questo tipo contengono, oltre ai monomeri, una miscela di solventi organici aventi lo scopo di controllare il tempo di gelificazione e separazione di fase durante la polimerizzazione. Nello specifico, un quantitativo di 3,5 g di 2-octanone, 3,5 g di 2-etil-1-esanolo e 3 g di esadecano è stato impiegato in aggiunta a 12

g di etanolo come solvente volatile e 3 g di glicerolo. Il rapporto di combinazione tra i due monomeri è stato poi variato mantenendo costanti le quantità dei solventi, dei co-solventi e di glicerolo in tutte le formulazioni. Particelle nanometriche di TRIS/TMPTA sono state ottenute con rapporti a partire da 1:1 fino a 1:8. Combinazioni non stechiometriche dei monomeri tiolico e acrilico sono identificate come reazioni con meccanismo tiolenico misto.

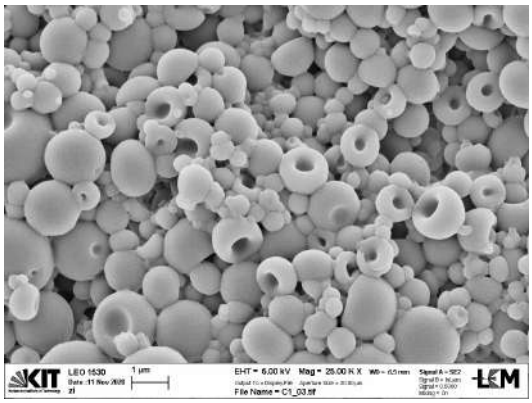

(a) TRIS/TMPTA rapporto 1:1.

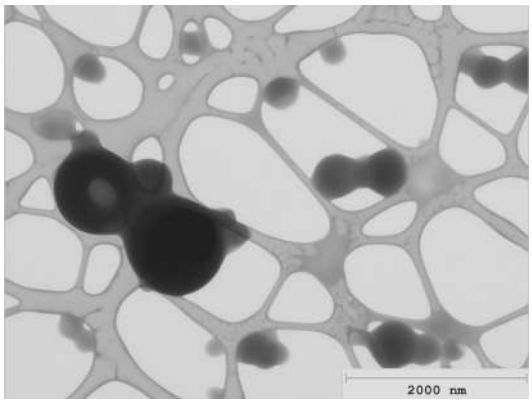

(b) TRIS/TMPTA rapporto 1:1.

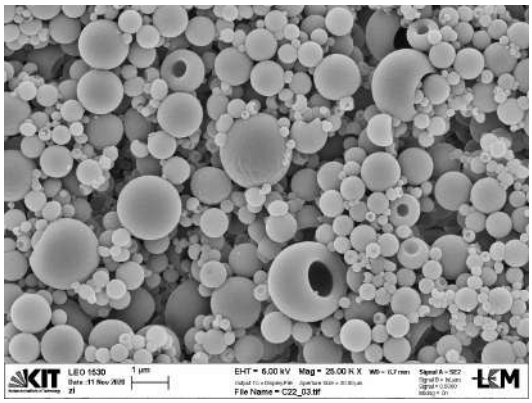

(c) TRIS/TMPTA rapporto 1:2.

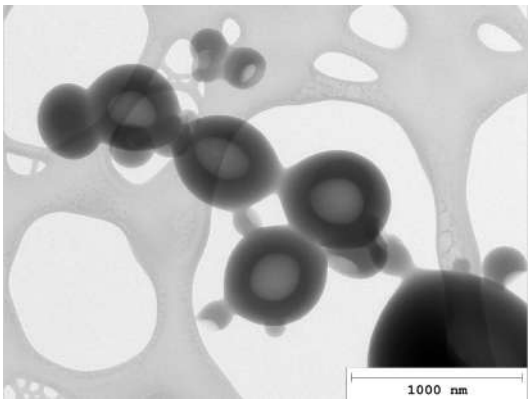

(d) TRIS/TMPTA rapporto 1:2.

Figure 2: Immagini al SEM e TEM di particelle ottenute con rapporti di TRIS/TMPTA di 1:1 e 1:2.

Particelle in cui la struttura nucleo-guscio è poco distinguibile sono state ottenute con concentrazioni maggiori di TRIS (Figura 2b). Presenza di agglomerati e necking tra le particelle sono causati dalla minore conversione del tiolo che, a sua volta, è provocata dall'effetto predominante del meccanismo di trasferimento di catena su quello di propagazione. Con l'aumento della concentrazione di TMPTA un chiaro miglioramento nella morfologia delle particelle è osservabile (Figure 3b e 3d). L'aumento della concentrazione del monomero acrilico aumenta l'influenza della reazione di propagazione rispetto a quella del trasferimento di catena e anticipa il processo di gelificazione. Le particelle presentano una riduzione nel fenomeno di necking ed hanno minore tendenza ad incollarsi tra di loro e formare agglomerati. In tutti i casi la separazione di fase avviene prima della gelificazione e la presenza di un nucleo contenente la fase solvente è osservabile nelle immagini al TEM. Aumentando ulteriormente la concentrazione di TMPTA da 1:4 fino a 1:8 è ancora possibile ottenere capsule senza sostanziali modifiche strutturali. Tuttavia, si osserva una presenza maggiore di particelle con struttura spugnosa, in cui più di una concavità è presente per ogni singola particella. Le strutture migliori sono state ottenute con il rapporto 1:3 e 1:4.

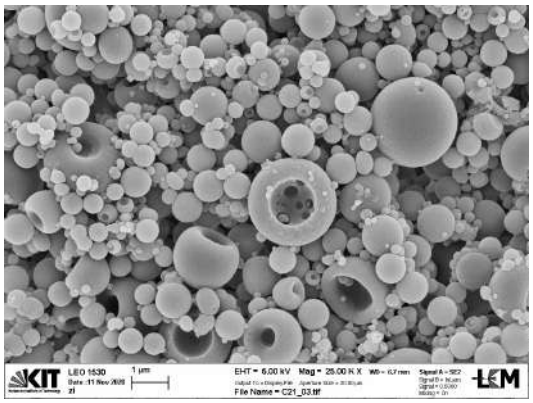

(a) TRIS/TMPTA con rapporto 1:3.

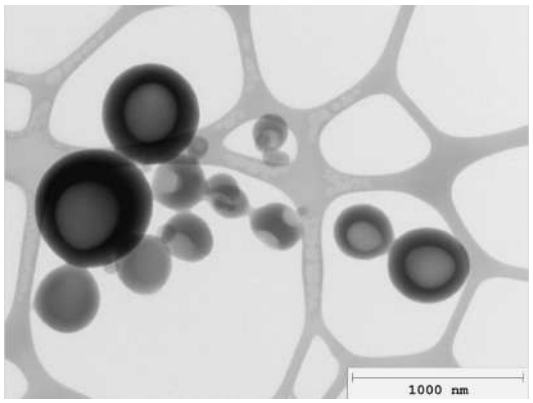

(b) TRIS/TMPTA con rapporto 1:3.

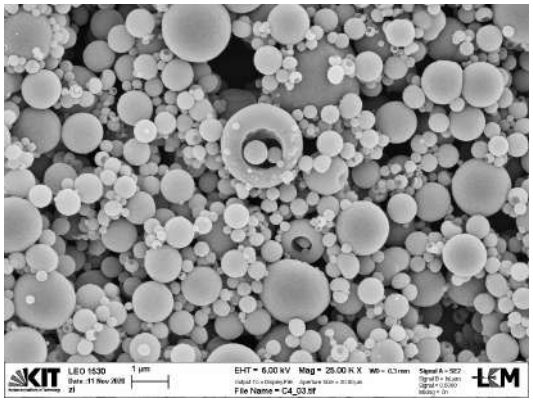

(c) TRIS/TMPTA con rapporto 1:4.

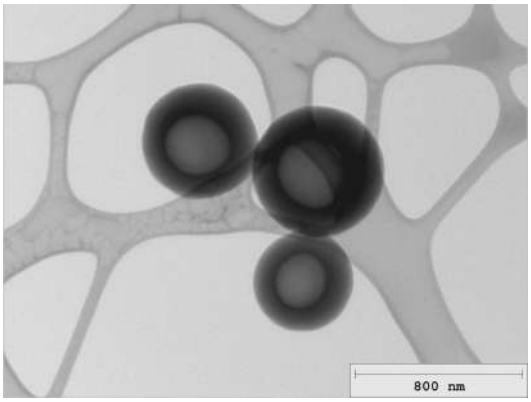

(d) TRIS/TMPTA con rapporto 1:4.

Figure 3: Immagini al SEM e TEM di particelle ottenute con rapporti di TRIS/TMPTA di 1:3 e 1:4.

Con l'obiettivo di trovare altre formulazioni in grado di generare nanocapsule, differenti monomeri acrilici con strutture e numeri di gruppi funzionali differenti sono stati impiegati. Formulazioni con TTT e DAA in rapporto equimolare rispetto al numero di gruppi funzionali e TAT in rapporto di 1:1, 1:2 e 1:4 con TRIS sono state analizzate. Comparando i risultati, nessuna delle nuove combinazione si è rivelata essere adatta a sostituire le particelle prodotte con TRIS/TMPTA.

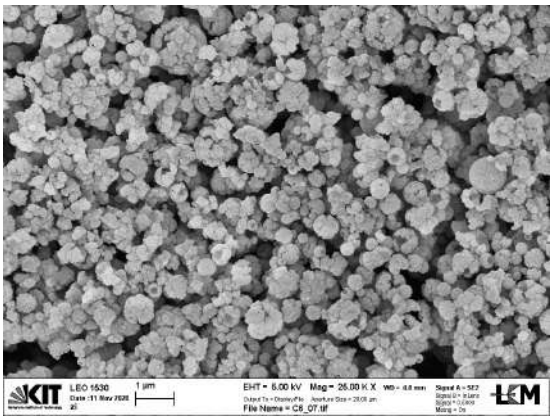

Figure 4: Particelle di TMPTA con struttura a mosaico ottenute tramite meccanismo radicalico.

Differenti monomeri acrilici hanno differenti reattività, influenzate dalla loro struttura ed in particolare dal numero di gruppi funzionali. La resa riferita al materiale raccolto si è rivelata inferiore per tutte le varianti e in alcuni casi è stato impossibile collezionare un campione. Un esperimento con solo TMPTA è stato effettuato (Figura 4). In questo caso, l'assenza del meccanismo di trasferimento di catena causata dalla mancanza del tiolo fa sì che la reazione di polimerizzazione proceda con meccanismo radicalico. L'evoluzione del peso molecolare medio in questa reazione è molto più rapida e tale da causare una prematura separazione di fase nelle singole gocce che polimerizzeranno formando una struttura a mosaico.

L'impiego di glicerolo si è rivelato essenziale per la formazione di nanocapsule. Formulazioni in cui il Gly è assente hanno generato particelle sferiche solide prive di nucleo (Figura 5a).

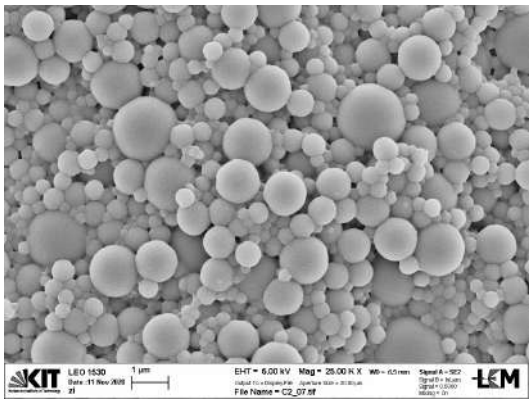

(a) TRIS/TMPTA senza glicerolo.

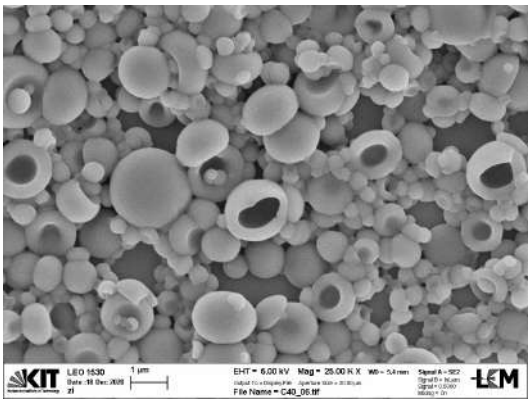

(b) TRIS/TMPTA con 6 g di glicerolo.

Figure 5: Immagini al SEM di particelle di TRIS/TMPTA con e senza glicerolo.

Un quantitativo maggiore di EtOH e 2Oct è stato usato in sostituzione al glicerolo con risultati generalmente peggiori. D'altra parte, formulazioni con 6 g di glicerolo a posto di 3 hanno generato capsule collose e tendenti deformarsi (Figura 5b) e un quantitativo maggiore di caps, ovvero capsule collassate osservabili al SEM. Un aumento nel quantitativo di glicerolo è stato applicato anche a formulazioni con rapporti TRIS/TMPTA di 1:4 e 1:5 con risultati strutturali migliori. L'aumento del necking e della tendenza delle particelle ad incollarsi causato dal glicerolo viene controbilanciato dall'aumento della concentrazione di TMPTA che genera un guscio polimerico più rigido.

0.3.2 Produzione di nanocapsule ibride

Una volta ottenuta una formulazione in grado di generare nanocapsule in modo riproducibile si è passati alla produzione di strutture ibride contenenti nanoparticelle di argento (Ag-NPs). La ricerca è stata focalizzata sull'ottenimento di nanocapsule contenenti nanoparticelle di argento non agglomerate all'interno del nucleo interno. Per ottenere ciò, alle soluzioni spray precedentemente testate sono state aggiunte Ag-NPs provenienti da varie fonti. Le Ag-NPs state prima disperse in etanolo e poi aggiunte alle formulazioni sotto l'effetto di una vigorosa agitazione. Nanoparticelle di argento con diametro medio di 25 e 50 nm sono state impiegate, nella forma di nanoparticelle rivestite con PVP e in forma di inchiostro di argento.

Come primi esperimenti, un basso carico di nanoparticelle rivestite da PVP è stato aggiunto alle formulazioni contenenti TRIS/TMPTA con rapporto 1:1 e 1:4. Nei campioni analizzati nessuna traccia di argento è stata osservata né all'interno né all'esterno delle cap-

sule. Successivamente, sono stati aggiunti, a parità di condizioni, 6 mg di ALA o MUL al fine di stabilizzare la dispersione di Ag-NPs. A queste concentrazioni di stabilizzanti, i campioni prodotti presentavano argento, ma in quello contenente MUL (Figura 6a) le Ag-NPs erano presenti in agglomerati all'interno delle particelle, mentre in quello contenente ALA (Figura 6b), queste erano isolate e sparse all'esterno.

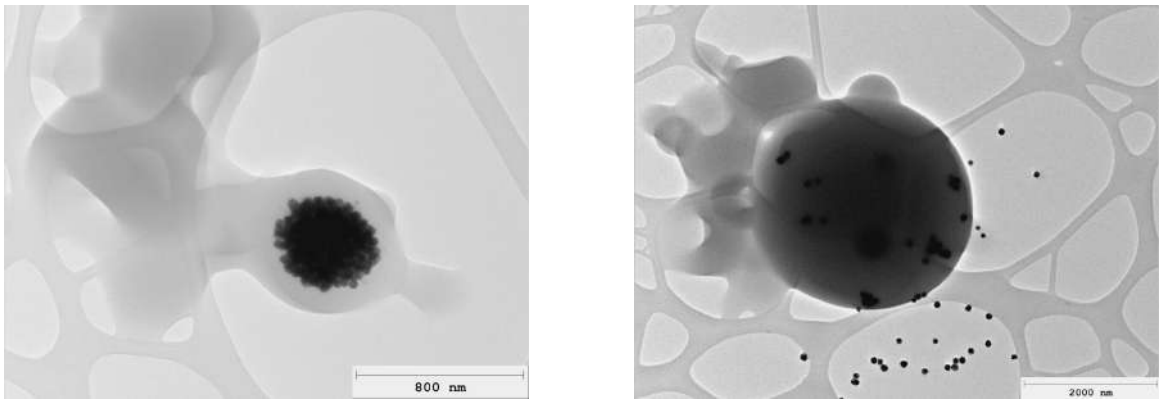

(a) TRIS/TMPTA con Ag-PVP e MUL. (b) TRIS/TMPTA con Ag-PVP e ALA.

Figure 6: Immagini al TEM di particelle TRIS/TMPTA con Ag-NPs e stabilizzanti.

Esperimenti con valori di 10 e 80 mg di ALA sono stati effettuati con le stessi condizioni di carico di argento senza ottenere buoni risultati. Inoltre, per valori di 80 mg di ALA modifiche strutturali quali riduzione del volume di nucleo nelle particelle sono state osservate. Analogamente, gli stessi esperimenti sono stati condotti usando una massa comparabile di inchiostro di argento e di MUL e ALA. Rapporti TRIS/TMPTA di 1:1, 1:2, 1:3 e 1:4 sono stati considerati.

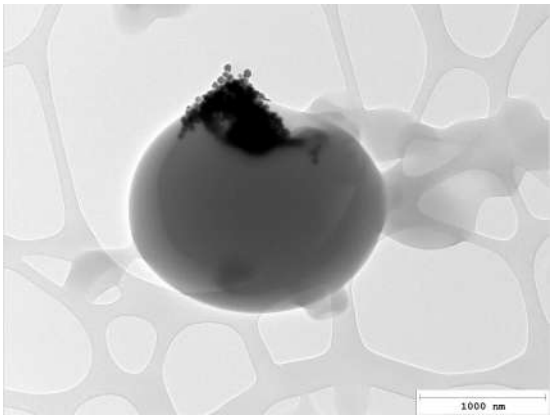

Figure 7: TRIS/TMPTA con Ag-Ink 30-35% e MUL.

Nessun campione analizzato presenta argento isolato all'interno delle capsule e in alcuni casi la presenza di stabilizzante influenza negativamente la morfologia delle particelle polimeriche. La tendenza dell'inchiostro di argento ad aggregarsi si è rivelata maggiore rispetto a quella dell'Ag-PVP.

Un effetto stabilizzante migliore è stato ottenuto sostituendo MUL e ALA con 1-propanolo. Il quantitativo di argento utilizzato è stato incrementato più volte di un fattore 3 senza

incontrare problemi di stabilità della dispersione. Tutte le formulazioni usate sono accomunate dal rapporto TRIS/TMPTA di 1:3, rivelatosi dare le migliori capsule. L'effetto dell'incremento di massa di argento ha un risultato positivo sulla stabilità dell'argento, anche senza l'introduzione del 1-propanolo. Questo effetto è visibile in particolar modo nei campioni con argento PVP.

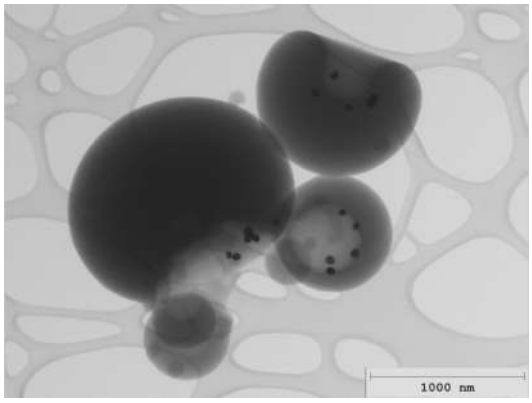

(a) TRIS/TMPTA con Ag-PVP e PrOH.

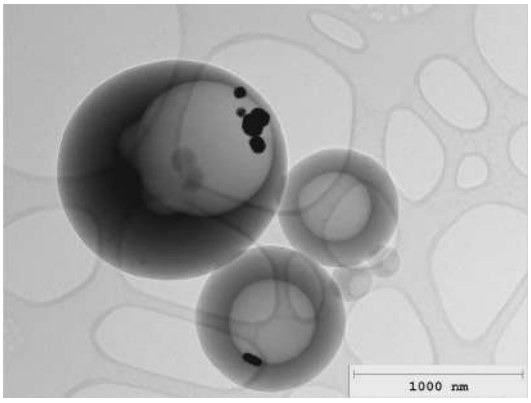

(b) TRIS/TMPTA con Ag-Ink 50% e PrOH.

Figure 8: Immagini al TEM di particelle TRIS/TMPTA con 0,05 g Ag-NPs e PrOH.

Introducendo 5 g di PrOH gli effetti osservabili sulle capsule prodotte con i due tipi di argento sono differenti. Nel campione contenente Ag-PVP le nanoparticelle di argento sono presenti fuori dalle nanocapsule (Figura 8a). Mentre nel campione con inchiostro di argento l'effetto stabilizzante del PrOH è maggiore (Figura 8b). Le Ag-NPs non sono agglomerate, ma ben separate e meglio distribuite all'interno delle particelle polimeriche. Allo stesso modo sono stati condotti esperimenti con un quantitativo pari a 0,15 g di argento con e senza PrOH. Anche in questo caso l'Ag-PVP è risultato più stabile nelle formulazioni senza PrOH rispetto all'Ag-ink.

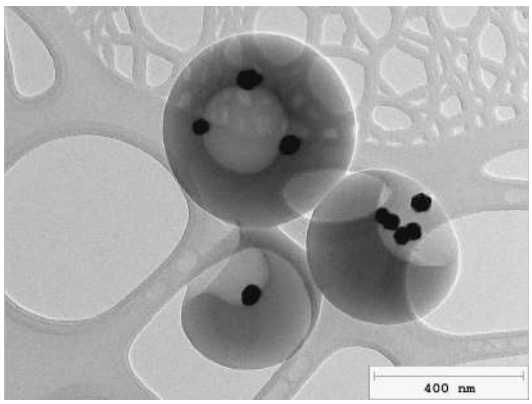

(a) TRIS/TMPTA con Ag-PVP e PrOH.

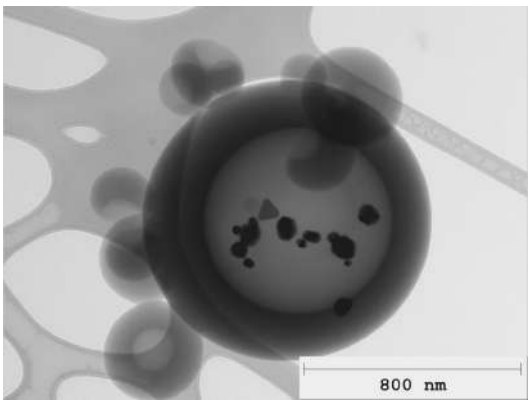

(b) TRIS/TMPTA con Ag-Ink 50% e PrOH.

Figure 9: Immagini al TEM di particelle TRIS/TMPTA con 0,15 g di Ag-NPs e PrOH.

Risultati ottenuti con Ag-PVP e 3 g di PrOH al posto di 5 g si sono rivelati migliori. La quasi totalità delle nanoparticelle prodotte contenevano argento ben distribuito al loro interno senza nessuna dispersione esterna (Figura 9a). La distribuzione delle nanoparticelle

di argento nel caso di impiego di Ag-Ink è meno uniforme e, come si può notare nella Figura 9b, la distribuzione dimensionale delle Ag-NPs stesse è meno uniforme.

Esperimenti con un quantitativo ancor maggiore di argento pari a 0,45 g sono stati effettuati per ottenere un ibridi con uno rivestimento più uniforme del nucleo con il metallo. I campioni con Ag-Ink hanno dato risultati negativi, mostrando particelle di argento agglomerate sia in presenza che in assenza di PrOH. Buoni risultati sono stati raccolti invece con Ag-PVP, ottenendo con successo nanocapsule con interfaccia del nucleo rivestita di nanoparticelle di argento (Figura 10).

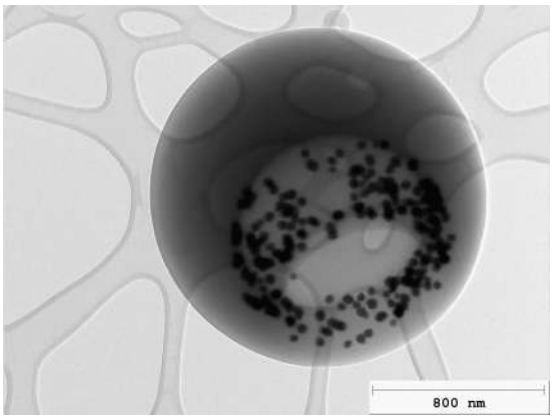

Figure 10: TRIS/TMPTA con 0,45 g Ag-PVP e PrOH.

Prove simili sono state condotte con l'utilizzo di Ag-PVP con diametro medio di 25 nm e diversi stabilizzanti. Un carico di 0,15 g di Ag è stato usato in combinazione con PrOH, TPGME e LipoA. Le dimensioni minori delle particelle di argento hanno causato maggiori problemi di agglomerazione e hanno possibilmente influito sul processo di spraying delle formulazioni.

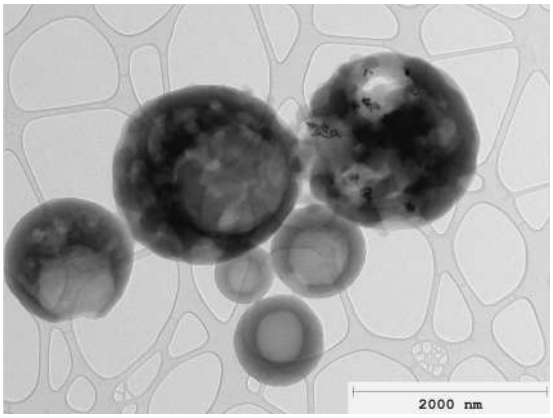

Figure 11: Strutture a mosaico di TRIS/TMPTA con Ag-PVP (25 nm) e TPGME.

L'effetto stabilizzante del PrOH non ha restituito risultati simili agli esperimenti in cui Ag-PVP 50 nm è stato impiegato. Infatti, le NPs hanno dimensione media maggiore e presentano una struttura spugnosa con più cavità superficiali. L'uso di 3 g di TPGME, il solvente usato per l'inchiostro di argento, ha generato particelle con caratteristiche intermedie

tra capsule e particelle a mosaico (in Figura 11), probabile conseguenza di un processo di strutturazione secondaria.

L'utilizzo di LipoA non ha causato modifiche strutturali e ha ridotto la tendenza delle particelle di argento ad agglomerarsi. Tuttavia, l'impiego dell'argento con diametro medio minore ha influito negativamente sulla stabilità del prodotto finale. La scelta di una buona fonte di Ag-NPs si è rivelata essenziale per il successo nella produzione di ibridi ben strutturati. Parametri come la stabilità della dispersione, gli additivi presenti e la distribuzione dimensionale media delle particelle variano a seconda del tipo di argento impiegato.

Per concludere, sono state effettuate diverse prove variando il rapporto monomeri su solvente (M/S) e mantenendo inalterato il rapporto tra le masse di monomero e argento e il rapporto relativo tra i solventi. I valori di M/S analizzati corrispondenti a 1/2, 2/5, 5/14, 3/10 e 1/4 hanno influenzato particolarmente la struttura delle particelle prodotte.

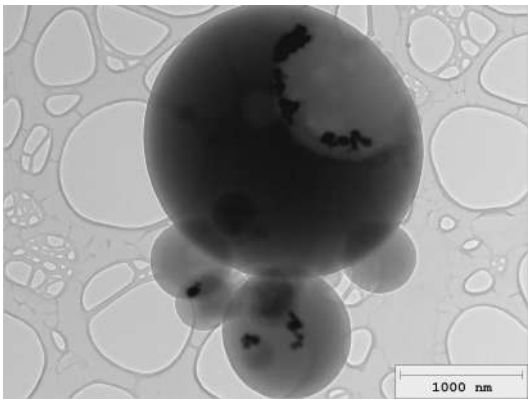

(a) TRIS/TMPTA con M/S pari a 1/2.

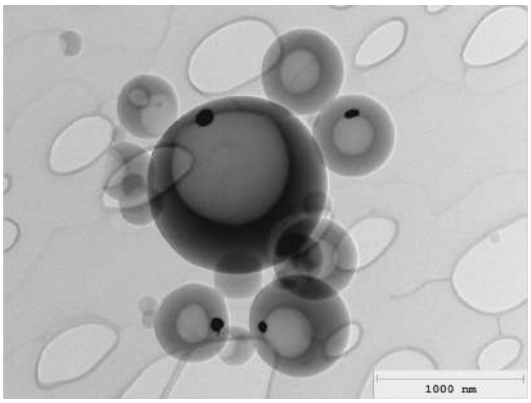

(b) TRIS/TMPTA con M/S pari a 3/10.

Figure 12: Immagini al TEM di particelle TRIS/TMPTA con variazione M/S.

Nello specifico, una riduzione della quantità di solvente ha portato alla produzione capsule in minor numero e caratterizzate da una guscio polimerico più spesso (Figura 12a). Al contrario, un aumento della frazione di solventi corrisponde alla formazione di capsule con un nucleo che occupa al maggior parte del volume della particella e con un guscio polimerico molto più sottile (Figura 12b)

0.3.3 Coniugazione con maleimide

Nell'ultima parte di questo studio, l'attenzione si è focalizzata sulla ricerca di gruppi funzionali sulfidrilici in alcuni dei campioni prodotti con meccanismo tiolenico puro e misto. In seguito una coniugazione con la bio molecola maleimide è stata portata a termine. I campioni di nanoparticelle scelti per questo tipo di analisi sono stati ottenuti con concentrazioni crescenti di TMPTA con rapporti che variano da 1:1 fino ad 1:8 TRIS/TMPTA. Come prima analisi qualitativa, i campioni sono stati sottoposti a reazione di Ellman. Questa prevede l'impiego di un reagente in grado di legarsi con i gruppo SH e dare come prodotto un composto di colore giallo. In base all'intensità della colorazione assunta dalle soluzioni preparate con i diversi campioni più il reagente di Ellman si può determinare quali di questi contengono ancora gruppi SH disponibili per future funzionalizzazioni.

Campioni con rapporti di TRIS/TMPTA pari a 1:4 o inferiori sono risultati positivi alla reazione con reattivo di Ellman, con intensità maggiore per quantitativi di TRIS maggiori, a conferma della non completa conversione del tiolo in meccanismi tiolenici con rapporto

stechiometrico tra i monomeri. Questi campioni sono poi stati sottoposti a reazione con maleimide (iFM) e l'effettivo successo della coniugazione analizzato con spettroscopia a fluorescenza.I campioni con le particelle disperse con iFM sono stati dapprima sottoposti a diversi cicli di purificazione (centrifugazione e ridispersione del campione in DMSO e EtOH) per rimuovere le molecole di iFM non legate alle particelle e successivamente analizzate con la spettroscopia a fluorescenza.

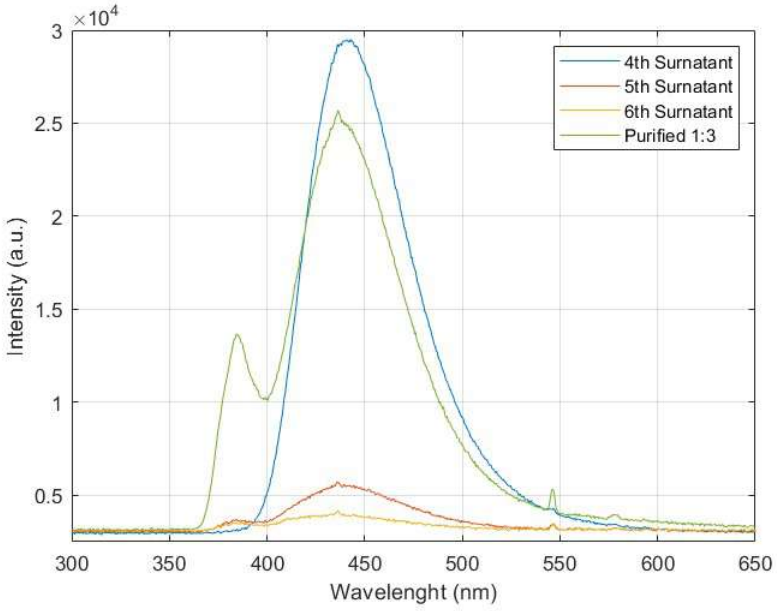

Figure 13: Spettri di fluorescenza registrati per particelle con rapporto TRIS/TMPTA pari a 1:3.

Gli spettri dei surnatanti prelevati dopo ogni ciclo di purificazione sono stati analizzati finché il picco di assorbimento di iFM non è risultato abbastanza basso da ritenere la purificazione conclusa. Una volta terminata la purificazione le particelle legate a iFM sono stata analizzate e i picchi relativi alla maleimide registrati. In Figura 13 è riportato lo spettro ottenuto con particelle prodotte con rapporto TRIS/TMPTA di 1:3 il cui picco a 430-440 nm conferma l'avvenuta coniugazione con iFM.

0.4 Conclusioni

In questo lavoro è stata dimostrata la possibilità di ottenere nanocapsule polimeriche e nanocapsule ibride polimero-argento attraverso un processo di fotopolimerizzazione in aerosol con meccanismo tiolenico. L'effetto dei vari additivi impiegati nelle formulazioni è stato indagato per comprendere come essi influenzino la morfologia delle particelle prodotte. Nello specifico, soluzioni spray contenenti diversi rapporti molari dei monomeri TRIS e TMPTA sono state studiate ed è stato possibile individuare nel rapporto TRIS/TMPTA di 1:3 una formulazione in grado di produrre nanocapsule ben strutturate in modo riproducibile. Nanocapsule polimeriche contenenti nanoparticelle di argento nel loro nucleo interno sono state prodotte per la prima volta attraverso il meccanismo tiolenico e l'effetto di diversi stabilizzanti sulle dispersioni contenenti nanoparticelle di argento è stato studiato. Infine, uno studio sulla presenza dei gruppi funzionali SH nelle strutture prodotte è stato portato a termine. La presenza dei gruppi sulfidrilici per campioni con rapporti di TRIS/TMPTA da 1:1 a 1:4 è stata dimostrata e una coniugazione con la biomolecola maleimide è stata portata a termine.

Studi ulteriori mirati al miglioramento della stabilità delle soluzioni spray contenenti argento sono necessari per l'ottimizzazione del processo in previsione di una applicazione su più ampia scala di questa tecnologia. Inoltre, problemi relativi alla polidispersità sono presenti e un migliore controllo della distribuzione dimensionale delle particelle polimeriche dovrà essere oggetto di sviluppi futuri. Una volta perfezionata la tecnica per la produzione di particelle monodisperse e eliminati problemi di stabilità, studi sull'immagazzinamento e rilascio di farmaci risulteranno necessari ai fini di sviluppare nano-sistemi terapeutici.

Chapter 1

Introduction

1.1 Overview on Polymeric Nanoparticles

Nowadays, the interest in nanoparticles (NPs) and hybrid-nanoparticles (HNPs) is rapidly increasing due to the numerous potential application in the field of nanomedicine, such as drug delivery (Farokhzad and Langer, 2009), disease diagnosis and bioimaging (Wang et al., 2008).

Among all, Polymeric NPs are considered a promising drug delivery system for their excellent surface modification properties, high loading capability and pharmacokinetics control (Faraji and Wipf, 2009). Depending on their internal structure, polymeric NPs can be further classified into nanospheres and nanocapsules. The first with a regular solid polymeric matrix while the latter having a solid or liquid core coated with a polymeric shell (Deng et al., 2020).

The use of nanocapsules can effectively increase drug-loading efficiency and at the same time shielding their load from degradation, lengthening its half-life in the organism and reducing undesirable spillover. More specifically, therapeutic agents encapsulated in the core-shell structure can be selectively transported to preferential targets. This way, it is possible to minimize drug dosage, exposure to cells and tissues where the agent is not needed and at the same time increase drug efficacy and drastically reduce its side effect (Calzoni et al., 2019). NPs loaded in such a way have been widely used in cancer therapy, but also in the treatment of respiratory, cardiovascular and neurodegenerative diseases as well as immunotherapy (Singh et al., 2019). Once the NP-drug system has reached its site of action, release can be controlled over time and triggered by difference in pH, oxidative stress, temperature differential or ultrasound activity (Colson and Grinstaff, 2012).

Hybrid nanomaterials contain two or more different component, typically organic and inorganic, brought together by specific interaction which results in the synergetic enhancement of their functional properties (Ananikov, 2019). This way it is possible to combine polymeric NPs characteristics with noble metals exceptional optical and photothermal properties in a single nanostructure. Metal nanoparticles can improve contrast in magnetic resonance imaging (MRI), fluorescence imaging and scatter or absorb light due to their unique plasmon resonance properties. The latter can be used for thermosensitive drug release and tuned by variation of particle size, shape and composition allowing to design nanostructures for specific bioapplications (Jain et al., 2008). NPs that are designed to work as a drug delivery system as well as a bioimaging device follow on the concept of "theranostic" device, in which both diagnostic and therapeutic functions are can be administered in a single dose (Sailor and Park, 2012).

1.2 Aerosol Photopolymerization (APP)

Photochemical induced polymerization has been largely used to produce micro and nanoparticles for a long time because of several advantageous features that make it an innovative technology. Among these the most important include: contactless stimulation, specific reactivity, temporal control, spatial resolution, reaction rate and molecular weight tunability by dosage of radiation, high decomposition rate of photochemical initiator and no temperature effect on initiation stage (Jasinski et al., 2018).

Photopolymerization techniques used to produce nanoparticles are various, each with its field of use (Jasinski et al., 2018): macroemulsion, microemulsion, miniemulsion, dispersion, precipitation and suspension. All of these are characterized by the presence of a liquid media where the droplet are formed.

Differently, aerosol photopolymerization (APP) is an alternative process to the wet chemical routes listed above, it consists of a spraying device necessary to form monomer droplets and a reactor where the droplets are polymerized into particles through UV radiation. This method offers significant advantages (Widmann and Davis, 1996; Gao et al., 2007; Esen and Schweiger, 1996):

- it avoids the use of additives and surfactants, allowing the production of ultra pure colloids
- there is no need of separation and drying of particles from the liquid suspension as they can be easily collected on a filter
- reduced volume used to generate spray solution
- no interaction of particles with container walls
- particle size depending on the primary droplet size
- size of particles can be controlled over a wide range
- possibility to tune particle characteristics and adding other particles to form hybrids *in situ*

Two main technologies based on aerosol photopolymerization are available: a gas phase synthesis (or gas-to-particle) and a liquid phase synthesis (or liquid-to-particle). The first one has been used in the earliest study on aerosol photopolymerization (Nakamura et al., 1984; Partch et al., 1985) and it consists in the material evaporation followed by subsequent nucleation and growth by condensation and coagulation in an inert gas. This way it is possible to produce high purity particles with a good production rate, but multi-component structures are difficult to produce because of the differences in the pressures and in the nucleation/condensation rates of the involved vapours (Biskos et al., 2008). In addition, the rates of evaporation and condensations depend strongly on liquid volatility and to enhance the production efficiency a high temperature of evaporation and a low temperature of condensation are required, otherwise the rate of production is generally low. The second method allows to produce droplets by atomizing a solution of specific composition that crystallize into solid particles upon subsequent evaporation of the solvent (Biskos et al., 2008). In this case, pneumatic atomization (nebulization) is used to generate droplets from the liquid solution: pressurized air is introduced via an orifice in such a way that the expanding air stream moves perpendicularly to the end of a tube connected to the liquid reservoir. Due to the Bernoulli effect, the low pressure created at the tube end draws the liquid from the reservoir into the air stream. The high forces occurring at the air-liquid interface cause the solution to break up into small liquid droplets which are carried away by the airflow. The

spray stream is then directed onto an impactor plate where the larger droplets directed back to the liquid reservoir or break up into smaller droplets and exit the atomizer in the outlet stream (Biskos et al., 2008). The droplets formed this way are carried into the photoreactor by a nitrogen stream and are polymerized into NPs. Average particle dimensions obtained with aerosol photopolymerization techniques can reach a minimum of less than 100 nm in diameter.

1.3 Production of Nanospheres and Nanocapsules

Recently, intensive progress has been made in the production of different nanoparticles structures via aerosol photopolymerization using different reaction mechanisms. In the work of Akgün based on radical mechanism, a mixture of butyl acrylate (BA) and methyl methacrylate (MMA) with 1,6-hexanediol diacrylate (HDDA) as crosslinker was used to produce spherical nanoparticles (Akgün et al., 2013), nanocapsules, mosaic nanoparticles (Akgün et al, 2014a; Akgün et al., 2014b) and shell nanoparticles (Sigmund et al., 2014). Similar structures were obtained working with a cationic mechanism using diethylene glycol divinyl ether (DVE) as a repetitive monomer (Bazzano et al., 2017; Akgün et al., 2015). In order to reproduce each type, different spraying conditions and additives are required. Variables affecting the nanoparticles final structure are many and to be able to control the final morphology it is essential to understand the structuring process.

Typically, aerosol spray formulations are composed of the monomer or monomers combination, with the possibility of a crosslinker added to increases reticulation, a solvent, in which the monomers are dissolved and a photoinitiator to trigger the polymerization process by producing the propagating species (radical or ions depending on the mechanism). When the droplet is generated it is transferred into the photoreactor where UV light triggers the photoinitiator and propagating species start to form in the droplet. At the same time, the solvent evaporates decreasing the droplet size. Solvent evaporation will proceed until no more will be left, simultaneously, polymerization will turn the propagating chains into a single big reticulated molecule occupying the whole available volume, thus turning the initial droplet into a solid particle. Final particle diameter depends on the primary droplet diameter, monomer concentration, reaction rate, temperature and evaporation rate (Gao et al., 2007). In particular, particle diameter can be reduced by increasing the concentration of solvent and reducing the concentration of monomers in the formulation.

During polymerization, it is important to distinguish a few different phases based on polymer cross-linking density (Figure 1.1).

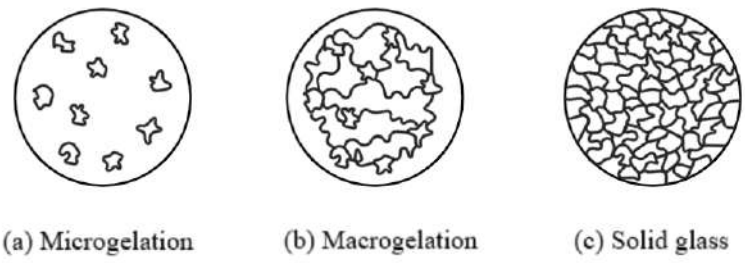

Figure 1.1: Phases of polymeric gelation in an aerosol droplet.

Initially, the polymeric chains are forming isolated small volumes of microgel (Figure

1.1a), diffusion inside this system is still possible through dispersion and chains are somehow free to move. Eventually, the mass of growing polymer becomes crosslinked into one infinite network occupying all the volume of the droplet (Figure 1.1b). The diffusion, as well as chain movement, is hindered, when this happens the system reaches its "gel-point". In the end, all monomers in the solution will be consumed and the crosslinked structure will assume a solid glass morphology (Figure 1.1c)(Sherrington, 1998). Once the polymerization process has reached the gel-point, structural modifications are no longer possible due to the impaired chain mobility and the particle morphology will no longer change. For that reason, to produce nanoparticles with more complex morphologies (superordinate structures) additional additives with the purpose of modifying the time this event occurs are required.

In order to produce the typical core-shell structure of nanocapsules, phase separation between solvents and polymer has to occur before polymer gelation so to allow oligomers or polymeric material to migrate to the outer layer of the droplet before the final structure is formed (Bazzano, 2017). Spray solutions used to produce capsule-like particles contain, in addition to the basic formulation, co-solvents or porogens and possibly a soft-maker. Porogens are organic solvents with a certain affinity with the polymer used. These solvents interact more or less favourably with the polymeric chains and if the solvent-polymer interactions are greater than the polymer-polymer interactions the solvent is sorbed into the polymer structure solvating the chains that will expand and be more free to move. Solvents producing this effect are called thermodynamically "good". Solvents that hardly interact with the polymer are termed thermodynamically "bad" and will cause the polymer to shrink and eventually phase separate and precipitate (Sherrington, 1998; Raula et al, 2004).

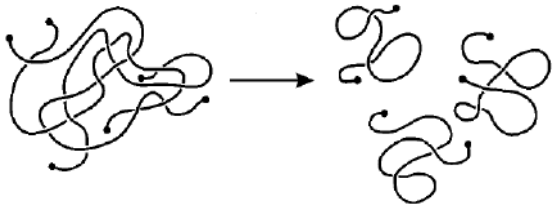

Figure 1.2: Polymeric chains expanding in the presence of a good solvent (Sherrington, 1998).

A mixture of "good" and "bad" solvents are to be used to carefully design the solubility of the monomer in the spray solution and its oligomers in the formed droplets. It is therefore possible to obtain nanocapsules and different particles morphologies simply by varying the ratio between the two solvents. For example, it is possible to delay the gelation of the polymeric structure, thus providing more time for the structuring process (Bazzano, 2017). Indeed, as the crosslinking process proceeds towards the point of gelation, the time at which the "bad" solvent-induced phase separation occurs determines the final particle structure. For example, for a capsule to be formed, it is essential for the phase separation to occur before the gelation. In this work, the "good" solvent of choice was the 2-octanone while the "bad" solvent used was the hexadecane. A second "bad" solvent (2-ethyl-1-hexanol) was used as well as a solvent for monomers and to give more homogeneity to the spray solution. The use of 2-ethyl-1-hexanol is of key importance also because it solubilizes hexadecane which is insoluble in both ethanol and 2-octanone. When the photopolymerization process begins, monomers start to bond together to form chains and 2-octanone has the role of solvating the forming oligomers for a time long enough for them to grow bigger and migrate to the outer droplet layer. The longer the oligomers stay solvated the more time they have to grow and the less amount of monomers will be left in the porogens solution inside the droplet so that it will be less likely to have a successive polymerization inside the particle core. Once the

oligomer chains have reached a certain degree of polymerization the solvent will no longer be able to sorb into them and they will precipitate to form the crosslinked structure. The gel point will be reached, but only locally as the inner particle will be mainly composed of porogens, thus leaving a double phase capsule structure. The value of the polymer molecular weight capable of triggering the precipitation will depend on the relative concentration of 2-octanone, hexadecane and 2-ethyl-1-hexanol.

Generally, thermodynamically good solvents push the polymer domain towards higher crosslinking ratios, whereas thermodynamically poor porogens shift the polymer domain to lower crosslinking ratios (Sherrington, 1998). The effect of this trend is depicted in Figure 1.3.

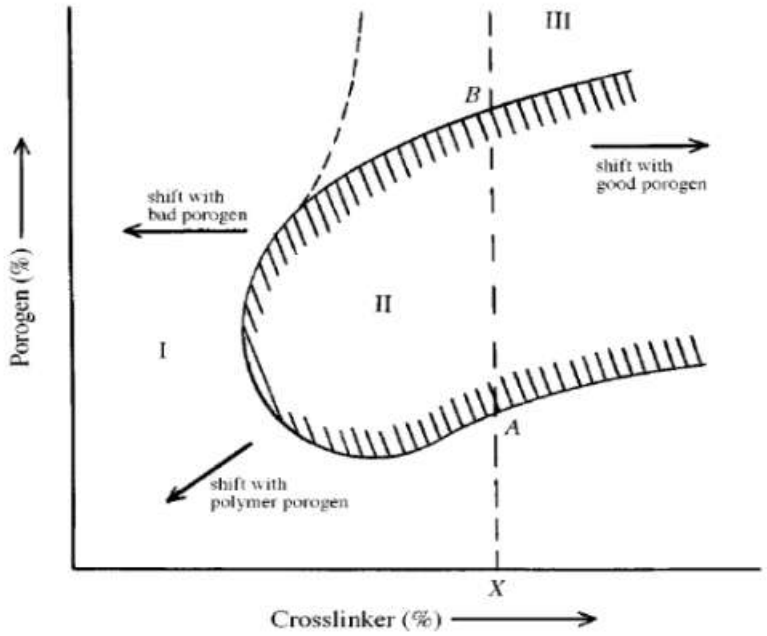

Figure 1.3: Polymer pseudo-phase diagram (Sherrington, 1998).

If gelation time is delayed for too long, porogens will still be sorbed in the polymers once the process is terminated and the structure will result in being sticky and not defined. On the other hand, premature gelation will result in an early polymer precipitation and the final structure will be the one of a mosaic particle (Figure 1.5). In mosaic structures polymeric chains precipitate from the solution before they had time to go to the outer droplet layer, multiple porogen and polymer phases are present within a single droplet and this will create isolated microgel beads inside the main droplet causing the formation of superordinate structures in the final particle. Porogen phase will be more concentrated in monomers, as the oligomers did not propagate long enough to reduce it so that further polymerization in the porogen phase creates additional polymers which will fuse microgel particles in a channel network (Figure 1.4a).

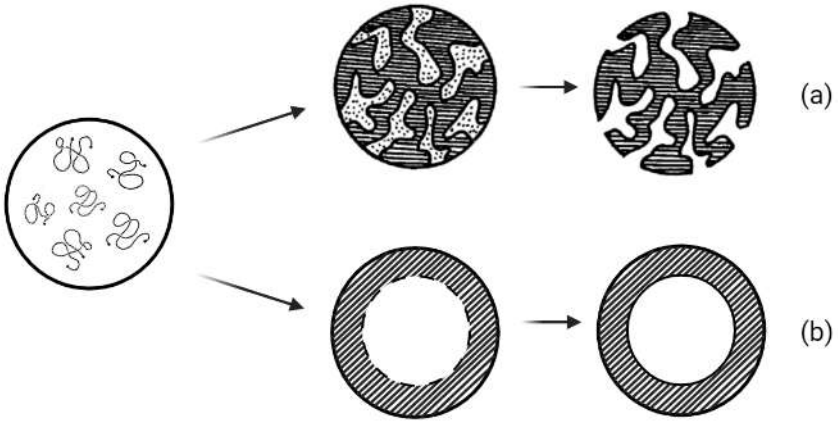

Figure 1.4: Nanoparticle formation in case of: (a) Early gelation and (b) delayed gelation (Modified from Sherrington, 1998).

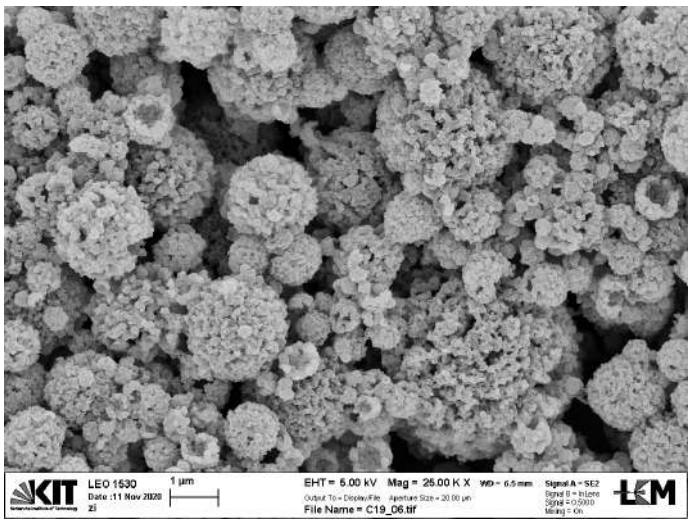

Figure 1.5: Image of a mosaic structure obtained by radical chain polymerization via APP.

The accurate mixing of good and bad solvent is not always enough to tune precisely when polymer gelation will occur. In a complex dispersed system like the one intended to use in this work, other factors are influencing polymer precipitation and/or gelation and they have to be taken into account if the goal is to produce well-structured capsules. The temperature has the same effect of solvent addition: expanding and shrinking polymeric chains, but will not be considered as not a process variable. Photoinitiator concentration influences the initiation step of reaction and consequently the mean average molecular weight. More photoinitiator means a greater number of propagating chains, under the same conditions of monomer concentration it will result in the faster consumption of monomers and shorter chains with lower mean average molecular weight. Despite having shorter chains the oligomers will stay solvated longer, faster propagation will eventually cause the polymers to occupy the whole available volume and crosslinking will cause polymers to reach gelation faster compared to conditions in which less photoinitiator is used. Besides, the faster the polymer molecular weight will evolve, the earlier phase separation will occur. Gelation time is also highly influenced by the reaction rate of the polymerization reaction, the faster the reactivity of the monomers, the faster the oligomers will grow bigger and the faster gelation

will occur. The reaction rate depends on the monomer type employed and the specific reaction mechanism, but it is also influenced by other parameters. For example, depending on the reaction mechanism, the addition of specific molecules can trigger Chain Transfer Mechanism (CTM) in the propagating reaction and halt the polymer growth. These substances can subtract the radical or ions from the reactive species and stop the chain propagation by transferring this active site to another chain. The overall effect of chain transfer species is the crosslinking density reduction and the consequent reduction of the total gel content (Bazzano, 2017). Another additive used to delay gelation time is glycerol. It also acts as a plasticizer, it moderates polymer crosslinking and holds the polymer shell elastic. Its presence is a prerequisite for capsules formation as it occupies the inner core of the droplet forcing the precipitating polymer to accumulate in the outer layers of the forming particle (Akgün et al., 2014b). The modulation of the aforementioned additives and variables and the comprehension of which one is influencing the most the time of gelation and polymer phase separation is of the uttermost importance to be able to produce structured capsules.

1.4 Mechanisms of Polymerization

In order to understand the importance of the polymerization rate and the type of polymerization in the structuring process described so far, insight into the polymerization reaction mechanism is needed. Depending on the scheme that monomers follow to build polymeric chains, polymerization can occur in two different ways: by step-growth mechanism or by a chain-growth mechanism. In chain-growth polymerization, only monomers can react with the propagating chain which has the reactive centre. At any time, there will be only a limited number of active sites located on growing chains and the rest of the molecules will be spare monomers. Radical, cationic and anionic polymerization all follow the chain-growth mechanism.

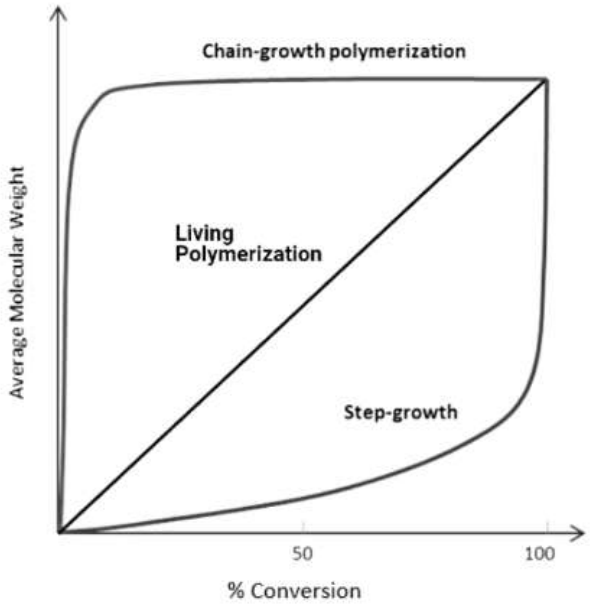

Figure 1.6: Conversion-average molecular weight diagram for chain-growth, step-growth and living polymerization mechanism (Polymer Properties Database).

On the other hand, condensation polymers and generally polymers made up of bifunctional and multifunctional monomers usually follow the step-growth mechanism. In this case, polymers are formed by any number of repetitive units assembling. For instance, a monomer bonds with another monomer to form a dimer that can, in turn, bond with another monomer to form a trimer, two dimers can bond together or they can bond with longer oligomers and so on. In these terms, a bigger number of reactive sites will be active simultaneously. Step-growth polymerization, differently from chain-growth, have no termination step and the end groups of the oligomers and polymers are reactive throughout the polymerization process. In step-growth polymerization average molecular weight increases slowly at low conversions. The explanation is that having a greater number of reactive sites implies that monomers are consumed in a great amount to lengthen a big number of short chains instead of adding up to a single big chain. A higher monomer conversion will be required to have oligomers of a certain length to increase molecular weight substantially. Nevertheless, at high conversion, monomers will be scarce and fairly big oligomers will only be able to bond between each other increasing exponentially the molecular weight. Chain-growth follows the opposite trend, at lower conversions chain will rapidly add monomers to their active site increasing the average molecular weight of few molecules. At higher conversions monomer concentration will be lower and growth will stabilize because the addition of single monomers is no longer influencing that much the molecular weight. The third curve in Figure 1.6 is the living polymerization and represents a chain-growth mechanism where there is no termination and all chains start propagating at the same time and with the same rate.

1.4.1 Thiol-ene Mechanism

Thiol-ene reaction mechanism occurs when a thiol and an alkene react together to form a polymer via a radical mechanism. Thiol-ene reaction are included in the family of "click" chemistry reaction, characterized by high yields, short reaction times, wide functional groups and solvent tolerance, regio- and chemo-selectivity, insensitivity to oxygen, few to no byproducts, facile purification, and high to 100% atom economy (Northrop and Coffey, 2012).

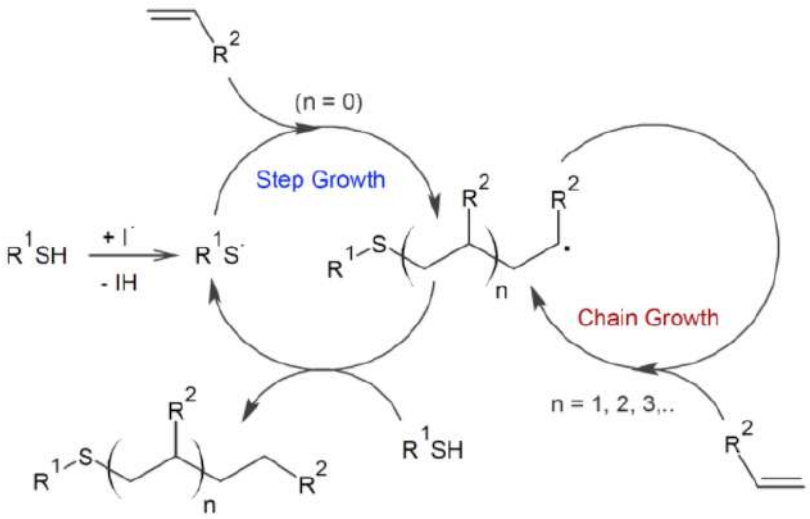

Figure 1.7: Thiol-ene reaction mechanism (Polymer Properties Database).

Under photochemically induced conditions the thiol-ene reaction proceeds as a typical chain process with initiation, propagation and termination step (Lowe, 2010). Nonethe-

less, thiol-ene reactions present the specific characteristic of a step-growth polymerization in which the formation of multiple low molecular weight species is favoured, resulting in high conversion at the gel point and a largely homogeneous network (Northrop and Coffey, 2012). This characteristic duality depends on the competition between two different pathway that in this kind of reactions are interconnected and happen simultaneously (Figure 1.7).

The initiation process starts with the irradiation of the photoinitiator (step 1) and the consequent thiyl radicals formation (step 2).

$$\mathrm{PI} + \mathrm{h}\nu \longrightarrow \mathrm{I}^{\bullet} \qquad \text{(step1)}$$

$$\mathrm{I}^{\bullet} + \mathrm{RSH} \longrightarrow \mathrm{RS}^{\bullet} + \mathrm{IH} \qquad \text{(step2)}$$

Once the thiyl radical is formed it transfers its active centre to another molecule by reacting with an alkene. A carbon centred radical intermediate (thioether) is formed in a step known as thiyl radical propagation (step 3):

$$\mathrm{RS}^{\bullet} + \mathrm{R}^{'}\mathrm{CH{=}CH_2} \xrightarrow{Kp} \mathrm{R}^{'}\mathrm{HC}^{\bullet}{-}\mathrm{CH_2}{-}\mathrm{SR} \qquad \text{(step3)}$$

The thioether formed in step 3 can follow two different propagation pathways: it can either react with another thiol in a chain transfer reaction (step 4) or bond to another alkene, propagating the carbon radical in a homopolymerization process (step 5):

$$\mathrm{RSH} + \mathrm{R}^{'}\mathrm{HC}^{\bullet}{-}\mathrm{CH_2}{-}\mathrm{SR} \xrightarrow{K_{\mathrm{CT}}} \mathrm{R}^{'}\mathrm{CH_2}{-}\mathrm{CH_2}{-}\mathrm{SR} + \mathrm{RS}^{\bullet} \qquad \text{(step4)}$$

$$\mathrm{R}^{'}\mathrm{HC}^{\bullet}{-}\mathrm{CH_2}{-}\mathrm{SR} + \mathrm{R}^{'}\mathrm{CH{=}CH_2} \xrightarrow{K_{\mathrm{CP}}} \mathrm{R}^{'}\mathrm{C}(-\mathrm{CH_2SR})(-\mathrm{CH_2C}^{\bullet}\mathrm{HR}^{'})\mathrm{H} \qquad \text{(step5)}$$

The chain transfer reaction (step 4) is a step-growth mechanism and its products are a thioether and a thiyl radical. This newly formed thiyl radical can now give rise to another propagating chain by reacting with an alkene molecule as in step 3 (see Figure 1.7) or go through a termination reaction. However, if is the thioether radical the one to react with another alkene, the product will be a propagating polymer based on chain transfer mechanism (right pathway in Figure 1.7). The resulting oligomer can now follow again step 5 and keep on adding monomers or switch to the step-growth pathway and stop its propagation. In conclusion, the whole reaction mechanism consists of two competing reactions: an acrylate homopolymerization and a thiol-acrylate step-growth reaction. When two radicals of the same species or two different species bond together chain propagation stops. Termination reactions are all considered equally likely:

$$2\ \mathrm{RS}^{\bullet} \longrightarrow \mathrm{RS}{-}\mathrm{SR} \qquad \text{(step6)}$$

$$2\ \mathrm{R}^{'}\mathrm{HC}^{\bullet}{-}\mathrm{CH_2}{-}\mathrm{SR} \longrightarrow \mathrm{R}^{'}\mathrm{CH}(-\mathrm{R}^{'}\mathrm{CHCH_2}{-}\mathrm{SR}){-}\mathrm{CH_2}{-}\mathrm{SR} \qquad \text{(step7)}$$

$$\mathrm{RS}^{\bullet} + \mathrm{R}^{'}\mathrm{CH_2}{-}\mathrm{CH_2}{-}\mathrm{SR} \longrightarrow \mathrm{R}^{'}\mathrm{CH}(-\mathrm{RS}){-}\mathrm{CH_2}{-}\mathrm{SR} \qquad \text{(step8)}$$

Generally, given the initial stoichiometric mixture of thiol and ene monomers functional groups, it is expected for the monomers to be consumed at identical rates in what is described

as a pure thiol-ene mechanism (Cramer and Bowman, 2001). In reality, this does not occur and one of the mechanisms prevail over the other. Whether a step- or a chain-growth pathway is followed depends on the relative kinetics of chain transfer and homopolymerization which, in turn, depends on the nature of the carbon centred radical and the alkene (Northrop and Coffey, 2012). The dominance of either of the two mechanisms has a major effect on network structure and material properties (Reddy et al., 2006)

In the thiol-acrylate mechanism, the one used in this work, the chain-growth pathway often prevails. Indeed, it was observed in previous research, that the acrylic chain grows at a faster rate compared to the step-growth counterpart. The reason for this behaviour can be explained by two factors: the first is that thiol monomers are not able to bond together to give a homopolymerization reaction as acrylates monomers do. The second is that when thiyl radicals can be reformed in the chain transfer mechanism and participate in repeated reactions with no net thiol consumption. Thus, it is likely that the thiol monomer will have a lower conversion when compared to the acrylic monomer (Cramer and Bowman, 2001).

1.4.2 Mixed Thiol-Acrylic Polymerization

Given that the termination reactions are all considered equally likely and their rates negligible compared to the ones of the propagations steps, the relative variation of ene monomer and thiol monomer concentration can be expressed as (Cramer and Bowman, 2001):

$$\frac{d[\mathrm{C{=}C}]}{d[SH]} = 1 + \left(\frac{k_{\mathrm{CP}}}{k_{\mathrm{CT}}}\right)\frac{[\mathrm{C{=}C}]}{[SH]} \tag{1.1}$$

Where [C=C] represents the concentration of the ene functional group and [SH] represents the concentration of the thiol functionalities. $\mathrm{k_{CP}}$ and $\mathrm{k_{CT}}$ are the reaction rates of the propagation step and the chain transfer step respectively. The ratio between these two constants is the main factor determining the overall kinetics. If $k_{\mathrm{CP}} >> {}_{\mathrm{CT}}$ the chain transfer step is rate-limiting and the overall rate is first order with respect to the thiol concentrations. On the other hand, if $k_{\mathrm{CP}} << k_{\mathrm{CT}}$ the rate-limiting step will be the ene homopolymerization and the overall reaction will be first order with respect to the ene monomer concentration. When the terms are similar the rate will be depending on both concentrations (Northrop and Coffey, 2012). The $\left(\frac{k_{\mathrm{CP}}}{k_{\mathrm{CT}}}\right)$ ratio can be also used as a measure of polymeric gelation; the greater is the influence of the homopolymerization chain-growth step compared to the chain transfer one the less delayed will be the gelation in the polymer network as is the chain transfer mechanism that hinders the molecular weight increase. Therefore, by modifying the concentration of thiol and ene monomers in the starting solution it is possible to design gelation point and final polymer structural characteristic. Thiol-ene reactions occurring with non-stochiometric monomers concentrations are depicted as mixed thiol-ene mechanism. Models have been developed displaying that an increase in thiol concentration will result in an increase in the gel point conversion caused by an increase in the contribution of the step-growth mechanism (Reddy et al., 2006).

1.5 Conjugation

In order to be biologically active, polymeric NPs have to undergo a process of bio-conjugation. More specifically, a chemical surface reaction with the objective of combining through a covalent bond the synthetic polymeric NPs with a biomolecule (Sperling and Parlak, 2010). This process is a fundamental requirement to obtain nanomaterials able to interact with a biological system, thus assolving drug delivery or bio medical activities. The most common thiol-ene polymer surface modification is the Maleimide-thiol reaction (Figure 1.8). It consists of joining the maleimide functional groups to the sulfhydryls groups present on the NPs surface through a Michael addition "click" reaction (Lee at al., 2020).

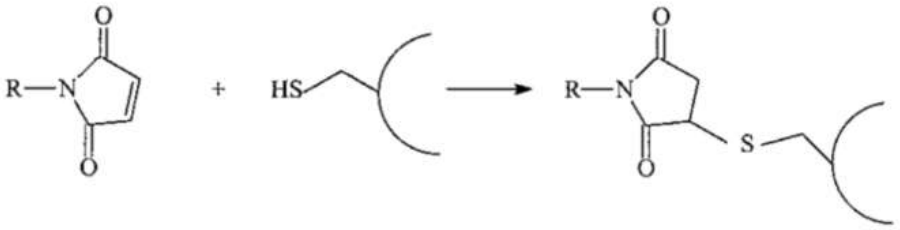

Figure 1.8: Maleimide-thiol reaction: sulfhydryl group on NP surface reacts with the substituted maleimide, where R group can be a biomolecule of interest. The product of the reaction is a maleimide bioconjugated to a polymeric NP through a thioether bond (modified from Geest and Lolkema, 2000).

Maleimide exhibits a high selectivity towards thiol functional group and maleimide bonded NPs show good long-term stability in physiological environments (Fontaine et al., 2014). Maleimide can be easily bonded with biomolecules such as peptides, proteins, or carbohydrates so to create systems with both NPs and biomolecule characteristics.

Chapter 2

Experimental section

2.1 Materials

For this work, various chemicals were used to produce spray formulations. These are divided in monomers, porogens, solvents, silver compounds and stabilizers.

- **THIOL monomers:**
  - Thrimethylolpropane tris(3-mercaptopropionate), TRIS (Figure 2.1a). Purity $\geq$ 95.0%, density of 1.21 g/mL at 25 °C and molecular weight of 398.56 g/mol. Purchased from Sigma-Aldrich.
  - Pentaerythritol tetrakis (3-mercaptopropionate), TETRA (Figure 2.1b). Purity $\geq$ 95.0%, density of 1.28 g/mL at 25 °C and molecular weight of 488.66 g/mol. Purchased from Sigma-Aldrich.

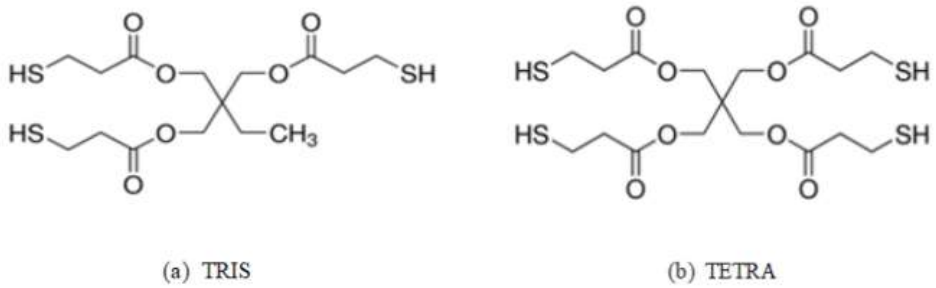

(a) TRIS (b) TETRA

Figure 2.1: THIOL monomers.

- **ENE monomers:**
  - Trimethylolpropane triacrylate, TMPTA (Figure 2.2a). Contains 600 ppm monomethyl ether hydroquinone as inhibitor, technical grade. Density of 1.1 g/mL at 25 °C and molecular weight of 296.32 g/mol. Purchased from Sigma-Aldrich.
  - 2,4,6-Triallyloxy-1,3,5-triazine, TAT (Figure 2.2b). Purity 97%, density of 1,11 g/mL at 25 °C and molecular weight of 249,27 g/mol. Purchased from Sigma-Aldrich.
  - 1,3,5-Triallyl-1,3,5-triazine-2,4,6(1H,3H,5H)-trione, TTT (Figure 2.2c). Purity 98%, density of 1.159 g/mL at 25 °C and molecular weight of 249.27 g/mol. Purchased from Sigma-Aldrich.

– Diallyl adipate, DAA (Figure 2.2d). Density of 1.02 g/mL at 25 °C and molecular weight of 226.27 g/mol. Purchased from Tokyo Chemical Industry Co., Ltd. (TCI)

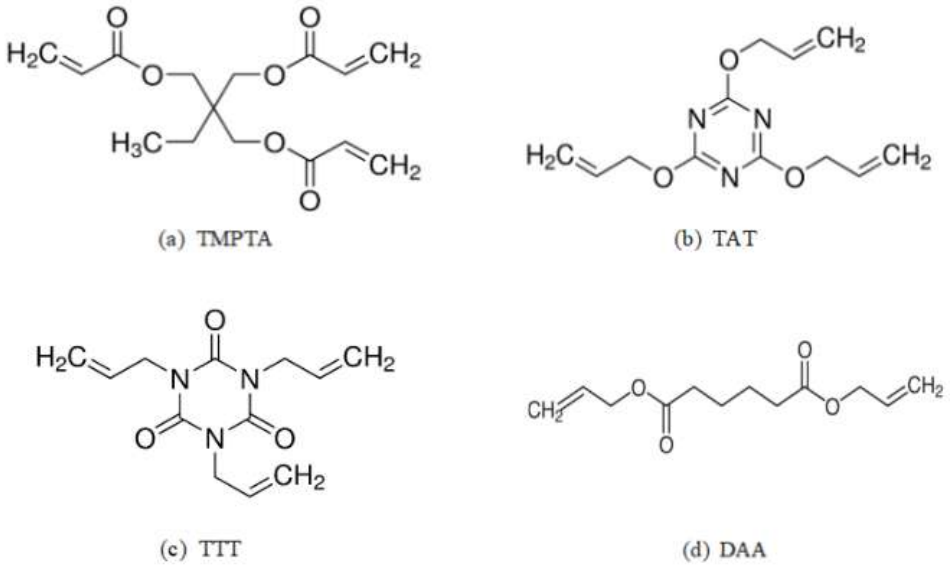

Figure 2.2: ENE monomers.

- **Porogens:**
  - 2-Octanone, 2-Oct (Figure 2.3a). Reagent grade, 98%. Density of 0,819 g/mL at 25 °C, molecular weight of 128,21 g/mol and boiling point of 173 °C. Purchased from Sigma-Aldrich.
  - 2-Ethyl-1-hexanol, IsoOct (Figure 2.3b). Purity $\geq$ 99.6%, density of 0,833 g/mL at 25 °C, molecular weight of 130,23 g/mol and boiling point of 183-186 °C. Purchased from Sigma-Aldrich.
  - Hexadecane, HD (Figure 2.3c). Purity 99%, density of 0,773 g/mL at 25 °C, molecular weight of 226,41 g/mol and boiling point of 287 °C. Purchased from Sigma-Aldrich.

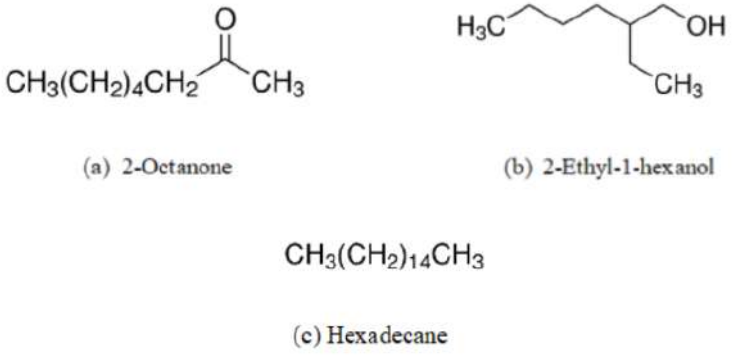

Figure 2.3: Porogens.

- **Solvents and additives:**
  - Ethanol, EtOH. Density of 0.789 g/mL at 25 °C and boiling point of 78.37 °C. Purchased from Sigma-Aldrich.
  - 1-Propanol, PrOH ROTIPURAN®, purity ≥ 99.5%, density of 0.784 g/mL at 25 °C and boiling point of 97 °C. Purchased from Roth.
  - Glycerol, Gly. Purity ≥ 99.5%, density of 1.26 g/mL at 25°C and boiling point of 290 °C. Purchased from Sigma-Aldrich.
  - Dimethylsulfoxid, DMSO. Purity ≥ 99.5%, density of 1.1 g/mL at 25 °C and boiling point of 189 °C. Purchased from Roth.
  - Tri(propylene glycol) methyl ether, TPGME, mixture of isomers. Purity ≥ 97.5%, density of 0.963 g/mL at 25 °C and boiling point at 100°C/2 mmHg. Purchased from Sigma-Aldrich.
- **Stabilizers:**
  - 11-Mercapto-1-undecanol, MUL. Purity 97%, molecular weight of 204,37 g/mol. Purchased from Sigma-Aldrich.
  - α-Lipoic acid, ALA. Purity ≥ 99.0% and molecular weight of 206.33 g/mol. Purchased from Sigma-Aldrich.
  - m-dPEG®$_8$-Lipoamide, LipoA. Molecular weight of 571.79 g/mol. Purchased from Quanta Biodesign.
- **Silver:**
  - Silver nanoparticles ink, dispersion in tripropylene glycol mono methyl ether, 30-35wt%, 50 nm average nanoparticle diameter. Purchased from Sigma-Aldrich.
  - Silver nanoparticles ink, dispersion in tripropylene glycol mono methyl ether, 50wt%, 50 nm average nanoparticle diameter. Purchased from Sigma-Aldrich.
  - Silver nanospheres with 25 nm average diameter, coated in Polyvinylpyrollidone (PVP). Purchasd from nanoComposix.
  - Silver nanospheres with 50 nm average diameter, coated in Polyvinylpyrollidone (PVP). Purchasd from nanoComposix.
- **Other:**
  - Photoinitiator, 2-Methyl-4'-(methylthio)-2-morpholinopropiophenone, PI. Purity 98%. Purchased from Sigma-Aldrich.
  - Nitrogen, purity ≥ 99.999%. Purchased from Air Liquide.
  - 5,5'-dithiobis-(2-nitrobenzoic acid), DTNB. Purity 99%. Purchased from Sigma-Aldrich.
  - iFluor ^{TM} 350 maleimide, iFluor-M. Purchased from AAT Bioquest.

2.2 Equipment and Instrumentation

The instrumentation used in this work consists mainly of an atomizer and a photoreactor. The solution to be sprayed is prepared in 100 mL brown flasks (to avoid early photopolymerization triggered by environmental light) and mounted in the atomizer. The atomizer employed was the AerosolGenerator ATM 220 by TOPAS GmbH (Figure 2.4) employing nozzles with a spray aperture diameter of 0.3 mm. Here, the spray dilution is atomized and conveyed through the photoreactor where the photopolymerization occurs. Droplets with an average concentration of $10^8 particles/cm^3$ are produced by this atomizer and are then separated by an impact separator that avoids particles with a diameter greater than 1 μm to be sprayed in the reactor, these are instead sent back to the flask by reflux.

Figure 2.4: Atomizer by TOPAS.

When using silver nanoparticles the spray solution was continuously agitated using a magnetic stirrer during the whole duration of the experiment to prevent phase separation. Both the flask containing spray solution and the tube connecting the atomizer to the reactor are covered with aluminium foil or black rubber to avoid exposition to light and premature photoinitiation (see Figure 2.5a).

(a) Atomizer plus stirrer.

(b) 4 tubes photoreactor.

The photoreactor (Figure 2.5b) is where the actual photopolymerization takes place and consists of 4 FEP (Fluorinated Ethylene Propylene) tubes through which droplets are exposed to UV radiation. Tube length is 56 cm and inner diameter is 1,5 cm. This reactor is placed between 6 UV lamps with an electrical input power of 15 W and emitting light in a wavelength range between 270 and 360 nm with a peak of maximum 312 nm. Nitrogen is used as a carrier gas that conveys the droplets towards the reactor. Inlet pressure used in all experiments was maintained constant and equal to 1 bar so that the residence time could be calculated knowing the nozzle spray flow rate (1,46 L/min). The residence time was sufficient considered the short polymerization time required by the thiol-ene mechanism.

Once the polymer particles are formed they are collected in a filter housing at the end of the photoreactor. Filter used were polyvinylidene difluoride (PVDF) hydrophilic membranes with 0.1 μm pore diameter purchased by Durapore. The duration of each experiment was established on the base of the sample collection rate and was generally comprised between 90 and 120 minutes. Filters were exchanged to avoid clogging every 30 or 60 minutes also depending on the sample collection rate.

2.3 Analysis Techniques

Samples obtained in this work employing Aerosol Photopolymerization (APP) were analysed using SEM, TEM and Fluorescence Spectroscopy.

Scanning Electron Microscopy (SEM) is used to produce 2D images of solid samples where the surface topography is outlined. Crystalline structure and chemical composition can also be analysed with this characterization method. SEM employs a high energy beam of the electrons emitted by a source called "Gun" that interacts with the surface of the solid specimen. The electronic beam's kinetic energy is dissipated because of the impact with the sample and different signals are generated, with the main part being the, so-called, secondary electrons. This signal is captured by a detector that, using the position of the emitted beam and its intensity, can produce an image of the sample. SEM works in a vacuum and has a maximum resolution reaching 1-10 nm. In this work a Field Emission Scanning Electron Microscope (FE-SEM) has been used, having a better spatial resolution (up to 1 and 1/2 nm) and being able to produce clearer and less electrostatically distorted images.

Transmission Electron Microscopy (TEM) uses a similar working principle as light microscopy, but instead of light, it uses a beam of electrons. The electron beam has a far smaller wavelength compared to light and thus it is possible to achieve a far greater resolution, in some cases atomic scale resolution is attainable. The beam is transmitted through the solid sample with the help of focus lenses and its energy is modified by it, then it strikes a fluorescent screen where the image is generated. The sample should be prepared on a specific grid and it must have a maximum thickness of 100 nm for the beam to be able to pass through. TEM requires high vacuum as well.

Fluorescence Spectroscopy (FS) analyses fluorescence emitted by a sample triggered by radiation excitation. Molecules in the sample absorb photons from an emission source and become excited, meaning that they go from a ground electronic state to a higher energy level. When the molecules drop to a lower energy level, they are capable of emitting a photon, generally with a different frequency, which is then captured by a detector. By knowing the emission wavelength of various functional groups and molecules it is possible to characterize the chemical nature of a sample. Excitation light passes through a monochromator which

filters the radiation before it hits the sample, after that the light is directed to another monochromator before arriving at a detector to be analysed . The incident light hits the sample from a certain direction and fluorescence light is emitted in all directions, detector is usually placed at a 90° angle to minimize stray light from the excitation source.

Chapter 3

Results and Discussion

3.1 Production of Capsules

The starting formulation adopted in this work is based on previous studies employing Aerosol Photopolymerization (Longo, 2019; Zappitelli, 2017). It consists of an equimolar combination of the Thiol-ene monomers TRIS/TMPTA and a certain ratio of porogens and solvents (C01 in Table 3.1). This formulation exhibits the prerequisites to form capsule-like particles and was thus chosen as the starting point for this research.

3.1.1 Effect of Thiol-ene monomer relative ratio

Monomers relative ratio is modified with the goal of altering the relative influence of the step-growth reaction and chain-growth reaction in the Thiol-ene mechanism. During the polymerization, the thiol monomer acts as a chain transfer agent or regulator, its effect is to acquire the free radical site from the growing polymer and in this way promote chain termination. Chain transfer has a strong effect on the degree of polymerization. In fact, by increasing the amount of regulator the overall molecular weight decreases as well as the crosslinking density. As the chain propagation process step is hindered, polymeric chains do not reach the same length as they would without the addition of these regulators and the gelation process is delayed. On the other hand, by adding more ene monomer to the formulation, chain propagation reaction rate increases and the gelation occurs earlier as the homopolymerization of the alkene is the main reaction pathway followed and the average molecular weight evolution is faster.

All experiment in this mixed-mode series have been performed by maintaining constant all variables: including M/S ratio, amount of solvents and porogens and by only varying the monomers relative ratio. TMPTA percentage was increased from a molar ratio of 1:1 to 1:8, the sum of TRIS and TMPTA was kept constant and equal to 10 g. Details of the spray solutions employed are present in Table 3.1.

Table 3.1: Experiments with different Thiol-ene monomer ratio.

Exp.	Monomers		Ratio	HD/2Oct/IsoOct [g]	Gly [g]	Solvent [g]	M/S
C01	TRIS	TMPTA	1:1	3/3,5/3,5	3	12 EtOH	2/5
C22	TRIS	TMPTA	1:2	3/3,5/3,5	3	12 EtOH	2/5
C21	TRIS	TMPTA	1:3	3/3,5/3,5	3	12 EtOH	2/5
C04	TRIS	TMPTA	1:4	3/3,5/3,5	3	12 EtOH	2/5
C20	TRIS	TMPTA	1:5	3/3,5/3,5	3	12 EtOH	2/5
C37	TRIS	TMPTA	1:6	3/3,5/3,5	3	12 EtOH	2/5
C38	TRIS	TMPTA	1:8	3/3,5/3,5	3	12 EtOH	2/5

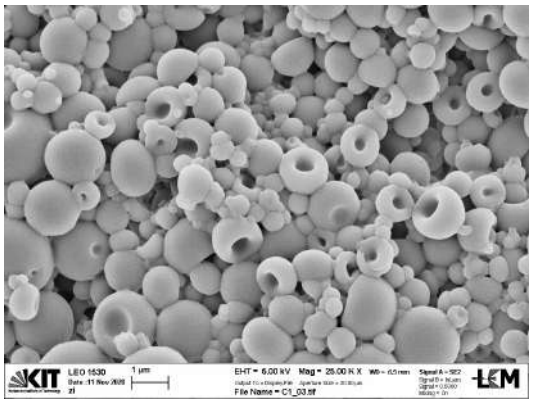

(a) SEM image of experiment C01 (1:1).

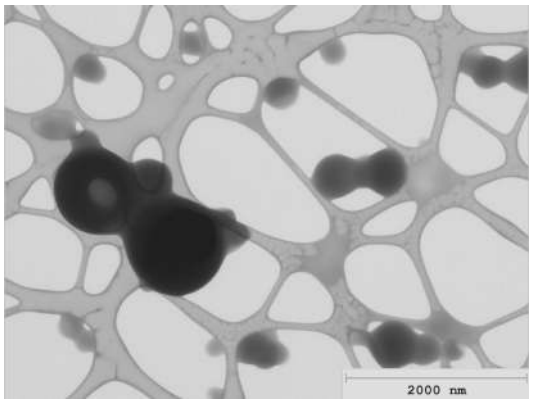

(b) TEM image of experiment C01 (1:1).

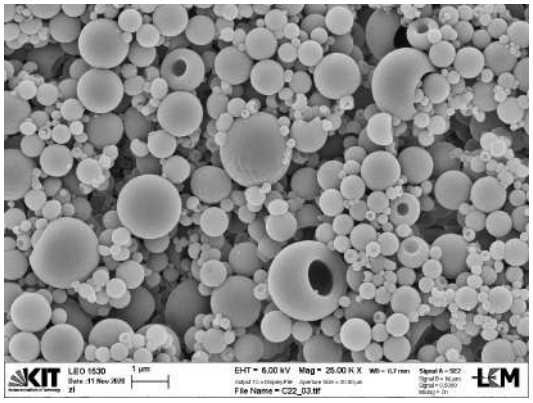

(c) SEM image of experiment C22 (1:2).

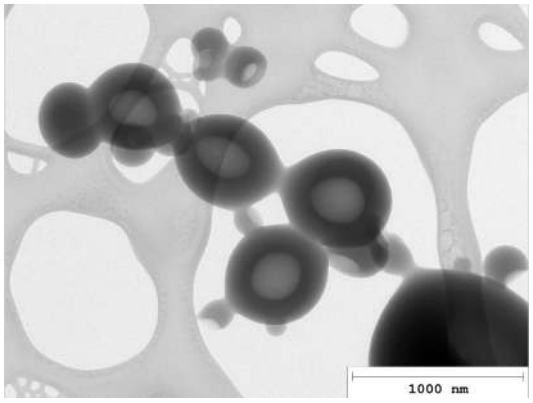

(d) TEM image of experiment C22 (1:2).

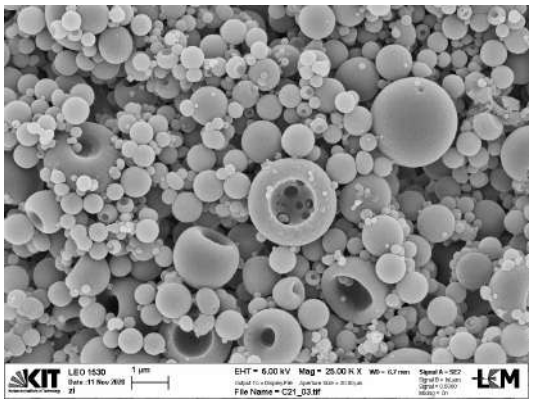

(e) SEM image of experiment C21 (1:3).

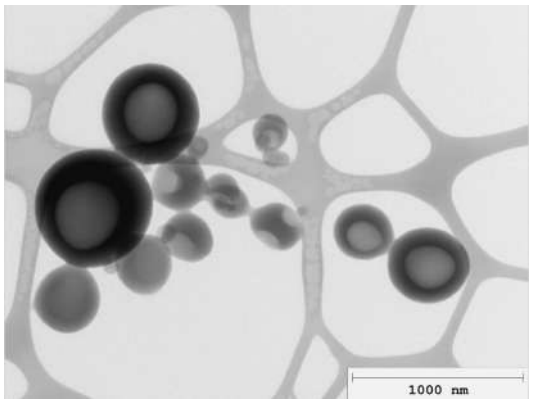

(f) TEM image of experiment C21 (1:3).

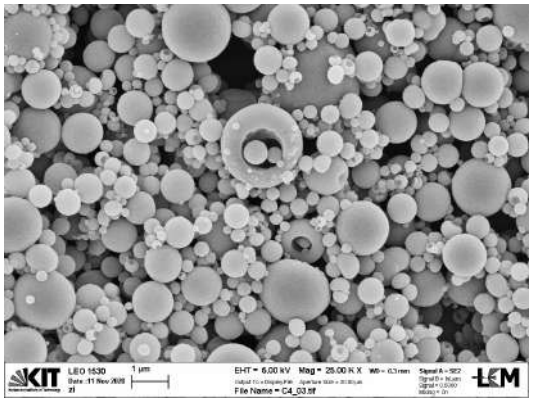

(g) SEM image of experiment C04 (1:4).

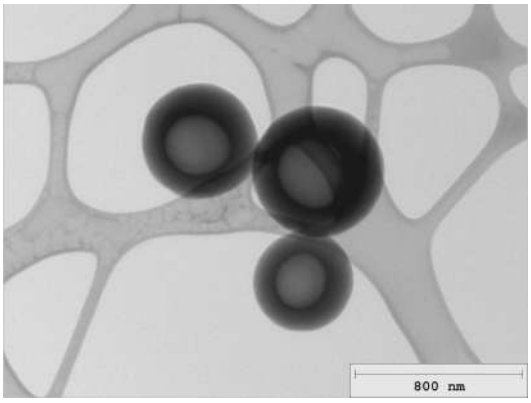

(h) TEM image of experiment C04 (1:4).

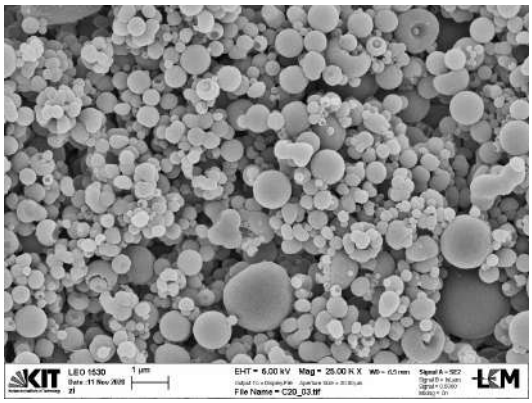

(i) SEM image of experiment C20 (1:5).

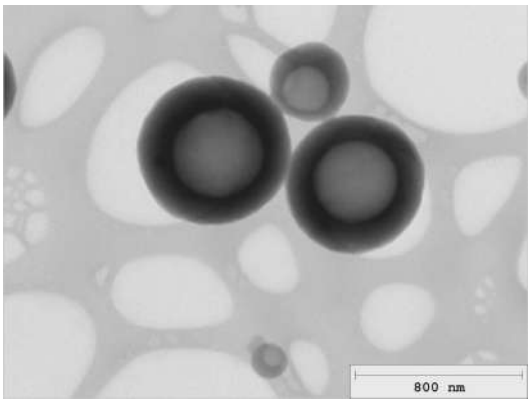

(j) TEM image of experiment C20 (1:5).

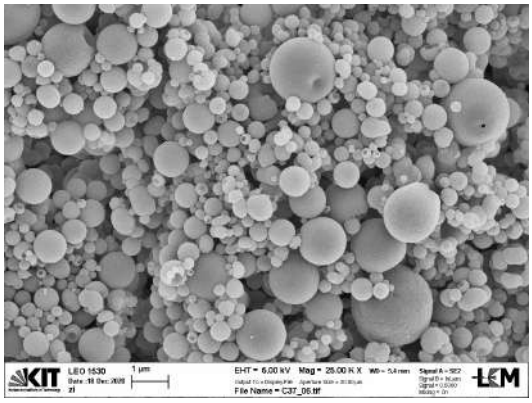

(k) SEM image of experiment C37 (1:6).

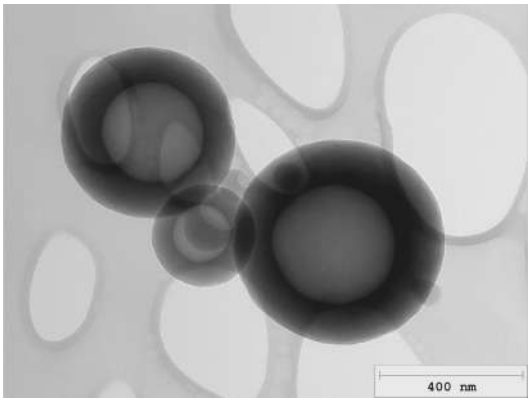

(l) TEM image of experiment C37 (1:6).

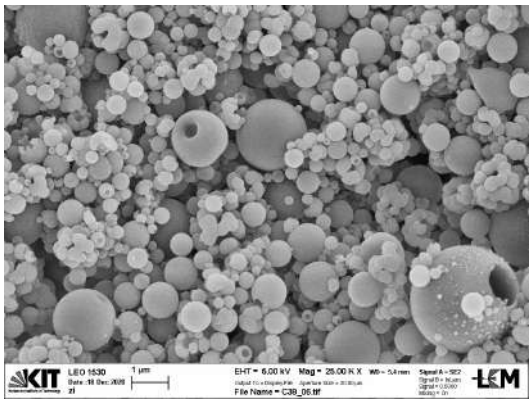

(m) SEM image of experiment C38 (1:8).

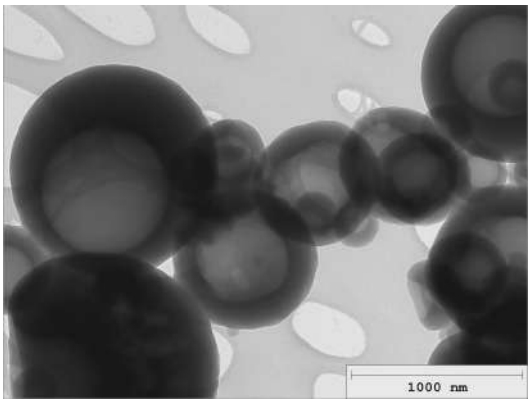

(n) TEM image of experiment C38 (1:8).

Figure 3.1: SEM and TEM images of experiments with different Thiol-ene monomer ratios.

Considering the large amount of nanometric particles present in each sample, all SEM and TEM pictures are selected to represent the most likely structure outcome of the studied formulation. Images showing shapes and structures which are not repeated frequently enough or that are the possible outcome of outside not controlled effects are not considered.

In almost every experiment of the series, SEM images show the presence of capsule-like particles. In samples with higher TRIS content (C01, C22, C21) the number of collapsed capsules is higher. Where present, capsules seem to be size-dependent with smaller than 2 μm particles being more likely to show the collapsed structure. In some cases, more cavities with different sizes are present in one single particle creating a sponge-like morphology as it can be seen in SEM Figure 3.1e. This occurs because the evaporation rate for bigger droplets is smaller and the driving force for oligomers/polymers accumulation in the outer shell is

decreased. Size distribution is generally broad, varying from 200 nm to few micrometres, with a slight increase in the average diameter in the experiment with a bigger amount of TMPTA. In SEM images of experiment 3.1k and 3.1m particles can be found in agglomerates with bigger ones surrounded by smaller ones. Apart from the sample of experiment C01, all SEM images show particles that are generally isolated and without excessive stickiness. By only analysing SEM images it is impossible to draw conclusions about the particle internal structure, indeed a lot of particles are capsules in which the outer shell is rigid enough to prevent collapse and thus cannot be recognized with scanning microscopy. TEM images are particularly required in order to understand the actual percentage of particles in which a liquid core is present.

When looking at TEM Figure 3.1b, it is easy to observe that not all particles have a liquid core or cavities and most of them are fused together forming small sticky agglomerates. The reason for the sample stickiness is supposedly the low conversion of thiol monomers in the pure Thiol-ene chemistry. For the 1:1 ratio, step-growth reaction rate is smaller than chain-growth rate and TRIS is consumed at a slower rate. Residual unreacted thiols act as a plasticizer by further polymerizing after the collection. The late polymerization can be triggered by the high energy TEM electron beam. SEM analysis can also trigger necking in some samples, but given that the energy employed is far less compared to TEM's one necking phenomena are more difficult to observe.

Increasing the amount of TMPTA in the monomers relative ratio results in a decrease of observed necking phenomena and stickiness. In Figure 3.1d a transition from a stickier sample as C01 to a less sticky one (C22) is explicit. Some necking is still visible and particles stuck together can be observed, but most of them still show cavities and consist of well-formed capsules. Increasing even more the TMPTA amount a clear trend in necking reduction is observed, particles are isolated and do not show bonding behaviour even when they are particularly close together. TRIS is thus responsible for the increase of the necking phenomena and ratios of TRIS/TMPTA smaller than 1:3 are not suitable to produce isolated capsule-like nanoparticles. Furthermore, Figures 3.1f, 3.1h, 3.1j, 3.1l and 3.1n show that almost all particles have cavities independently of the size, thus phase separation always occurs before gelation and the particles all show the same morphology.
In conclusion, formulations with a greater amount of TMPTA result in giving better quality capsules. The main reason being the predominant effect of the chain-growth step in the polymerization mechanism, causing the average molecular weight to increase faster and consequently the gelation to occur earlier. Nevertheless, gelation is not happening earlier than phase separation and the structuring process is not hindered. Samples with a too high amount of TMPTA (1:6 and 1:8) were not considered for further experiments as too few sulfhydryl groups are expected to be present for a possible future bioconjugation.

3.1.2 Using different monomer combinations

To confirm TRIS/TMPTA to be the best monomer combination for the formation of capsule-like particles different ENE monomers were employed in combination with TRIS. Such formulations were obtained by keeping constant and equal to 10 g the total amount of monomers. The amount of porogens, solvent and their relative ratio was kept constant as well as the monomer to solvent ratio in order to better confront the results. Molar ratio or Thiol-ene monomer combinations are varied (see Table 3.2). The given monomer ratios take into considerations the number of functional ene and thiol groups in the molecules. An experiment with only TMPTA as the monomer was also performed to compare the morphology of the particles formed in absence of the thiol specie. 1,3,5-Triallyl-1,3,5-triazine-2,4,6(1H,3H,5H)-trione (TTT), 2,4,6-triallyloxy-1,3,5-triazine (TAT) and diallyl adipate (DAA) were used instead of TMPTA.

Table 3.2: Experiments with different ENE monomer.

Exp.	Monomers		Ratio	HD/2Oct/IsoOct [g]	Gly [g]	Solvent [g]	M/S
C01	TRIS	TMPTA	1:1	3/3,5/3,5	3	12 EtOH	2/5
C06	/	TMPTA	0:1	3/3,5/3,5	3	12 EtOH	2/5
C45	TRIS	TTT	1:1	3/3,5/3,5	3	12 EtOH	2/5
C48	TRIS	DAA	1:1,5	3/3,5/3,5	3	12 EtOH	2/5
C43	TRIS	TAT	1:1	3/3,5/3,5	3	12 EtOH	2/5
C46	TRIS	TAT	1:2	3/3,5/3,5	3	12 EtOH	2/5
C44	TRIS	TAT	1:4	3/3,5/3,5	3	12 EtOH	2/5

When using different monomers combinations besides TRIS/TMPTA couple, the overall collection rate diminished at a point that in some cases was impossible to collect material from the filters as NPs were stuck to them (e.g. C44). The yield of experiment C48, performed using DAA was the lower of the series. The reason for that resides in the different structure of the monomer and the lower number of functional groups that highly affect the polymerization rate. On the other hand, experiments with TTT and TAT, which share the same amount of functional acrylic groups with the TMPTA molecule, both showed a higher reactivity.

Figure 3.2b representing experiment C06 shows a mosaic-like structure. Particles are not capsules or defined spheres but are observed in agglomerates of smaller entities, most likely generated in a single droplet during the polymerization process.

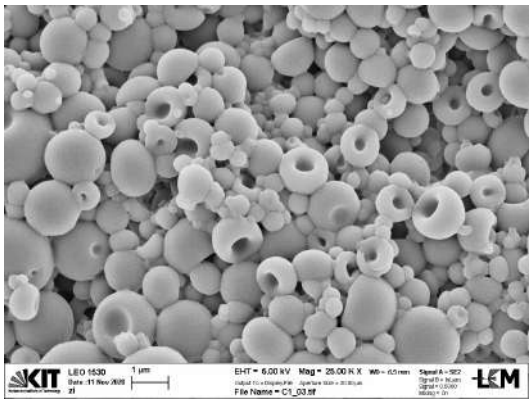

(a) SEM image of experiment C01.

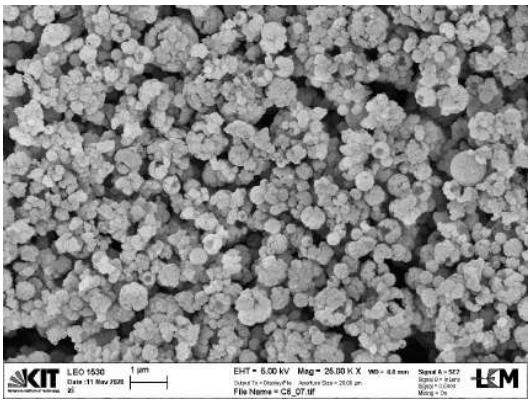

(b) SEM image of experiment C06 (TMPTA).

Figure 3.2: Experiments with TRIS/TMPTA (1:1) and only TMPTA.

TMPTA homopolymerization causes gelation to happen faster compared to polymerization with the TRIS/TMPTA Thiol-ene mechanism, because the absence of the step-growth reaction slows the molecular weight evolution. This trend is also confirmed by the higher collection rate of the sample compared to experiments employing both monomers. Mosaic-like structures are also most likely caused by early phase separation. When this happens, polymers phase-separate in multiple microgel superordinate structures giving no time to the polymers to migrate towards the outer droplet layer. Each microgel bead will go through gelation leaving the liquid phase all around as a template for the final solid structure formation. The liquid porogen phase will be highly concentrated in monomers and further polymerization will occur and fuse the microgel beads together forming the typical mosaic

morphology. In conclusion, when TMPTA is employed as the only monomer in the spray formulation nanoparticles morphology is highly affected. The presence of a chain trasfer mechanism is needed to slow down the ene polymerization process and hence the presence of a thiol to perform this task is required.

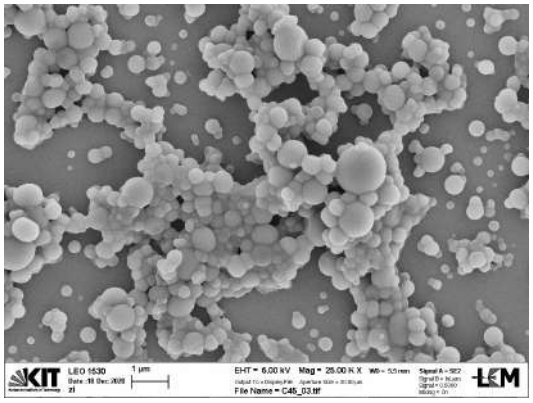

(a) SEM image of experiment C45.

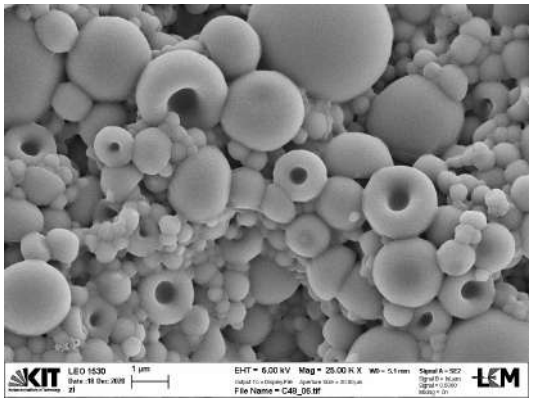

(b) SEM image of experiment C48.

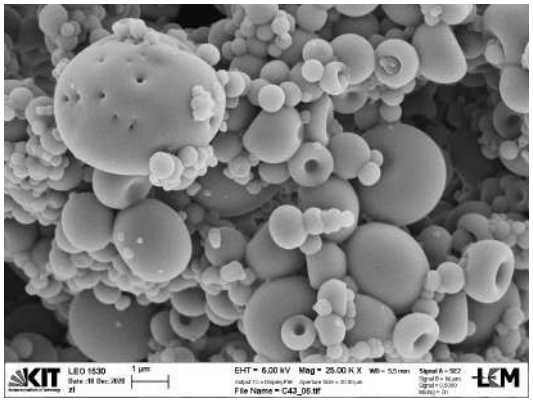

(c) SEM image of experiment C43.

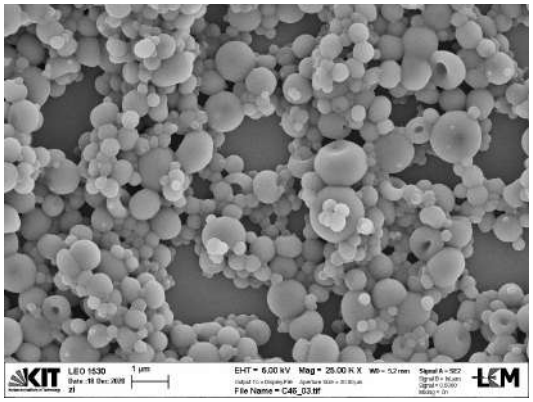

(d) SEM image of experiment C46.

Figure 3.3: SEM pictures of experiments using different monomer combinations.

SEM Figure 3.3a of experiment C45 using TTT as ene monomer shows agglomerated nanoparticles stuck together, almost no isolated particles can be spotted as the whole sample consist of a big cluster of polymeric material. Compared with C01, C48 and C43, where stoichiometric combinations of ene and thiol functional groups were used, there is no presence of "caps" (collapsed capsules). Experiment with DAA (Figure 3.3b) and TAT (Figure 3.3c) show a wider size distribution and a higher number of big sponge-like particles with surface defects compared to TRIS/TMPTA. Agglomeration is also an issue while using these reagents, sample 3.3b and 3.3c both have less isolated particles compared to 3.2a. Different TRIS/TAT molar combinations have been tried, increasing TAT concentration. For a 1:2 TRIS/TAT ratio, the sample shows a narrower size distribution and a smaller number of capsule-like particles (Figure 3.3d) while the stickiness is comparable to the experiment with a 1:1 ratio. The collection rate is reduced as TAT reactivity differs from TMPTA one. Increasing to 1:4 the monomer relative ratio resulted in no collection as the rate of production was not high enough and the material was too sticky to be scraped from the filter.

3.1.3 Effect of glycerol

Glycerol is a softmaker or plasticizer, its main effect when added to a polymeric matrix is that of decreasing intermolecular forces and consequently give more flexibility to the structure. Plasticizers also decrease polymer glass transition temperature leading to an increase in gelation time and polymeric chains mobility. Glycerol is also partially responsible for sample stickiness and agglomeration, but it generally helps particles to controllably collapse and consequently form caps. The starting formulation contains 3 g of glycerol in addition to the monomers and solvent/porogens mixture. In this series of experiments, in some cases the glycerol was replaced by a solvent or a porogen while the monomer to solvent ratio was kept constant. In other experiments, glycerol concentration was increased varying monomer to solvent ratio while keeping when possible the relative ratio of porogens constant.

Table 3.3: Experiments with different glycerol concentration.

Exp.	Monomers		Ratio	HD/2Oct/IsoOct [g]	Gly [g]	Solvent [g]	M/S
C02	TRIS	TMPTA	1:1	3/3,5/3,5	0	15 EtOH	2/5
C03	TRIS	TMPTA	1:1	3/6,5/3,5	0	12 EtOH	2/5
C40	TRIS	TMPTA	1:1	3/3,5/3,5	6	12 EtOH	5/14
C39	TRIS	TMPTA	1:4	3/3,5/3,5	6	12 EtOH	5/14
C41	TRIS	TMPTA	1:5	3/3,5/3,5	6	12 EtOH	1/3
C42	TRIS	TMPTA	1:4	3/0/3,5	6,5	12 EtOH	2/5

By replacing glycerol with EtOH in experiment C02 (Figure 3.4a) gel-type spheres were obtained and particles resulted in having no cavities. Porogens alone are not able to delay gelation long enough to allow capsule formation and EtOH addition cannot replace the glycerol effect in the structuring process. No liquid core is present (Figure 3.4b) suggesting that gelation occurs before phase separation and droplets polymerize in a solid sphere. Compared to experiment C01 with the same TRIS/TMPTA ratio, particles in sample C02 are more isolated and no necking is observed. Stickiness is likely to be influenced by glycerol presence besides thiol monomer conversion.

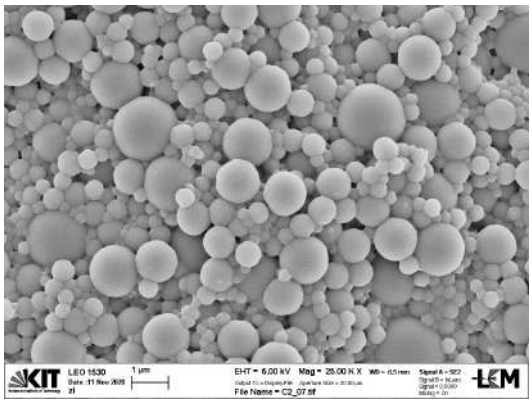

(a) SEM image of experiment C02.

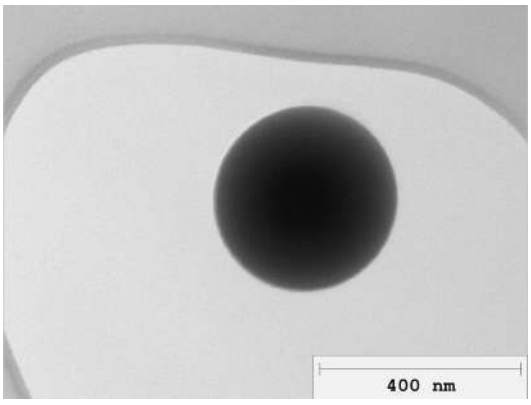

(b) TEM image of experiment C02.

Figure 3.4: SEM and TEM images of gel-type spheres obtained without glycerol.

In experiment C03, glycerol was replaced with the same amount of 2-octanone. As it can be observed from Figure 3.5a some cavities are present, but are far less compared to the formulation C01 with 3 g of glycerol. 2-Octanone has a similar softmaker effect, but

less effective compared to that of glycerol. Some caps are present and particles are generally isolated.

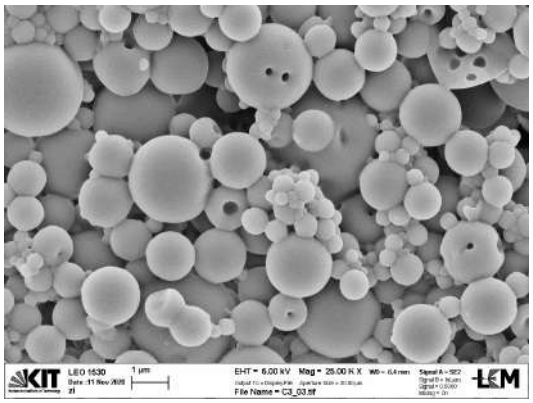

(a) SEM image of experiment C03.

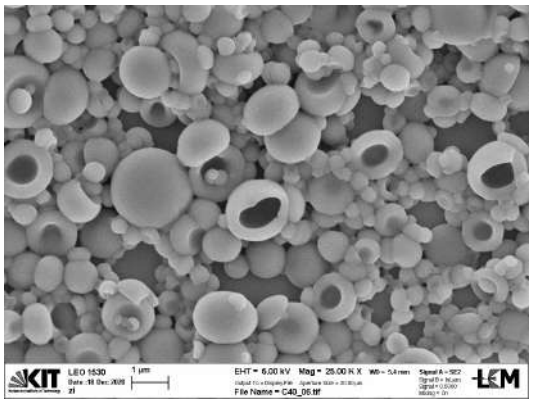

(b) SEM image of experiment C40.

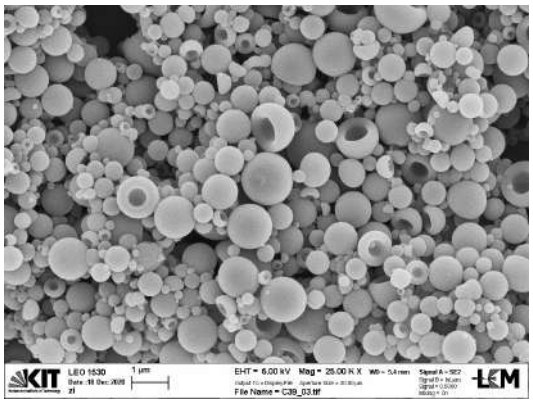

(c) SEM image of experiment C39.

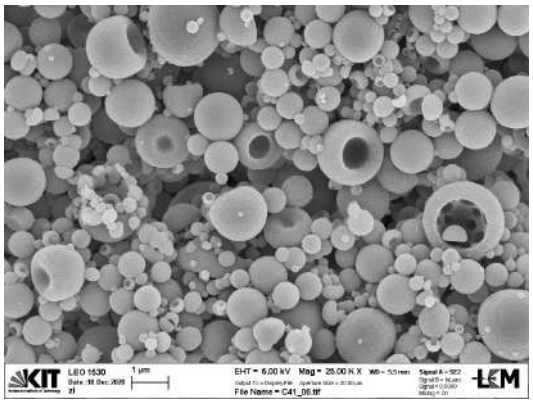

(d) SEM image of experiment C41.

Figure 3.5: SEM pictures of experiments with different glycerol concentration.

Increasing the amount of glycerol also led to worse results, in Figure 3.5b relative to experiment C40 glycerol amount was increased from 3 g to 6 g resulting in soft and sticky particles with a good number of caps. The polymeric matrix in this case results too flexible to generate durable structures and some of the caps appear compressed and stuck together. Given the results explained in subsection 3.1.1, the same increase in the amount of glycerol is performed with different TRIS/TMPTA molar combinations. When using 6 g of glycerol in a formulation with more TMPTA than TRIS the morphology modifications are less evident. Increasing the amount of glycerol and increasing the amount of TRIS have a similar effect on the particles stickiness. On the other hand, increasing the amount of TMPTA will counterbalance the effect of the increment of glycerol. In fact, with a 1:4 TRIS/TMPTA ratio (Figure 3.5c) and 6 g of glycerol particles are isolated and some caps are present, similarly to former experiments without an increased amount of glycerol and 1:1 monomer ratio. By decreasing even more TRIS concentration (experiment C41) particles remain isolated, but the structure is somehow less homogeneous as can be seen in Figure3.5d. Fewer caps and more spheres and broken particles are present, comparably to experiment C04 and C20 more TMPTA counteract the effect of glycerol.

It is plausible that as it happened for samples showed in TEM pictures in subsection 3.1.1 all the particles from experiment C39 and C41 have a liquid core and only some of them collapse, thus allowing us to see them in SEM.

3.2 Production of Hybrids

The term hybrids is used to describe all polymeric nanoparticles formed with metals as part of their internal structure. In this work, silver nanoparticles were used as the metal of choice and various mixing methods and formulations were tried in order to produce functional hybrid particles. As far as morphology is concerned, it is important for the hybrid to have all the silver nanoparticles inside their domain and not outside, so as not to give rise to possible health hazard aiming at a bio-application in the future. To achieve this result, it is fundamental to produce a stable silver NP dispersion in the spray solution, in fact, solution stability is a good indicator of silver presence in the produced particles. Silver dispersion and monomer solution were generally prepared separately and mixed together under vigorous stirring, the solution obtained was atomized under continuous stirring to avoid silver deposition. Spray solutions that were not stable for the whole duration of the experiment or in which phase separation occurred were discarded and not analysed. Spray solutions containing silver dispersion were collected after the end of each successful experiment and their stability checked over time.

3.2.1 Ag-PVP with ALA and MUL

In this series, silver nanoparticles coated with Polyvinylpyrrollidone (PVP) with an average size of 50 nm were used. The weight of silver indicated in Table 3.4 refers to the total amount of Ag-PVP material used, of which only 1/3 is actual silver and the rest consists of the coating. Along with silver nanoparticles, two different stabilizers were used: α-Lipoic acid (ALA) and 11-Mercapto-1-undecanol (MUL) to try to stabilize the silver dispersion and to avoid aggregation and deposition within the spray solution. All experiments have the same content of porogens, solvents and the same monomer to solvent ratio. The ratio between monomers has been changed from 1:1 to 1:4 as the latter resulted in better-formed capsules. ALA and MUL concentrations were increased starting from 6 mg.
Silver nanoparticles are difficult to spot using SEM analysis, for this reason, TEM characterization was used for each performed experiment.

Table 3.4: Experiments with Ag-PVP and different stabilizers.

Exp.	Monomers		Ratio	Solvent [g]	Silver NPs	Stabilizer	M/S
C07	TRIS	TMPTA	1:1	12 EtOH	0,05 g Ag-PVP	0	2/5
C08	TRIS	TMPTA	1:4	12 EtOH	0,05 g Ag-PVP	0	2/5
C14	TRIS	TMPTA	1:1	12 EtOH	0,05 g Ag-PVP	6 mg MUL	2/5
C13	TRIS	TMPTA	1:1	12 EtOH	0,05 g Ag-PVP	6 mg ALA	2/5
C23	TRIS	TMPTA	1:4	12 EtOH	0,05 g Ag-PVP	10 mg ALA	2/5
C31	TRIS	TMPTA	1:4	12 EtOH	0,05 g Ag-PVP	80 mg ALA	2/5

(1) All experiments in this table share the same amount of porogens and glycerol: 3,5 g 2Oct, 3,5 g of IsoOct, 3 g of HD and 3 g of Gly respectively.

In experiment C07 and C08 no stabilizer was added and TEM results show no particular difference in morphology compared to their analogous formulations without silver NP addition. A preliminary analysis outlines that PVP coated silver does not significantly affect nanoparticles morphology. As expected, particles from C08 have a more defined capsule shape while in C07 the increased stickiness given by a larger concentration of TRIS badly affects the morphology and the individuality of the particles.

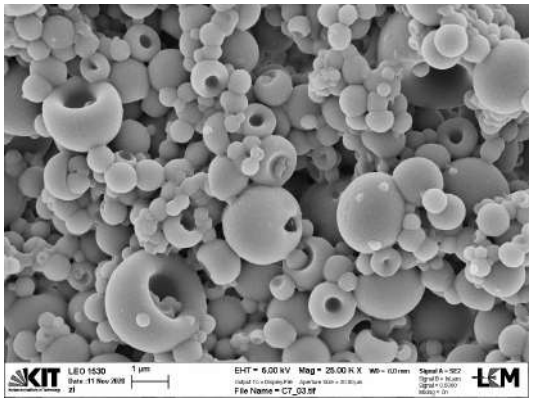

(a) SEM image of experiment C07.

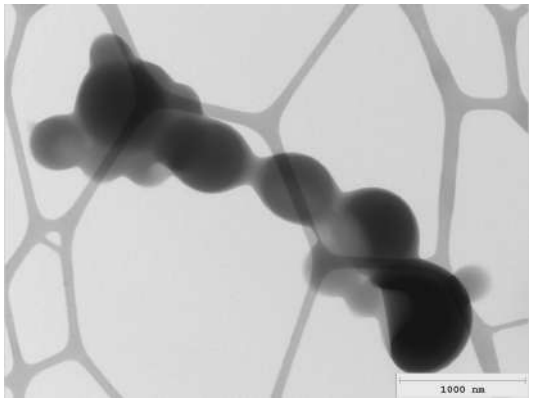

(b) TEM image of experiment C07.

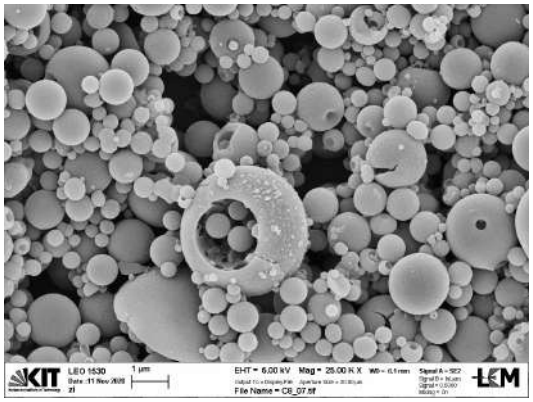

(c) SEM image of experiment C08.

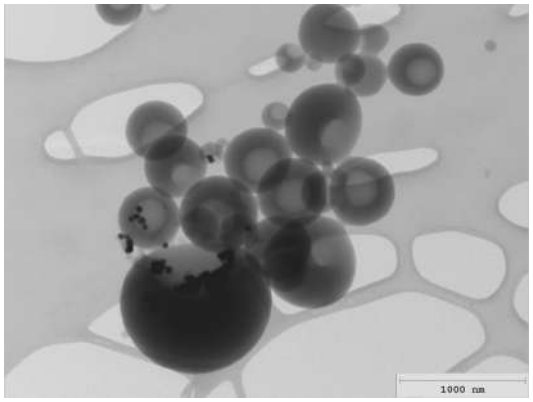

(d) TEM image of experiment C08.

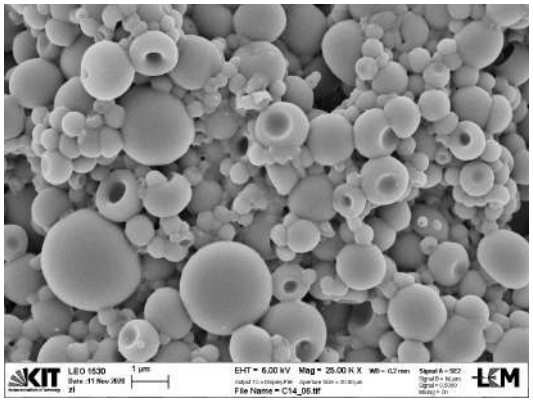

(e) SEM image of experiment C14.

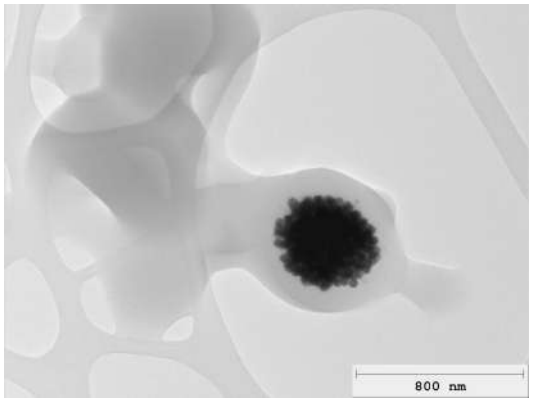

(f) TEM image of experiment C14.

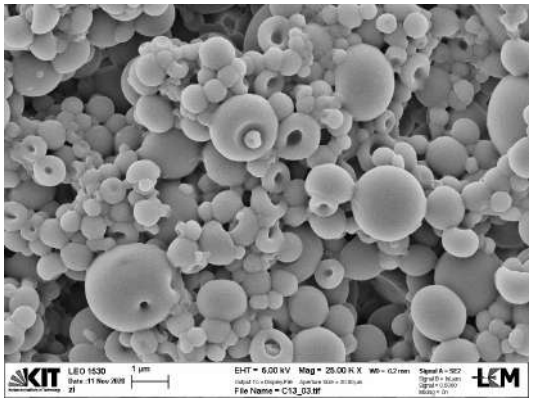

(g) SEM image of experiment C13.

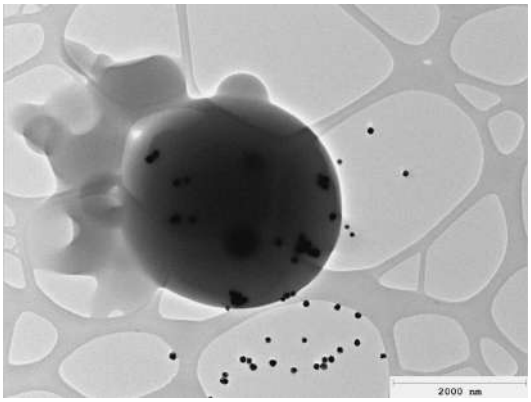

(h) TEM image of experiment C13.

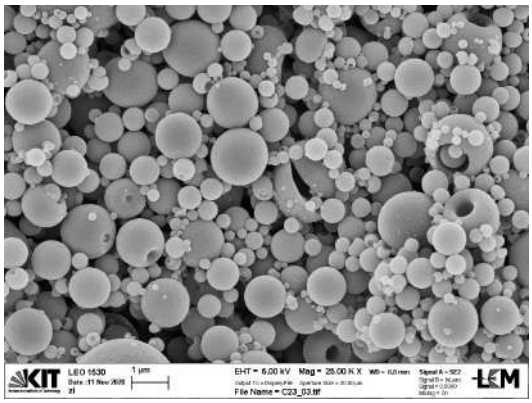

(i) SEM image of experiment C23.

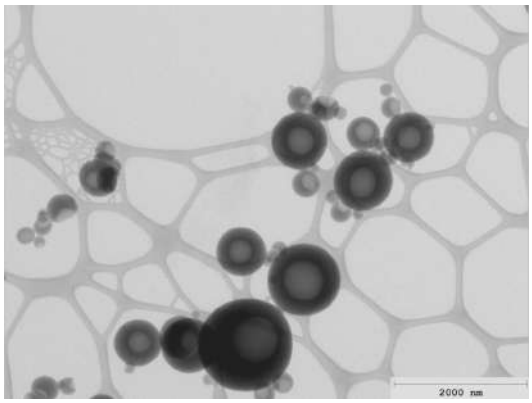

(j) TEM image of experiment C23.

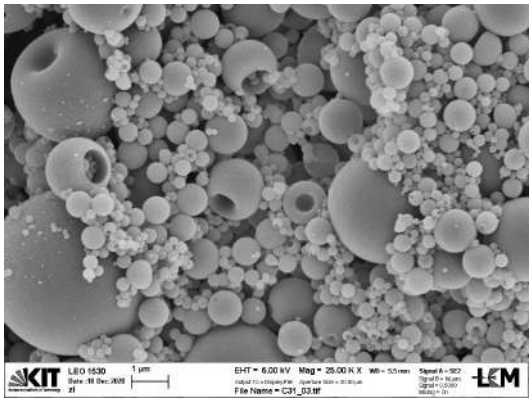

(k) SEM image of experiment C31.

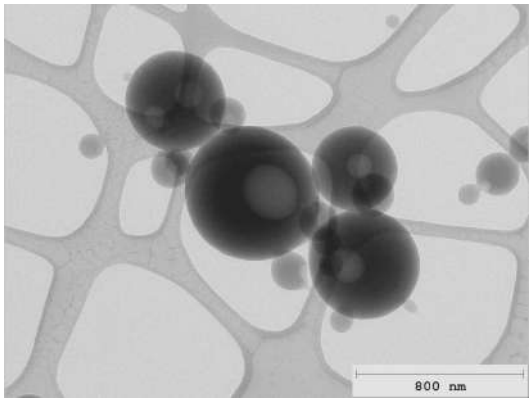

(l) TEM image of experiment C31.

Figure 3.6: SEM and TEM images of experiments with Ag-PVP and different stabilizers.

Experiment using TRIS/TMPTA ratio of 1:1 shows no silver neither inside nor outside the polymeric matrix (Figure 3.6b), while in experiment C08 using 1:4 ratio some silver particles can be observed, but mostly outside of polymeric NPs. The addition of a stabilizer was tested to try to keep the silver nanoparticles inside the polymeric matrix. In experiment C14, MUL was added to a 1:1 TRIS/TMPTA formulation, the difference with the previous experiment is easy to observe in Figure 3.6f. Here, all the silver is agglomerated in a few clusters, no silver is found outside, but almost all nanoparticles have no Ag-PVP loading. The same amount of a different stabilizer (ALA) was added to the same formulation in C13 and in this case almost all the Ag-PVP was found outside the matrix and very little inside (see Figure 3.6h). This may be caused by disruption of already formed big hybrid particles with consequent release of silver or by the simple presence of silver not yet incorporated in any polymeric structure. No silver agglomerates were found in this case, suggesting that ALA was more effective in keeping the silver NPs from sticking together in the spray solution. In both cases, the structure of the polymeric particles with the 1:1 formulation was confirmed to be too sticky and thus following experiments were performed with the 1:4 ratio. In C23 and C31 (Figures 3.6i and 3.6k) the difference in the polymer NPs structure conferred by the increased amount of TMPTA is clear. A higher concentration of ALA was used (10 mg and 80 mg respectively) as it was expected to have a better stabilizing effect. In both experiments, the samples show the presence of capsules, while no silver NPs could be seen in TEM images either in clusters or dispersed outside the matrix. Spray solution in experiment C23 was not stable for the entire duration of spraying, C31 had stability problems too and small silver deposits were found in the spray flask. While this may suggest that the concentration of the stabilizer was too high for the solution to be kept stable, it

is more likely that incorrect stirring may have caused the solution phase-separate. Indeed, vigorous and constant stirring during spraying was revealed to be fundamental to avoid phase separation within the spray solution. Comparing more closely C31 and C23 (Figures 3.6l and 3.6j), a difference in the shape of the NPs can be found suggesting that too much ALA influences the particle morphology. In C31 where 80 mg of ALA were employed, capsules with less liquid core and a thicker polymer shell are produced (Figure 3.6l). This effect can be hardly observed in experiments with a 1:1 monomers ratio as the core-shell structure is not well-distinguished. In all experiments, silver NPs were difficult to find and when spotted were either clustered in agglomerates or concentrated in few particles or locations. A bigger number of Ag-NPs is required to better recognize the effect of stabilizers and to increase the probability of spotting it on the TEM grids.

3.2.2 Ag-Ink with ALA and MUL

Silver Ink nanoparticles in a solution of tripropylene glycol monomethyl ether have been used instead of the PVP coated particles in this series of experiments. Silver concentration in the ink is 30-35wt% and the average particle size is 50nm. As for subsection 3.2.1, all the experiments share the same amount of porogens, solvents and monomer to solvent ratio. The ratio between monomers has been changed to investigate the effect of silver and stabilizers on morphology. MUL and ALA have been used as stabilizers. Details of the formulations can be seen in Table 3.5.

Table 3.5: Experiments with Ag-Ink 30-35wt% and different stabilizers.

Exp.	Monomers		Ratio	Solvent [g]	Silver NPs	Stabilizer	M/S
C11	TRIS	TMPTA	1:1	12 EtOH	200 μL Ag-Ink [(2)]	6 mg ALA	2/5
C10	TRIS	TMPTA	1:1	12 EtOH	200 μL Ag-Ink [(2)]	6 mg MUL	2/5
C34	TRIS	TMPTA	1:2	12 EtOH	200 μL Ag-Ink [(2)]	30 mg MUL	2/5
C35	TRIS	TMPTA	1:3	12 EtOH	200 μL Ag-Ink [(2)]	30 mg MUL	2/5
C33	TRIS	TMPTA	1:4	12 EtOH	200 μL Ag-Ink [(2)]	30 mg MUL	2/5

[(1)] All experiments in this table share the same amount of porogens and glycerol: 3,5 gof 2Oct, 3,5 g of IsoOct, 3 g of HD and 3 g of Gly respectively.

[(2)] Ag-Ink NPs used in this series is 30-35wt%.

Both experiment C10 and C11 performed with a 1:1 monomers ratio and a small content of stabilizers (respectively 6 mg of MUL and 6 mg of ALA) revealed silver aggregation and weak structuring of nanoparticles as expected for this type of monomers combination. To outline the stabilizer effect with various monomers ratios experiment C34, C35 and C33 were performed increasing TMPTA content in the monomers mixture and using a bigger amount of one of the stabilizers. For this series, MUL was chosen as the stabilizer in an arbitrary way as, differently from Ag-PVP, no particular major advantage has been observed in the use of MUL and ALA with the 1:1 formulation and silver ink.

In experiment C34 (Figure 3.7f) increased amount of MUL gives better isolated silver particles, even if they still tend to form agglomerates in few particles and not all the capsules have silver inside. Fewer capsules are present compared to previous experiments with 1:2 monomer ratio, meaning that at this concentration MUL seems to affect nanoparticle morphology. In experiments C35 and C33 where a greater amount of TMPTA was employed no silver was present in the sample, neither inside nor outside the polymeric nanoparticles.

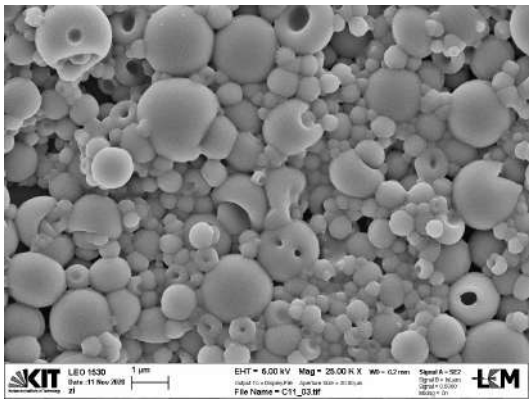

(a) SEM image of experiment C11.

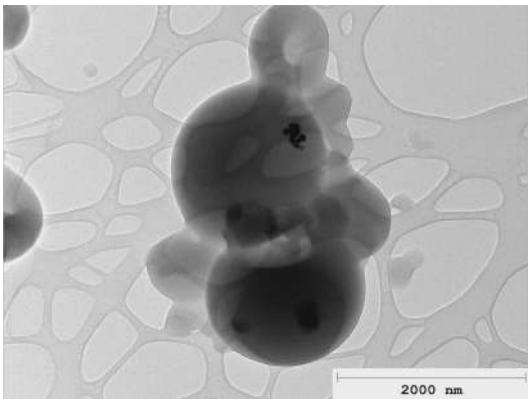

(b) TEM image of experiment C11.

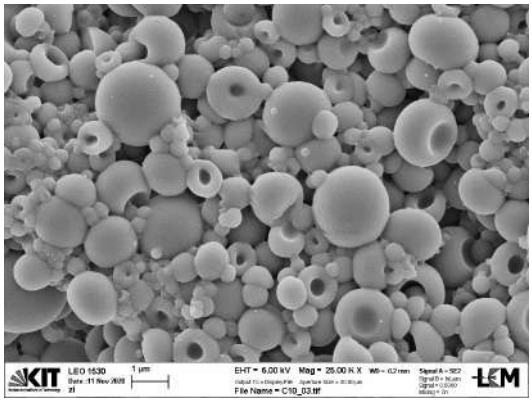

(c) SEM image of experiment C10.

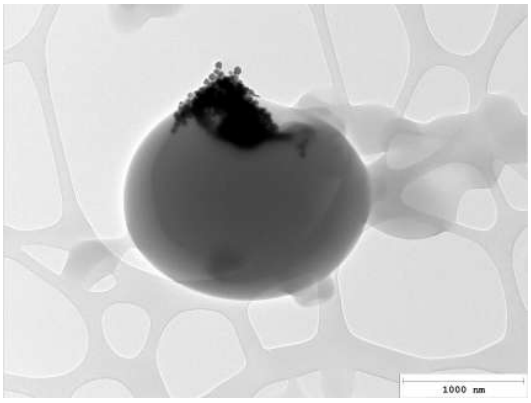

(d) TEM image of experiment C10.

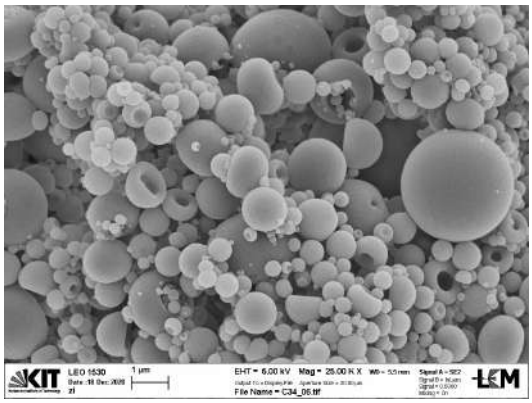

(e) SEM image of experiment C34.

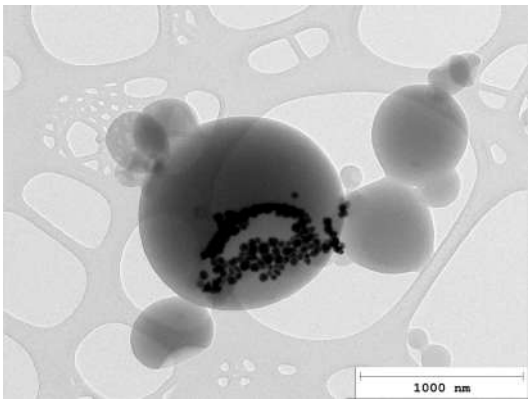

(f) TEM image of experiment C34.

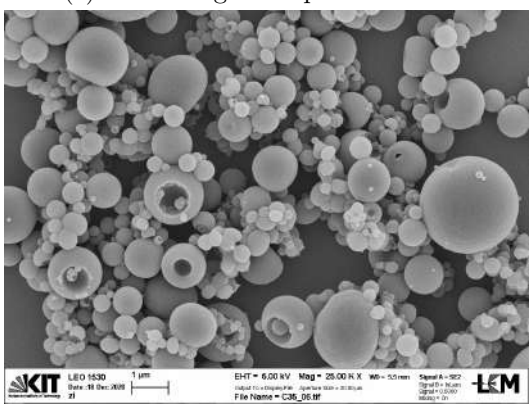

(g) SEM image of experiment C35.

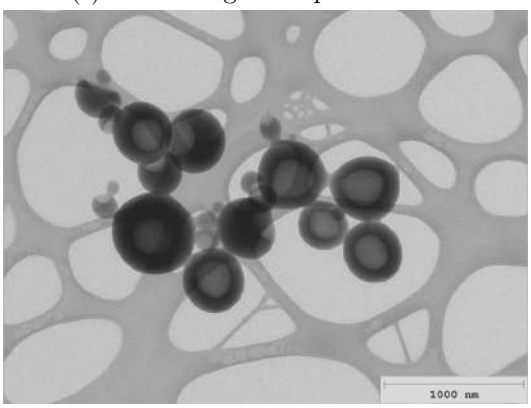

(h) TEM image of experiment C35.

Figure 3.7: SEM and TEM images of experiments with Ag-Ink 30-35wt% and different stabilizers.

Morphology was more similar to the formulations without stabilizer of subsection 3.2.1 even if more necking can be observed as in Figure 3.7h. This may be caused by the increased amount of MUL conferring the sample a stickier surface. This trend is more accentuated for a lower concentration of TMPTA.

3.2.3 Effect of 1-propanol on increasing loads of silver

1-Propanol has been added to the formulations as a stabilizer to increase silver dispersion stability. The silver type used was Ag-PVP in various concentrations and Ag-Ink 50wt% that, compared to the 30-35wt%, showed better behaviour against aggregation. Stability of spray formulations was inspected after each experiment. PrOH proved to be a good silver stabilizer when added to spray solution as they remained dispersed for a longer period compared to formulations where no PrOH was added. in this series experiment with and without PrOH have been performed and compared, spray formulations details are summarized in Table 3.6.

Table 3.6: Experiments with 0,05 g of silver NPs and PrOH.

Exp.	Monomers		Ratio	Solvent [g]	PrOH [g]	Silver NPs	M/S
C50	TRIS	TMPTA	1:3	12 EtOH	0	0,15 g Ag-PVP	2/5
C54	TRIS	TMPTA	1:3	12 EtOH	5	0,15 g Ag-PVP	1/3
C55	TRIS	TMPTA	1:3	12 EtOH	0	0,100 g Ag-Ink 50wt%	2/5
C56	TRIS	TMPTA	1:3	12 EtOH	5	0,100 g Ag-Ink 50wt%	1/3

(1) All experiments in this table share the same amount of porogens and glycerol: 3,5 g 2Oct, 3,5 g of IsoOct, 3 g of HD and 3 g of Gly respectively.

In all experiments, the 1:3 TRIS/TMPTA combination was used as it revealed to be the best compromise between the ability to form capsules and the expected minimum amount of TRIS for the resulting nanoparticles to have a good concentration of SH surface groups. Experiments using 1:1 monomers relative ratio show no difference compared to the other experiments performed with the same ratio and different load of silver, for that reason they were discarded and no longer analysed. The concentration of silver was increased by three times with no stability problems, but with the main effect of having a larger number of hybrids compared to experiments with reduced silver loads presented in Tables 3.4 and 3.5. All SEM pictures show defined and individual polymeric nanoparticles confirming that the 1:3 monomers ratio is a good formulation to achieve a low stickiness sample. In addition, almost all particles are capsules. Experiment C50 and C54 with Ag-PVP show a bigger amount of broken particles, more silver dots can be observed on the surface of nanoparticles compared to the samples containing Ag-Ink (see Figures 3.8a and 3.8c). In experiment C50 almost all silver is contained within the polymeric structure and little could be found outside the nanoparticles, not all the particles contained silver and not all the particles are capsules. No major aggregations were found and silver nanoparticles are overall well distributed within the samples (Figure 3.8b). By adding PrOH to the same formulation no major morphology change occurs, on the other hand, a greater amount of silver could be found outside the nanoparticles, especially in the vicinity of bigger ones. Particles bigger than 2 μm have a higher probability of containing a greater amount of silver and thus, they are more likely to go towards stability problems. Bigger particles also contain more solvent that may cause instability and rupture. No silver agglomerates were found, all Ag particles were separated even when found outside. A different trend can be observed when using Ag-Ink as a silver source. In experiment C55 all the silver is found in agglomerates inside few particles, leaving the majority of the other capsules without.

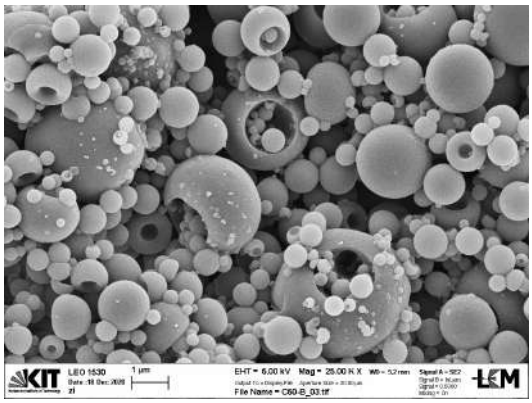

(a) SEM image of experiment C50.

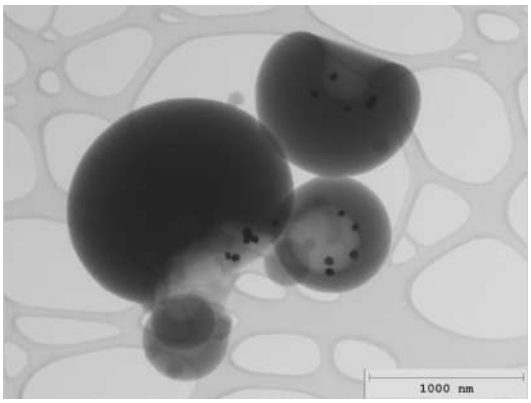

(b) TEM image of experiment C50.

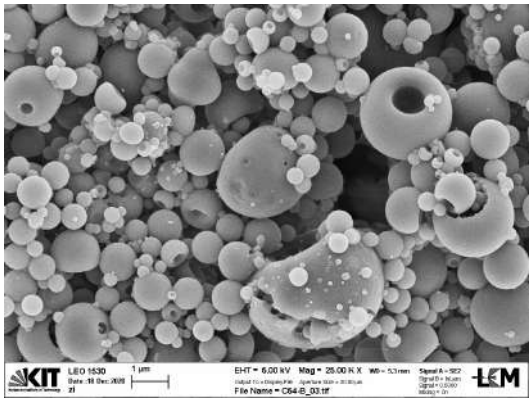

(c) SEM image of experiment C54.

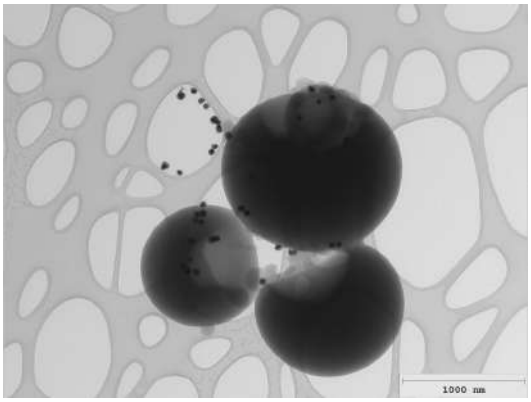

(d) TEM image of experiment C54.

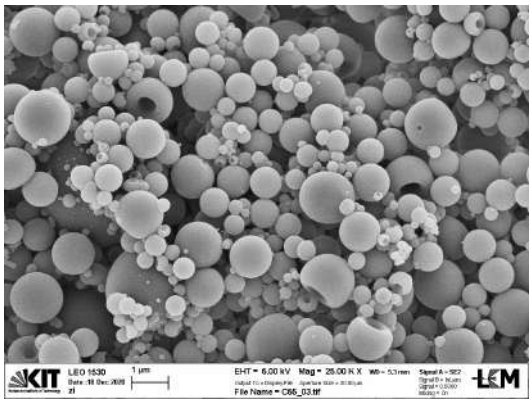

(e) SEM image of experiment C55.

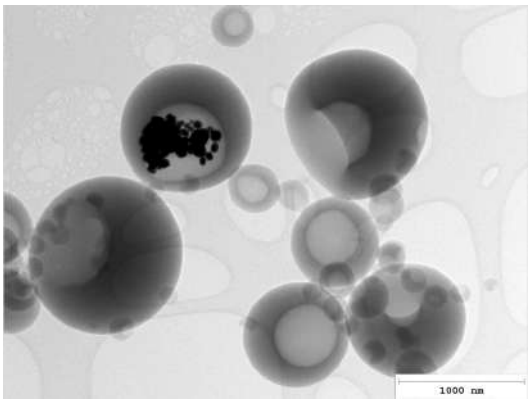

(f) TEM image of experiment C55.

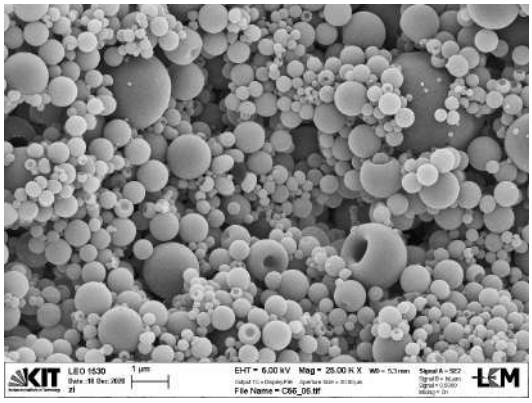

(g) SEM image of experiment C56.

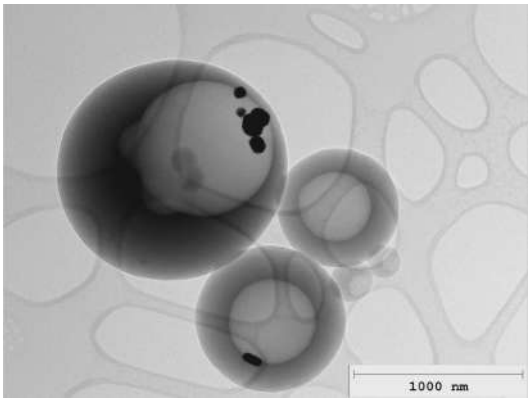

(h) TEM image of experiment C56.

Figure 3.8: SEM and TEM images of experiments with 0,05 g of silver with and without PrOH.

No silver was found outside and all the particles have a well-defined core and are capsule-like.

Adding 5 g of PrOH to the same formulation results in a clear stabilizing effect: no more agglomerates were found and more particles resulted in being hybrids, with silver better distributed within the matrix (see Figure 3.8h). No major morphology changes can be observed in this case as well. Experiments with samples using Ag-ink have particles generally less isolated compared to the ones with PVP coated silver. Besides, Ag-Ink particles have a broader size distribution compared to the Ag-PVP as shown in Figure 3.8h. This could be a drawback for bio-imaging applications for which different silver nanoparticles dimensions correspond to different light absorption characteristics.

A second series of experiments employing PrOH were performed using a higher amount of silver to increase the probability of having all polymeric nanoparticles with silver inside their structure. In order to achieve this, the amount of silver required to fill al capsules with at least one silver nanoparticle was calculated. The average silver particle size of 50 nm and average capsule size of 300 nm were used as starting parameters and a final load of 0.126 g of silver was obtained, corresponding to 0,415 g of Ag-PVP and 0,251 g of Ag-Ink 50wt%. A final load of 0,45 g of Ag-PVP and 0,3 g of Ag-Ink 50wt% was chosen as it corresponds to a three folds increase compared to previous experiments. Deviations from the calculated value of the silver load are likely because of the uncertainty on the exact average size of the polymeric nanoparticles. Experiments performed with such an increased amount of silver are listed in Table 3.7.

Table 3.7: Experiments with 0,15 g of silver NPs and PrOH.

Exp.	Monomers		Ratio	Solvent [g]	PrOH [g]	Silver NPs	M/S
C61	TRIS	TMPTA	1:3	12 EtOH	0	0,45 g Ag-PVP	2/5
C78	TRIS	TMPTA	1:3	12 EtOH	3	0,45 g Ag-PVP	4/14
C60	TRIS	TMPTA	1:3	12 EtOH	5	0,45 g Ag-PVP	1/3
C59	TRIS	TMPTA	1:3	12 EtOH	0	0,300 g Ag-Ink 50wt%	2/5
C63	TRIS	TMPTA	1:3	12 EtOH	3	0,300 g Ag-Ink 50wt%	5/14
C68	TRIS	TMPTA	1:3	12 EtOH	5	0,300 g Ag-Ink 50wt%	1/3

(1) All experiments in this table share the same amount of porogens and glycerol: 3,5 g 2Oct, 3,5 g of IsoOct, 3 g of HD and 3 g of Gly respectively.

All of the experiments show little or no modification of the shape of the particles, with the majority being capsules, meaning that neither the increment of silver loading nor the use of propanol has an important effect on the morphology of the hybrids. Experiments with PVP coated silver and the ones using silver ink show different results when PrOH is added, thus they are discussed separately.

SEM images from experiments with Ag-PVP and an increased amount of PrOH (C61, C78 and C60) all show isolated particles and no stickiness whatsoever. Silver dots can be spotted on the particles surface, in greater amount in Figure 3.9a and 3.9e, while in smaller percentage in Figure 3.9c where silver can be observed only in the vicinity of few big particles. The presence of Ag-NPs outside the polymeric particles can be caused by release from broken particles, occurring either because of instability or because of sample preparation. By looking at TEM images this trend is confirmed. In pictures from sample C61 where no propanol was used, all particles are capsules and the majority of silver is inside, with few exceptions where some Ag-NPs can be found on the surface of big particles.

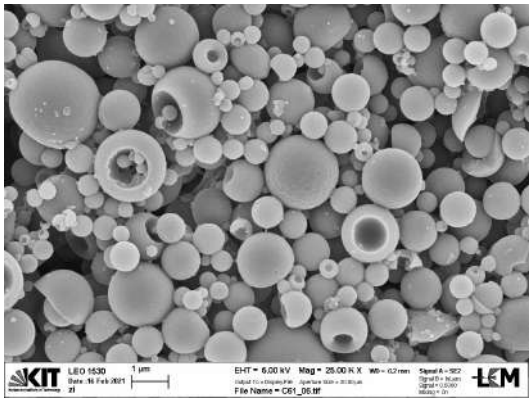

(a) SEM image of experiment C61.

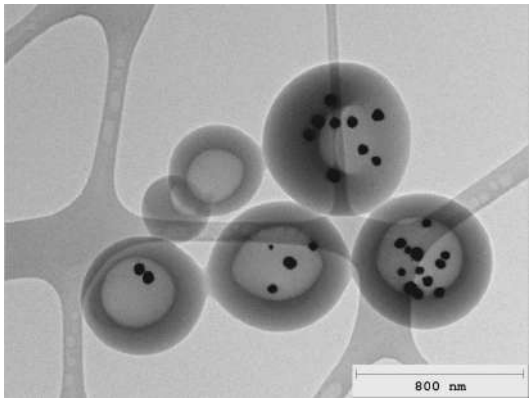

(b) TEM image of experiment C61.

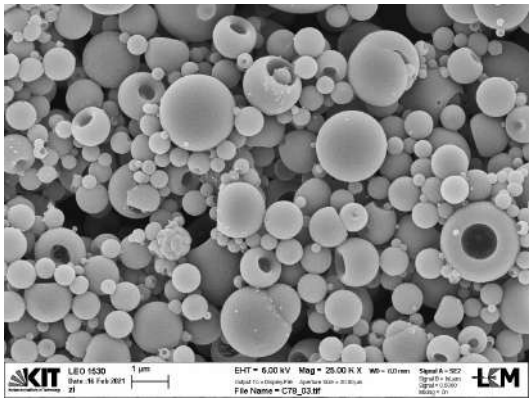

(c) SEM image of experiment C78.

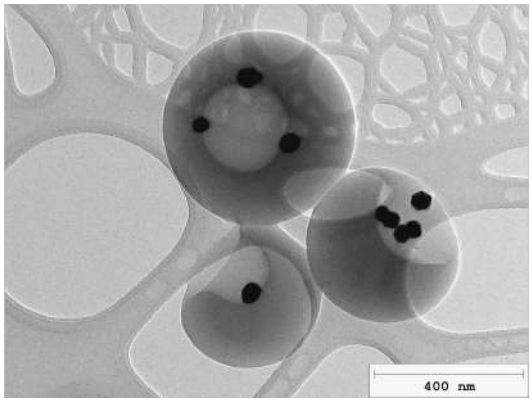

(d) TEM image of experiment C78.

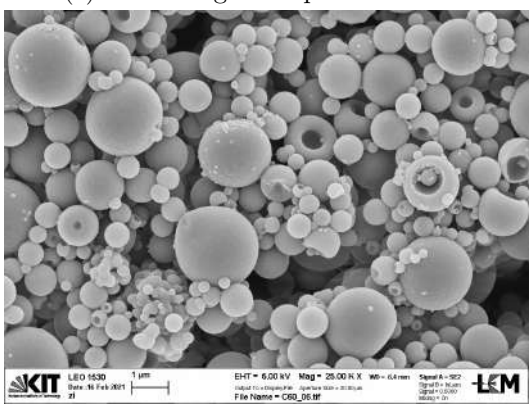

(e) SEM image of experiment C60.

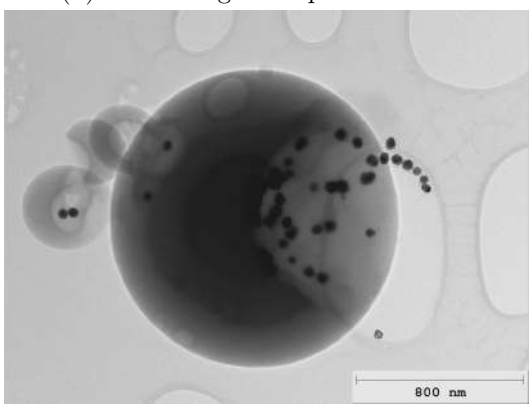

(f) TEM image of experiment C60.

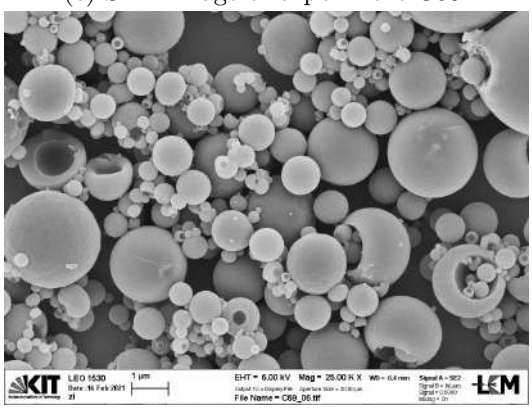

(g) SEM image of experiment C59.

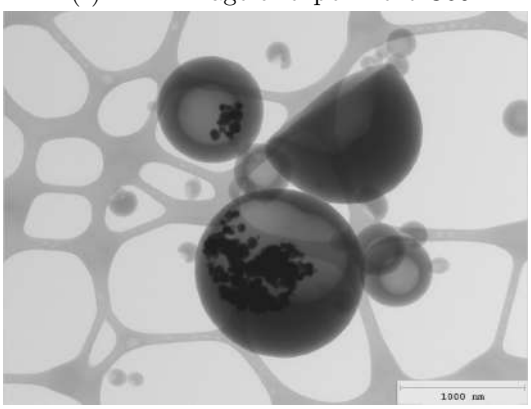

(h) TEM image of experiment C59.

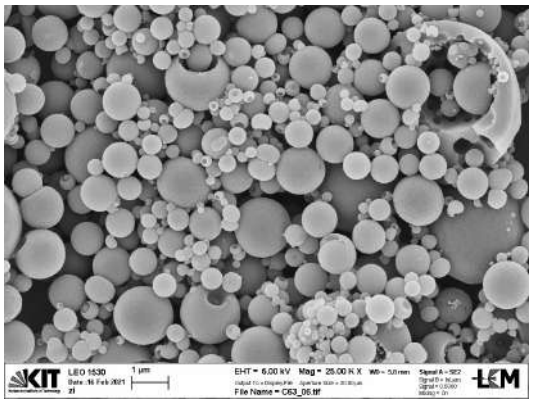

(i) SEM image of experiment C63.

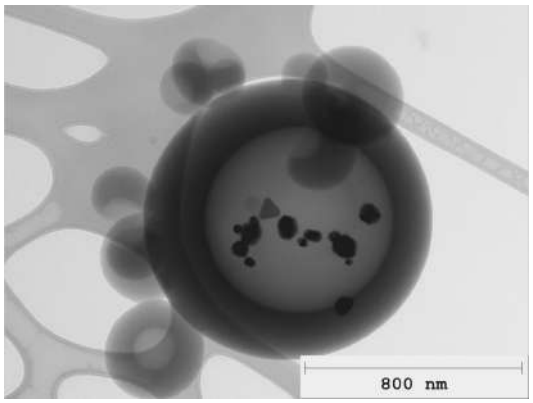

(j) TEM image of experiment C63.

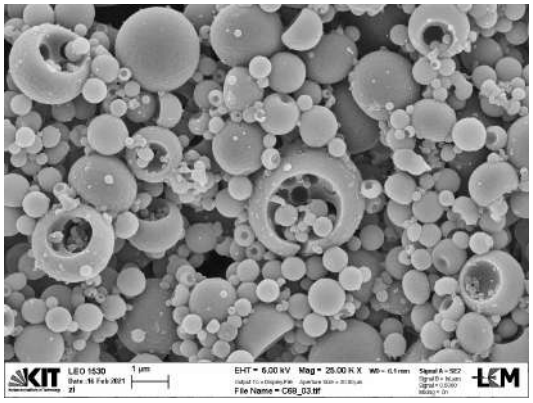

(k) SEM image of experiment C68.

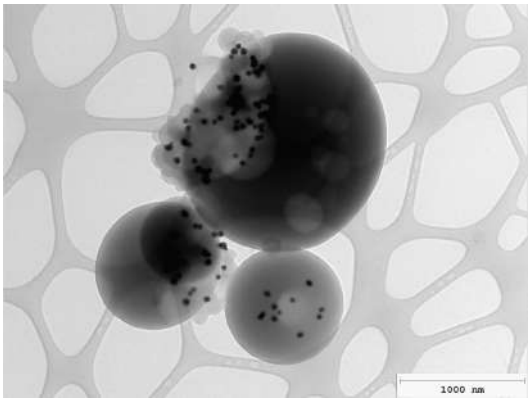

(l) TEM image of experiment C68.

Figure 3.9: SEM and TEM pictures of experiments with 0,15 g of Ag-NPs and PrOH.

A big percentage of the capsules contain silver, but not the totality as Figure 3.9b depicts. When adding 3 g of PrOH to the same formulation stability of the spray solution is improved and no silver can be found on TEM images, even big particles, outside which is common to find silver NPs, retain their structure without triggering release by rupture. Almost all capsules have silver inside and small empty ones can be also found (see Figure 3.9d). Adding more PrOH will result in the opposite effect: experiment C60 show more silver outside capsules even if all the polymeric particles have silver in their structure. It is confirmed that the addition of PrOH, to a certain extent, helps to improve the stability of the silver dispersion and helps silver to stay inside the capsules.

Experiments in which silver ink is present exhibit a different behaviour: PrOH has a far stronger stabilization effect and hinders silver aggregation. Figure 3.9h shows big clusters of silver nanoparticles in a formulation without propanol, the majority of the capsules have no silver inside and the one present is concentrated and aggregated in fewer bigger particles. Differently from experiment C61 (with Ag-PVP) no silver is released outside, mainly because it is difficult to find isolated Ag-NPs. Adding 3 g of PrOH to the same formulation with silver ink resulted in a better stabilization, it was easier to find more isolate silver throughout all the sample, more capsules had silver inside and fewer agglomerates were present. Increasing the amount of PrOH to 5 g resulted in a stickier sample and less isolated particles, more silver was found outside, some ruptured big particles and big agglomerates of polymeric NPs were present. Figure 3.9k shows a bigger number of broken particles and more silver dots on the surface compared to experiments with the same silver source and less PrOH. Compared to the same formulation with a different kind of silver, it was observed that PrOH affects more the stickiness of the samples, and even if particles did not show necking they stay together in big clusters. A similar agglomeration effect was observed with the same formulation and

a smaller load of silver but in a far smaller degree (experiment C56, Figure 3.8h).

To achieve a more complete integration of silver nanoparticles inside the polymeric nanoparticles an even higher amount of silver has been used. Silver weight has been increased three folds again and Ag-Ink 50wt% and Ag-PVP types were used. Formulation details are presented in Table 3.8.

Table 3.8: Experiments with 0,45 g of silver NPs and PrOH.

Exp.	Monomers		Ratio	Solvent [g]	PrOH	Silver NPs	M/S
C62	TRIS	TMPTA	1:3	12 EtOH	0	0,900 g Ag-Ink 50wt%	2/5
C64	TRIS	TMPTA	1:3	12 EtOH	3	0,900 g Ag-Ink 50wt%	5/14
C79	TRIS	TMPTA	1:3	12 EtOH	3	1,35 g Ag-PVP	5/14

(1) All experiments in this table share the same amount of porogens and glycerol: 3,5 g 2Oct, 3,5 g of IsoOct, 3 g of HD and 3 g of Gly respectively.

No stability problems were observed whatsoever when using this increased amount of silver, meaning that silver nanoparticles stability range in the monomer solution is broad. Experiments with PrOH showed longer stability compared to experiment without (C62) as expected, with spray solutions staying stable three times as long. Even with these high loads of silver the same trend as in experiments from Table 3.7 is present. When no PrOH is used in experiments with silver ink, silver is found in clusters and the majority of capsules are empty, no silver is found outside. Employing PrOH, a more stable dispersion is obtained and particles are as shown in Figure 3.10d, silver is more homogeneously distributed among the capsules and fewer clusters are present. Given the large amount, silver NPs still tend to agglomerate where present. In both experiment C62 and C64 nanoparticle structure is affected by the increased amount of silver ink, a bigger number of spherical particles can be observed and particles with a well-formed core a less frequent. This may be due to the higher concentration of silver ink solvent (tripropylene glycol monomethyl ether, TPGME) having an effect on gelation time.

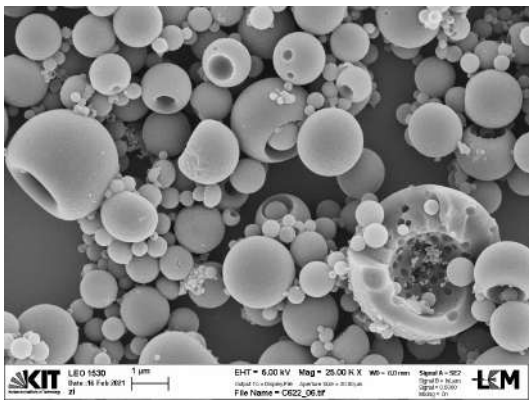

(a) SEM image of experiment C62.

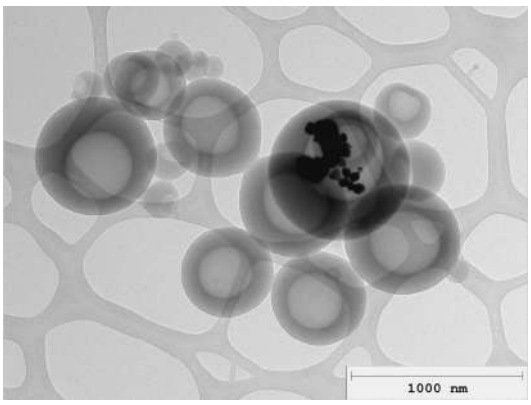

(b) TEM image of experiment C62.

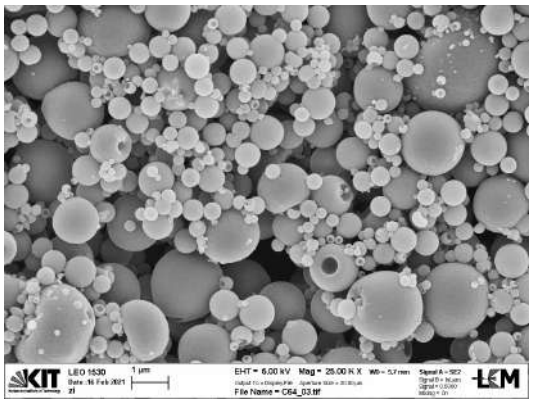

(c) SEM image of experiment C64.

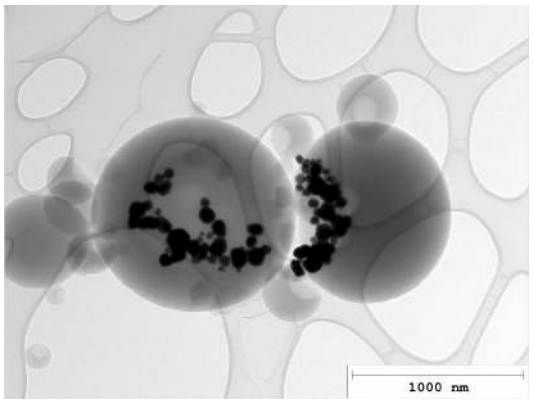

(d) TEM image of experiment C64.

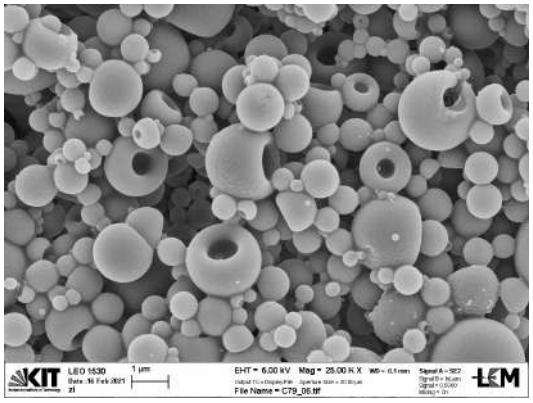

(e) SEM image of experiment C79.

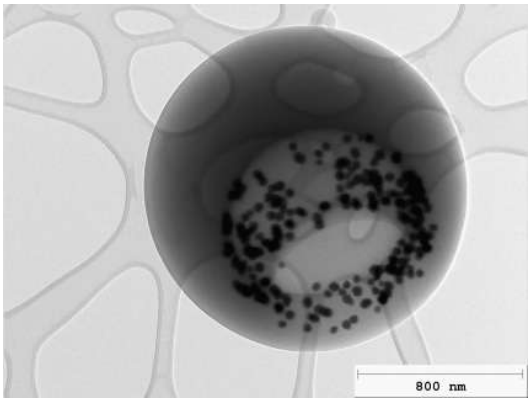

(f) TEM image of experiment C79.

Figure 3.10: SEM and TEM images of experiments with 0,45 g of silver NPs and PrOH.

On the other hand, experiment C79 with Ag-PVP show little agglomeration and more isolated polymeric nanoparticles, all silver is found inside and is not clustered. All particles are hybrids and capsules with almost none without silver. The amount of silver found inside each particle is far bigger compared to experiments with lower loading, with even capsules smaller than 400-300 nm having more than 3 or 4 silver nanoparticles inside. For bigger capsules, as shown in Figure 3.10f, the amount of silver stored inside their domain is big enough to create a corona of silver at the curved inner surface of the polymeric shell, where the indentation begins.

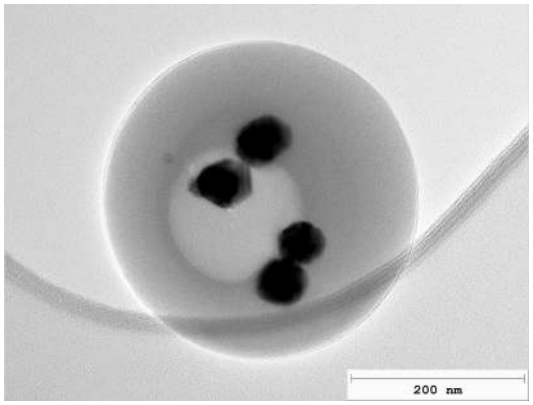

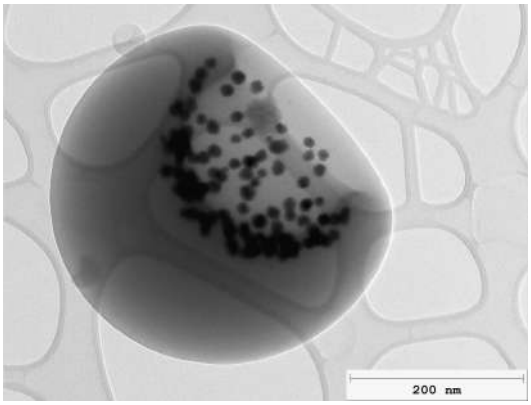

Figure 3.11: TEM images of hybrids from experiment C79.

3.2.4 Effect of Other Stabilizers

Silver PVP coated nanoparticles with a smaller average diameter (25 nm) were used in this series of experiments. The mass of silver used was kept equal to the one used in experiments of Table 3.3 in order to have a number 8 times bigger of silver NPs available. Stabilizers used in this series were: m-dPEG®$_8$-Lipoamide (LipoA), a modified ALA molecule and tripropylene glycol monomethyl ether (TPGME), the solvent already present in silver ink dispersions. The results obtained with formulations employing the two stabilizers were confronted with an experiment where PrOH was used. Details are presented in Table 3.9.

Table 3.9: Experiments with 0,15 g of silver NPs (25 nm) and different stabilizers.

Exp.	Monomers		Ratio	Solvent [g]	Stabilizer	Silver NPs	M/S
C73	TRIS	TMPTA	1:3	12 EtOH	3 g PrOH	0,45 g Ag-PVP [(2)]	3/5
C74	TRIS	TMPTA	1:3	12 EtOH	3 g TPGME	0,45 g Ag-PVP [(2)]	5/14
C75	TRIS	TMPTA	1:3	12 EtOH	0,100 g LipoA	0,45 g Ag-PVP [(2)]	2/5

[(1)] All experiments in this table share the same amount of porogens and glycerol: 3,5 g 2Oct, 3,5 g of IsoOct, 3 g of HD and 3 g of Gly respectively.

[(2)] Ag-PVP NPs used in this series have average size of 25 nm.

At first glance, Figures 3.12a and 3.12b from C73 look different compared to figures taken relative to experiment C78, in which Ag-PVP (50nm) is used.

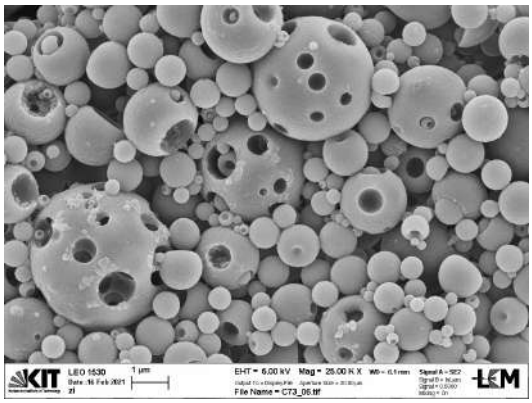

(a) SEM image of experiment C73.

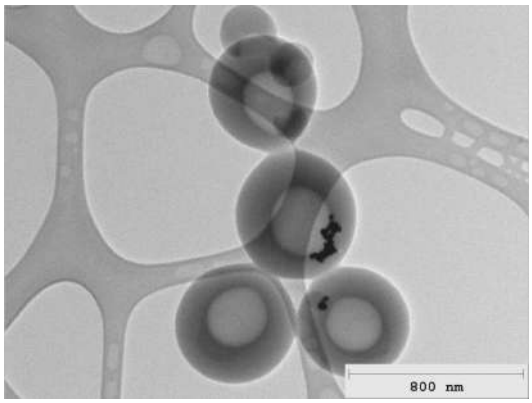

(b) TEM image of experiment C73.

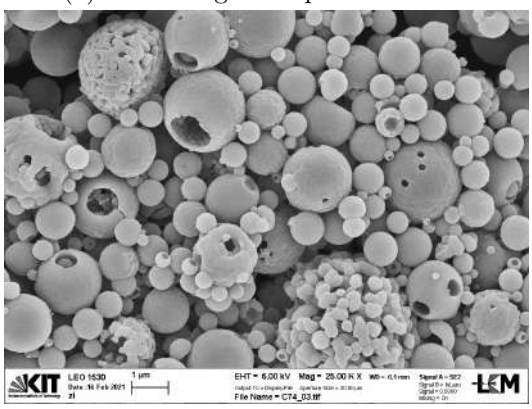

(c) SEM image of experiment C74.

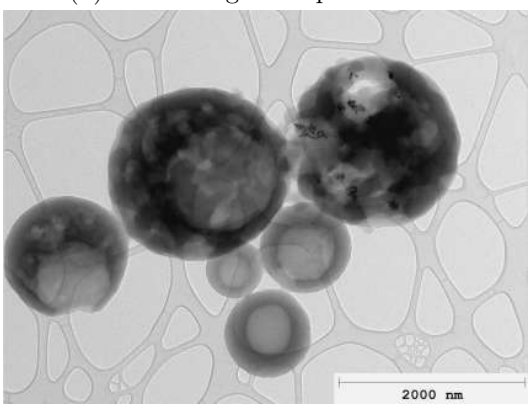

(d) TEM image of experiment C74.

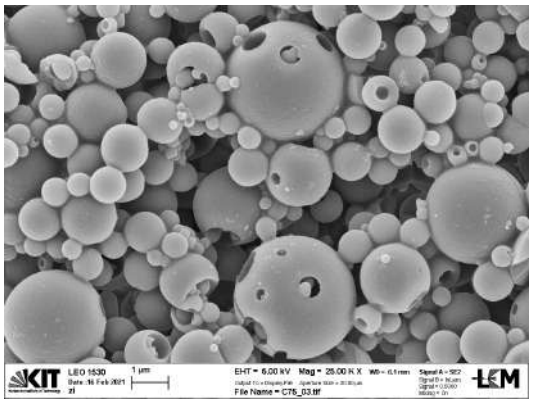

(e) SEM image of experiment C75.

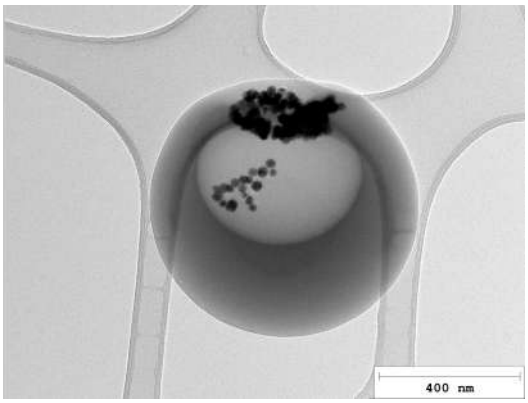

(f) TEM image of experiment C75.

Figure 3.12: SEM and TEM images of experiments with 0,15 g of silver and different stabilizers.

TEM image shows silver clusters and a big number of polymer NPs without any silver inside. No silver is found outside the NPs, confirming the good stabilizing effect of PrOH, but silver is not isolated either, suggesting that Ag-PVP with smaller particles diameter tend to agglomerate more easily. SEM images show a different NPs structure in all samples, characterized by a big number of particles having more than one cavity and a sponge-like structure. The presence of this particular structure can be caused by a secondary structuring that leads to the formation of sponge-like envelopes around preformed NPs. The particle size distribution is generally broader compared to the previous experiment and particles with a size bigger than 2 or 3 μm can be easily spotted. These characteristics are observed even in sample C73 suggesting that even without the addition of stabilizers a different silver source likely modifies the spraying process. Effects on morphology are bigger in sample C74. The use of TPGME has no distinguishable stabilizing effect on silver NPs, nonetheless, it affects capsule morphology creating mosaic structures. In Figures 3.12c and 3.12d a significant number of particles shows a mosaic structure or a mosaic-capsule structure, suggesting that the use of TPGME along with the particle size influence the phase separation process, anticipating it. A promising effect on silver particles stabilization is observed in sample C75 (see Figure 3.12f), where LipoA is employed. Silver clusters are still present and a few of the particles are hybrids, but no silver is found outside. Surface morphology is affected in the same way as in sample C73 by the use of LipoA, but in a smaller extent, very few sponge-like particles can be observed.

3.2.5 Changing monomer to solvent (M/S) ratio

In this section formulations with variations in monomers to solvents ratio were employed to check whether the formulation can be further optimized for a nanostructuring process. The total amount of monomers used was kept constant and equal to 10 g (TRIS + TMPTA) and the amount of silver was maintained constant and equal to 3wt% with respect to the monomer weight. In the solvents are included porogens, EtOH, glycerol and 1-propanol, the total amount was varied, but the relative ratio between each compound was kept constant. Starting formulation was the one of experiment C63, using 0,300 g Ag-Ink 50wt% as the amount calculated in subsection 3.2.3. Details are presented in Table 3.10.

In all formulations no silver was observed outside the polymeric nanoparticles, no big agglomerations were found outside either, since solvents increase or decrease is not as important as monomers to silver ratio in terms of dispersion stability. It is safer to assume that

Table 3.10: Experiments with different monomer to solvent (M/S) ratio.

Exp.	Monomers		Ratio	HD/2Oct/IsoOct [g]	EtOH [g]	Gly [g]	PrOH	M/S
C66	TRIS	TMPTA	1:3	2,14/2,50/2,50	8,60	2,15	2,15	1/2
C65	TRIS	TMPTA	1:3	2,67/3,12/3,12	10,75	2,70	2,70	2/5
C63	TRIS	TMPTA	1:3	3,00/3,50/3,50	12,00	3,00	3,00	5/14
C76	TRIS	TMPTA	1:3	3.56/4,16/4,16	14,30	3,59	3,59	3/10
C77	TRIS	TMPTA	1:3	4,28/5,00/5,00	17,16	4,28	4,28	1/4

(1) All experiments in this table share the same amount of silver: 0,300 g Ag-Ink 50wt%.

silver ink is generally less likely to spill outside nanoparticles as previous experiments have revealed, and in the range of M/S ratio used no instability of the dispersion was observed. In experiment C66 and C65 with higher M/S ratio particles morphology is highly affected: a lower percentage of capsules are present compared to M/S ratio of previous experiments. Silver is more likely found in the few particles which have a core (see Figure 3.13d). The smaller number of well-formed capsules it is due to the increased percentage of monomers that occupy the majority of the space in the droplet, the little volatile solvent present is bound to evaporate and the remaining part and the porogens are not enough to trigger phase separation right in time to form a perfect capsule. All particles are individual and no stickiness or necking between them is observed neither in Figure 3.13b nor in 3.13d. Larger amounts of porogens, softmaker or TRIS are capable of changing this bahaviour, as other experiments have already shown.

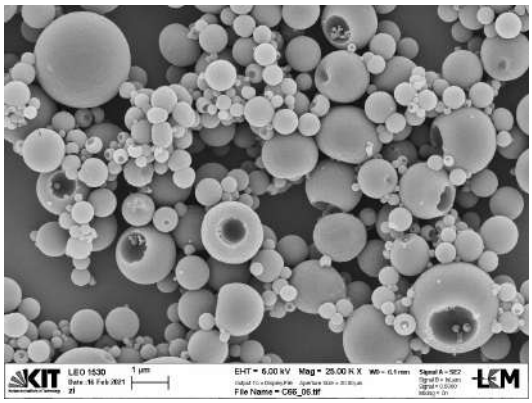

(a) SEM image of experiment C66.

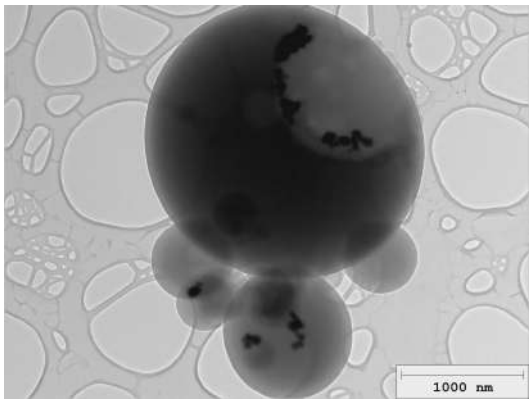

(b) TEM image of experiment C66.

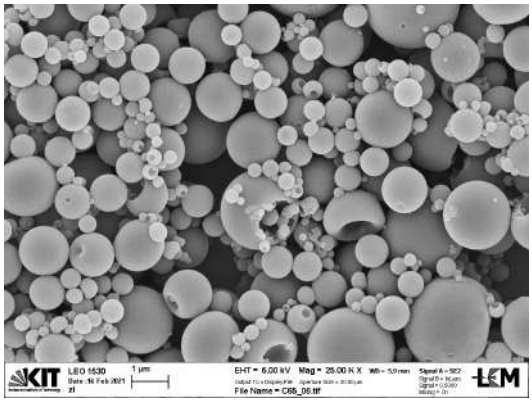

(c) SEM image of experiment C65.

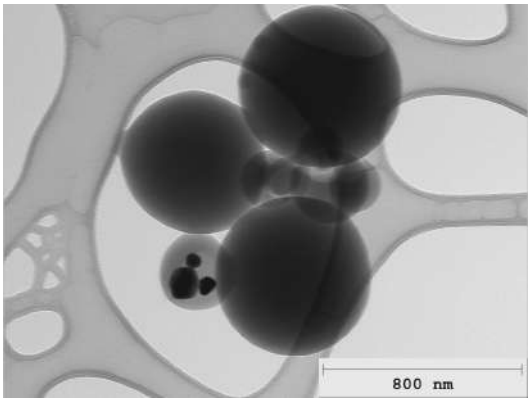

(d) TEM image of experiment C65.

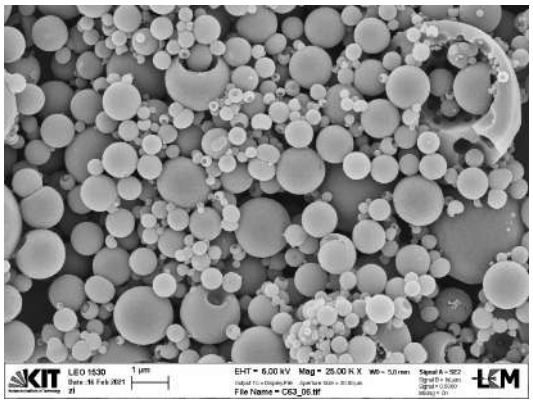

(e) SEM image of experiment C63.

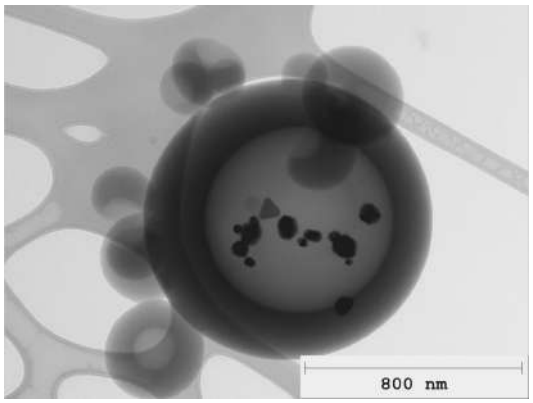

(f) TEM image of experiment C63.

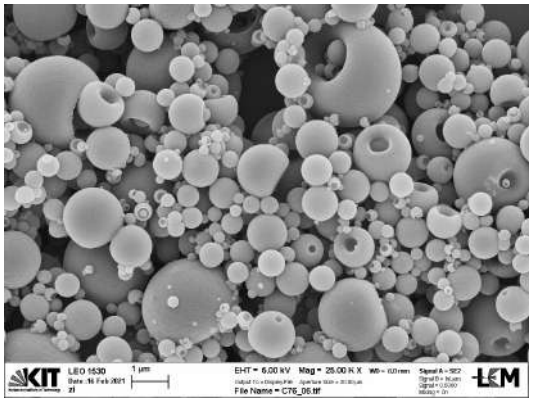

(g) SEM image of experiment C76.

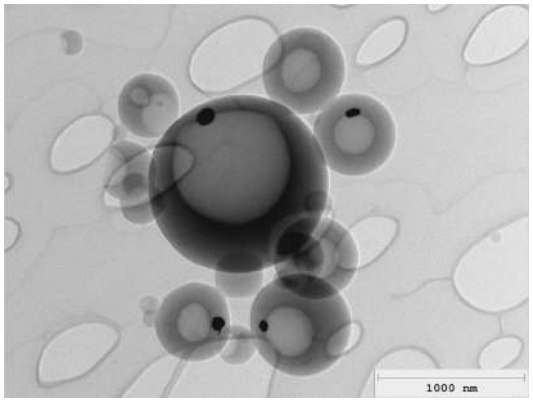

(h) TEM image of experiment C76.

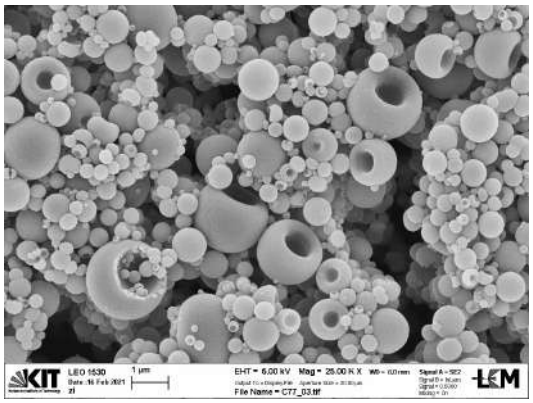

(i) SEM image of experiment C77.

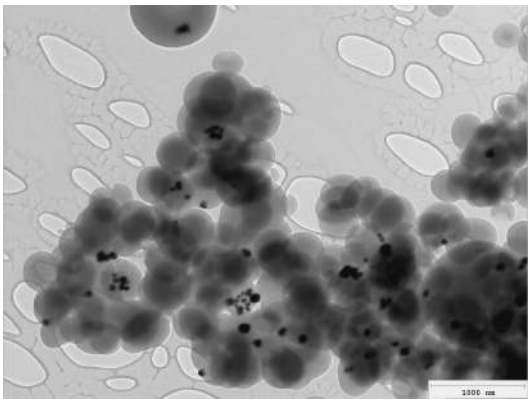

(j) TEM image of experiment C77.

Figure 3.13: SEM and TEM images of experiments with different monomer to solvent (M/S) ratio.

On the other hand, increasing the solvent content causes the sample's morphology to change in the opposite direction, particles have a bigger core and the monomeric shell is somehow thinner as can be seen in Figure 3.13h of experiment C76. More collapsed capsules are present as well, making it easier to get an indication of nanostructuring via SEM images (see Figures 3.13g and 3.13i) in accordance that thinner monomer shells bend more easily. In Figure 3.13h all particles are well-formed capsules in which the core occupies a large percentage of volume. Adding more solvent to the formulations means having more highly volatile species such as EtOH which by evaporating reduce the average size of the droplet, but also having a stronger presence of the good solvents 2-octanone and the bad solvent hexadecane. More 2-octanone results in more soluble polymeric chains which grow longer before

precipitation occurs hence resulting in delayed phase separation. 2-Octanone also increases the stickiness of the sample as well as glycerol and 1-propanol, each of which now present in higher content. This explains why increasing even more M/S ratio (to 1/4 as in experiment C77) will result in a sample with almost no capsules and higher agglomeration/stickiness (in Figure 3.13j big agglomerates of polymeric nanoparticles can be observed).

Having big clusters of particles makes the task of acquiring data about the size distribution more difficult, but it can be stated that fewer big particles are present in experiments with higher solvent amount. Managing to reduce hybrid particle size is important to reduce the probability of silver spillover due to the collapse of too fragile structures.

3.3 Thiol Groups Analysis

3.3.1 Ellman's reaction

Formulations using TRIS/TMPTA molar combination ratio of 1:3 and 1:4 showed to be more suitable for the production of individual and well-defined capsule-like particles. However, increasing the amount of ene monomer in the monomer mixture will result in the modification of the polymerization mechanism that will less likely be a pure thiol-ene step-growth one and determined more by a radical chain mechanism. In order to denote how far the mechanism is from the pure thiol-ene it is important to quantify the presence of the remaining SH groups after the polymerization process took place. To do so, Ellman's reaction has been employed. In this reaction, 5,5'-dithiobis-(2-nitrobenzoic acid) (DTNB) reacts with the sulfhydryl groups in the sample to give a disulfide compound and 2-nitro-5-thiobenzoate (TNB) as products (see Figure 3.14).

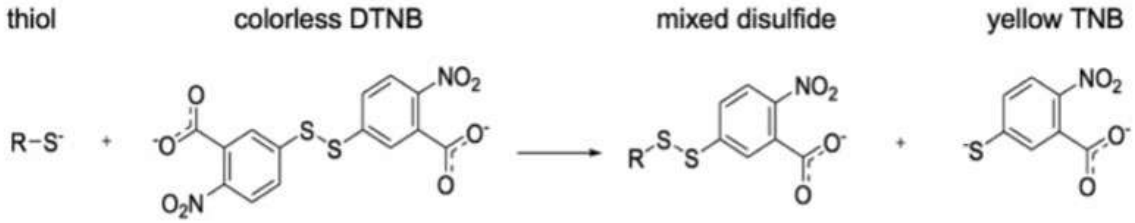

Figure 3.14: Ellman's reaction mechanism (Nieri et al., 2017).

The TNB specie formed has a yellow colour and can be used as an indicator of the presence of SH groups in the sample.

Thiol groups presence for different TRIS/TMPTA ratios (from 1:1 up to 1:8) were analysed using Ellman's reagent. The vials for the reaction were prepared by dispersing the dried nanoparticle samples in a phosphate buffer saline (PBS) solution. DMSO was added in a concentration of 5% to facilitate NPs dispersion. Dispersion pH was checked for neutrality and DTNB was added to each vial. Results are shown in Figure 3.15.

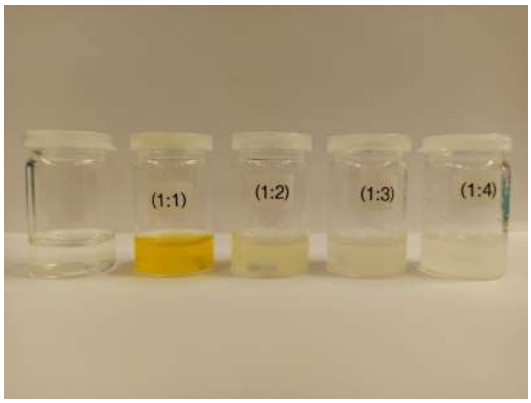

(a) Ellman's reaction of samples with TRIS/TMPTA ratios from 1:1 to 1:4.

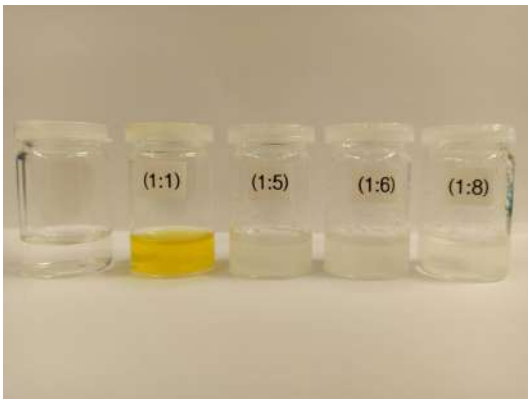

(b) Ellman's reaction of samples with TRIS/TMPTA ratios from 1:5 to 1:8.

Figure 3.15: Ellman's reaction of samples of TRIS/TMPTA with different monomer relative ratio.

The yellow colouration indicates the presence of SH groups due to a positive Ellman's reaction. For sample with 1:1 and 1:2 combinations, it is easy to detect the colour change. Sample 1:3 show a slight colouration too, while samples having a greater amount of TMPTA in their composition were negative to the test.

Ellman's reaction is a quantitative method if combined with the spectrophotometric measurement of TNB absorbance. In this study, the reaction was used solely as a qualitative assay to determine if thiol groups were present or not regardless of their concentration. Nevertheless, Figures 3.15a and 3.15b imply that only samples with more TRIS are suitable for successive surface conjugation via thiol groups and thus one can expect that samples with a ratio of 1:3 are the most promising in terms of ability to generate capsules and SH groups availability.

3.3.2 Maleimide conjugation

Once established that particles in experiments based on 1:1 up to 1:3 TRIS/TMPTA ratios have reactive SH groups, a surface conjugation technique was applied to determine whether the thiol groups are available for maleimide functionalization or not. Nanoparticles were treated with a fluorescence derivate of Maleimide, iFluor Maleimide (iFM), which bonds to SH groups and after a few purification cycles, bonded maleimide was characterized employing Fluorescence spectroscopy.

Dried nanoparticles were first dispersed in DMSO and stirred for about 3 hours. A solution of iFM in DMSO was prepared separately and 1 mL was added upon vigorous stirring to the nanoparticles dispersions, followed by moderate stirring overnight. Once the Maleimide-NPs were well dispersed, purification cycles by centrifugation were performed in order to separate the polymeric nanoparticles with bonded maleimide from the non reacted maleimide present in the DMSO. 6 or 7 purification cycles were needed, fluorescence spectroscopy was then performed to check for iFM presence. After the 3rd centrifugation cycle, DMSO was replaced by EtOH to redisperse the particle pellet. Once the iFM signal in the supernatant was barely detectable purification was considered to be concluded and the pellet containing the purified particles was analysed.

Figure 3.16 shows the fluorescence spectrum of the sample with 1:1 monomer ratio. A first peak due to stray light is present at around 380 nm while the peak relative to iFM is at 430-440 nm. In the same figure, supernatant fluorescence spectra are plotted as a reference.

1st to 3rd supernatants are not present as the concentration of unreacted maleimide is still too high to be used for comparison, successive supernatants show decreasing signal and thus are proof that the particles purification was successful.

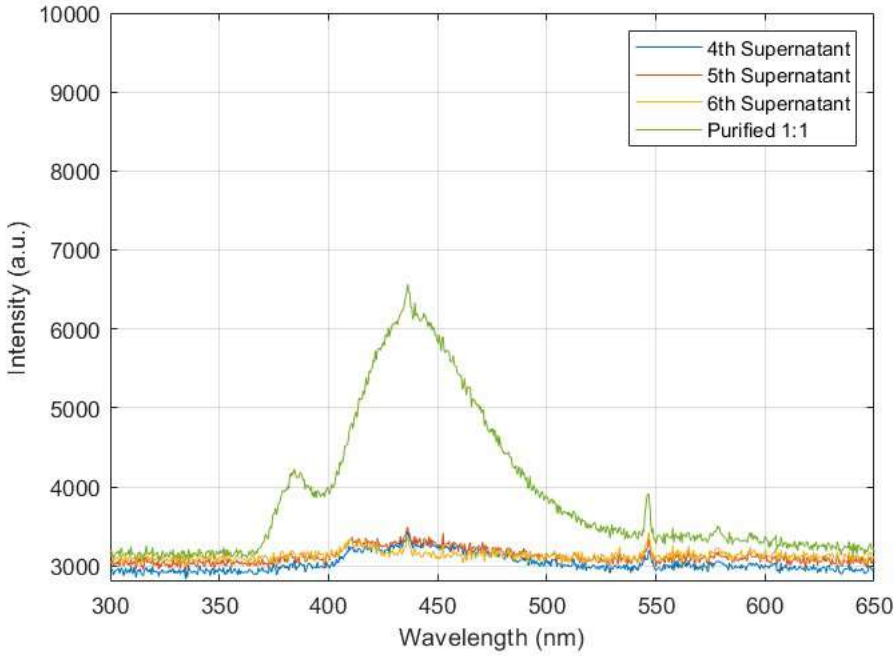

Figure 3.16: Fluorescence spectra recorded during purification of the sample based on 1:1 TRIS/TMPTA ratio.

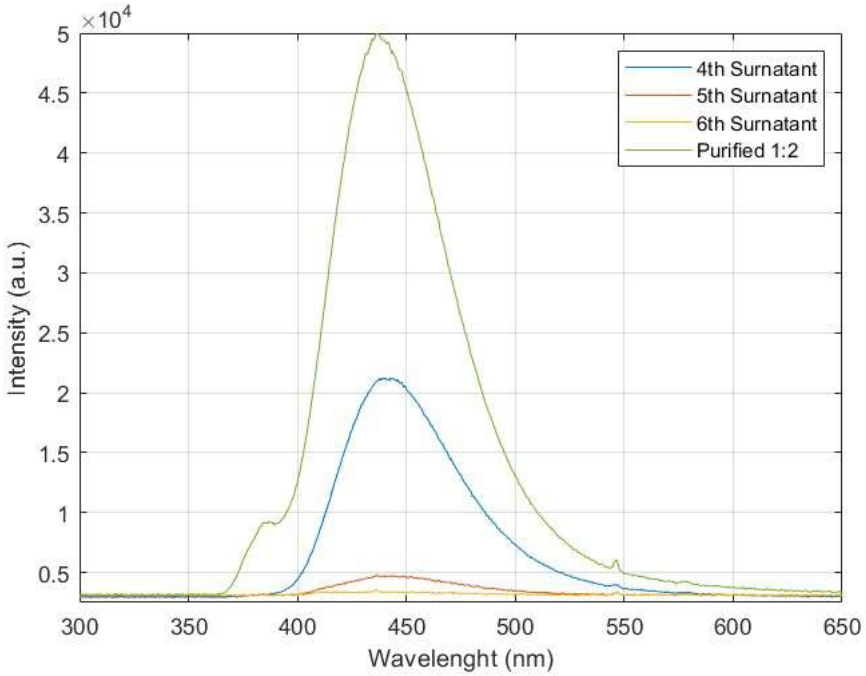

Figure 3.17: Fluorescence spectra recorded during purification of the sample based on 1:2 TRIS/TMPTA ratio.

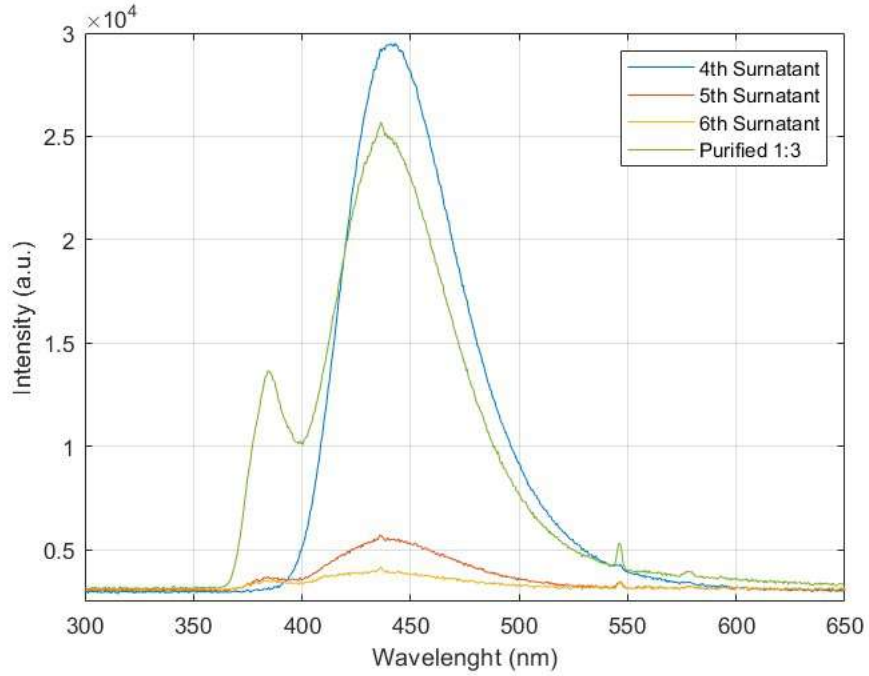

Figure 3.18: Fluorescence spectra recorded during purification of the sample based on 1:2 TRIS/TMPTA ratio.

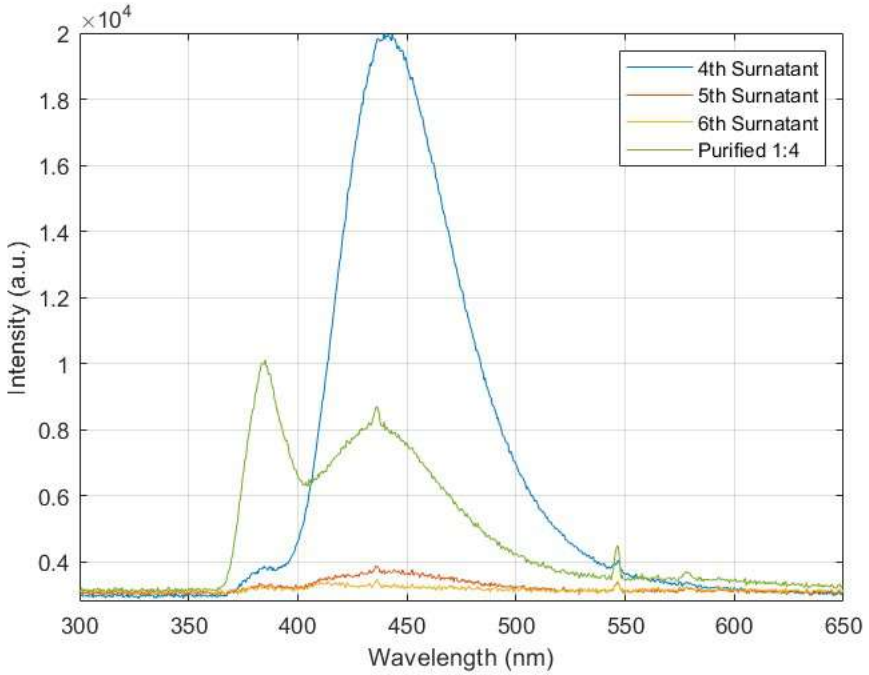

Figure 3.19: Fluorescence spectra recorded during purification of the sample based on 1:4 TRIS/TMPTA ratio.

The intensity of iFM signals in samples based on 1:2 up to 1:4 TRIS/TMPTA ratios suggest that SH groups are available for functionalization even at higher TMPTA ratios. The spectrum of 1:2 sample (Figure 3.17) has the peak with greater intensity and thus is the best candidate for a future conjugation process. Spectra of particles with higher TMPTA content (Figures 3.18 and 3.19) show a smaller iFM peak according to Ellman's reaction test.

Supernatant signals of Figure 3.18 are slightly higher compared to the 1:1 sample suggesting a less effective purification. Nonetheless, the last supernatant signal is small, so that is safe to say that unreacted maleimide is not responsible for the intense peak in the purified sample. Considering the results of subsection 3.3.1, a higher iFM signal was expected for the purified particles in the sample with a 1:1 TRIS/TMPTA ratio. This is because of the higher content of not converted TRIS monomer present in stoichiometric Thiol-ene reaction, confirmed by the intense yellow colour in Ellman's reaction test. Unreacted TRIS efficiently bonds with iFM, decreasing its concentration for reaction with SH groups present particles.

Despite 1:2 sample (Figure 3.17) having the more intense iFM peak, the sample based on a 1:3 TRIS/TMPTA ratio was chosen for further study because of the better capsules morphologies obtained with this ratio.

Chapter 4

Conclusions

In this work, polymeric nanocapsules and polymer-silver nanocapsules hybrids were obtained by aerosol photopolymerization (APP) with a Thiol-ene mechanism. Spray solutions used consisted of a TRIS/TMPTA monomer combination, a volatile solvent (EtOH), a mixture of porogens (2-octanone, 2-ethyl-1-hexanol and hexadecane) and glycerol. Different silver nanoparticles sources and stabilizers were added to produce hybrids. The role of each of the additives used in the spray formulation was inquired in order to understand their influence on particle morphology. More specifically, spray solutions with different TRIS/TMPTA combinations were studied and the effect of each monomer on the structuring process of the particles was underlined. It was found that a TRIS/TMPTA ratio of 1:3 was suitable for the production of well-structured capsules (Figure **??**).

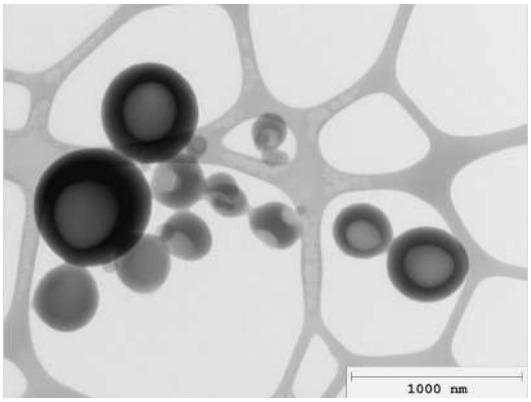

Figure 4.1: Capsules produced with a 1:3 TRIS/TMPTA ratio (mixed mode).

Polymeric capsules containing silver NPs were successfully obtained for the first time employing the mixed-mode Thiol-ene reaction mechanism. Different stabilizers were tested and their effect on Ag-NPs dispersion was studied. At the end, a formulation containing PVP coated silver nanoparticles and 1-propanol as a stabilizer was employed to produce well-structured hybrids with silver NPs uniformly distributed in their core (Figure 4.2). All the polymeric particles had capsule-like morphology and contained silver NPs inside, no Ag-NPs were found outside of the sample as well.

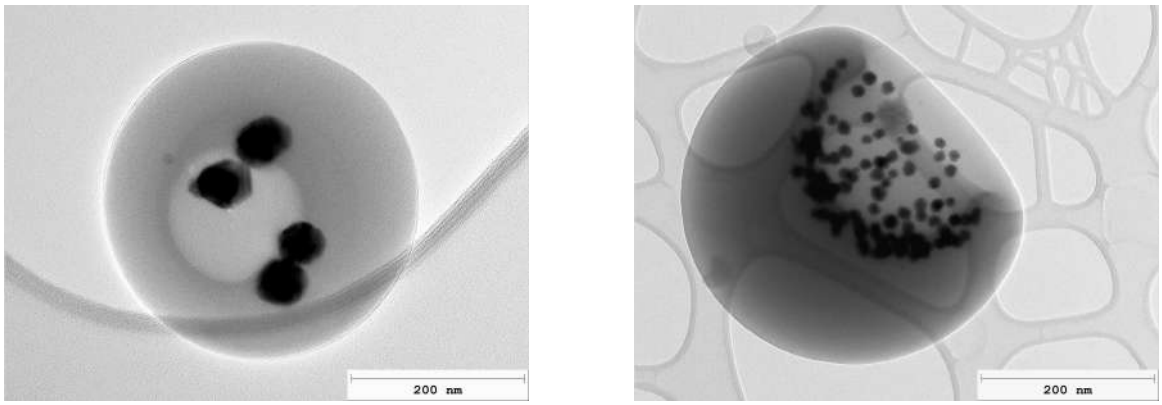

Figure 4.2: Hybrids produced with a 1:3 TRIS/TMPTA ratio plus Ag-PVP and PrOH.

The last part of the work was focused on the research of available SH functional groups in the nanoparticles samples. The presence of SH groups for sampòes with TRIS/TMPTA ratio from 1:1 up to 1:4 was proved via Ellman's reaction and the conjugation with the bio molecule maleimide was performed. Results of successful conjugation were analysed using fluorescence spectroscopy.

In order to optimize the hybrids production process, further studies aimed at increasing silver dispersion stability in the spray solutions are required. During this work, problems concerning the polydispersity of polymeric nanoparticles were encountered. Thus, better control of nanoparticles size distribution should be considered as a future addition to this research. Furthermore, an FT-IR analysis would be required for the study of the conversion of ene groups and thiol groups after the polymerization process so to give further support to the choice of the best TRIS/TMPTA ratio. Finally, a study regarding drug incorporation and release is necessary for a future application in therapeutic nanosystems.

List of Figures

1 Strumentazione completa: atomizzatore e fotoreattore con filtro di raccolta. . ii
2 Immagini al SEM e TEM di particelle ottenute con rapporti di TRIS/TMPTA di 1:1 e 1:2. iii
3 Immagini al SEM e TEM di particelle ottenute con rapporti di TRIS/TMPTA di 1:3 e 1:4. iv
4 Particelle di TMPTA con struttura a mosaico ottenute tramite meccanismo radicalico. iv
5 Immagini al SEM di particelle di TRIS/TMPTA con e senza glicerolo. v
6 Immagini al TEM di particelle TRIS/TMPTA con Ag-NPs e stabilizzanti. . . vi
7 TRIS/TMPTA con Ag-Ink 30-35% e MUL. vi
8 Immagini al TEM di particelle TRIS/TMPTA con 0,05 g Ag-NPs e PrOH. . vii
9 Immagini al TEM di particelle TRIS/TMPTA con 0,15 g di Ag-NPs e PrOH. vii
10 TRIS/TMPTA con 0,45 g Ag-PVP e PrOH. viii
11 Strutture a mosaico di TRIS/TMPTA con Ag-PVP (25 nm) e TPGME. . . . viii
12 Immagini al TEM di particelle TRIS/TMPTA con variazione M/S. ix
13 Spettri di fluorescenza registrati per particelle con rapporto TRIS/TMPTA pari a 1:3. x

1.1 Phases of polymeric gelation in an aerosol droplet. 3
1.2 Polymeric chains expanding in the presence of a good solvent (Sherrington, 1998). 4
1.3 Polymer pseudo-phase diagram (Sherrington, 1998). 5
1.4 Nanoparticle formation in case of: (a) Early gelation and (b) delayed gelation (Modified from Sherrington, 1998). 6
1.5 Image of a mosaic structure obtained by radical chain polymerization via APP. 6
1.6 Conversion-average molecular weight diagram for chain-growth, step-growth and living polymerization mechanism (Polymer Properties Database). 7
1.7 Thiol-ene reaction mechanism (Polymer Properties Database). 8
1.8 Maleimide-thiol reaction: sulfhydryl group on NP surface reacts with the substituted maleimide, where R group can be a biomolecule of interest. The product of the reaction is a maleimide bioconjugated to a polymeric NP through a thioether bond (modified from Geest and Lolkema, 2000). 11

2.1 THIOL monomers. 13
2.2 ENE monomers. 14
2.3 Porogens. 14
2.4 Atomizer by TOPAS. 16

3.1 SEM and TEM images of experiments with different Thiol-ene monomer ratios. 21
3.2 Experiments with TRIS/TMPTA (1:1) and only TMPTA. 23
3.3 SEM pictures of experiments using different monomer combinations. 24
3.4 SEM and TEM images of gel-type spheres obtained without glycerol. 25

3.5 SEM pictures of experiments with different glycerol concentration. 26
3.6 SEM and TEM images of experiments with Ag-PVP and different stabilizers. 29
3.7 SEM and TEM images of experiments with Ag-Ink 30-35wt% and different stabilizers. 31
3.8 SEM and TEM images of experiments with 0,05 g of silver with and without PrOH. 33
3.9 SEM and TEM pictures of experiments with 0,15 g of Ag-NPs and PrOH. . . 36
3.10 SEM and TEM images of experiments with 0,45 g of silver NPs and PrOH. . 38
3.11 TEM images of hybrids from experiment C79. 38
3.12 SEM and TEM images of experiments with 0,15 g of silver and different stabilizers. 40
3.13 SEM and TEM images of experiments with different monomer to solvent (M/S) ratio. 42
3.14 Ellman's reaction mechanism (Nieri et al., 2017). 43
3.15 Ellman's reaction of samples of TRIS/TMPTA with different monomer relative ratio. 44
3.16 Fluorescence spectra recorded during purification of the sample based on 1:1 TRIS/TMPTA ratio. 45
3.17 Fluorescence spectra recorded during purification of the sample based on 1:2 TRIS/TMPTA ratio. 45
3.18 Fluorescence spectra recorded during purification of the sample based on 1:2 TRIS/TMPTA ratio. 46
3.19 Fluorescence spectra recorded during purification of the sample based on 1:4 TRIS/TMPTA ratio. 46

4.1 Capsules produced with a 1:3 TRIS/TMPTA ratio (mixed mode). 49
4.2 Hybrids produced with a 1:3 TRIS/TMPTA ratio plus Ag-PVP and PrOH. . 50

List of Tables

3.1 Experiments with different Thiol-ene monomer ratio. 19
3.2 Experiments with different ENE monomer. 23
3.3 Experiments with different glycerol concentration. 25
3.4 Experiments with Ag-PVP and different stabilizers. 27
3.5 Experiments with Ag-Ink 30-35wt% and different stabilizers. 30
3.6 Experiments with 0,05 g of silver NPs and PrOH. 32
3.7 Experiments with 0,15 g of silver NPs and PrOH. 34
3.8 Experiments with 0,45 g of silver NPs and PrOH. 37
3.9 Experiments with 0,15 g of silver NPs (25 nm) and different stabilizers. . . . 39
3.10 Experiments with different monomer to solvent (M/S) ratio. 41

Acronyms

NPs	Nanoparticles
HNPs	Hybrid Nanoparticles
APP	Aerosol Photopolymerization
CTM	Chain Transfer Mechanism
TRIS	Thrimethylolpropane tris(3-mercaptopropionate)
TETRA	Pentaerythritol tetrakis (3-mercaptopropionate)
TMPTA	Trimethylolpropane triacrylate
TAT	2,4,6-Triallyloxy-1,3,5-triazine
TTT	1,3,5-Triallyl-1,3,5-triazine-2,4,6(1H,3H,5H)-trione
DAA	Diallyl adipate
2Oct	2-Octanone
IsoOct	2-Ethyl-1-hexanol
HD	Hexadecane
EtOH	Ethanol
PrOH	1-Propanol
Gly	Glycerol
DMSO	Dimethylsulfoxid
TPGME	Tri(propylene glycol) methyl ether
MUL	11-Mercapto-1-undecanol
ALA	α-Lipoic acid
LipoA	m-dPEG®$_8$-Lipoamide
Ag-NPs	Silver Nanoparticles
Ag-Ink50wt%	Silver nanoparticles ink 50wt%
Ag-Ink30-35wt%	Silver nanoparticles ink 30-35wt%
Ag-PVP(50 nm)	Silver nanospheres (50 nm), PVP coated
Ag-PVP(25 nm)	Silver nanospheres (25 nm), PVP coated
iFM	iFluor ^{TM} 350 maleimide
DTNB	5,5'-dithiobis-(2-nitrbenzoic acid)
PBS	Phosphate Buffer Saline
PI	Photoinitiator
SEM	Scanning Electron Microscopy
TEM	Transmission Electron Miscoscopy
FS	Fluorescence Spectroscopy

Bibliography

Akgün E., Hubbuch J. and Wörner M. (2013). Perspective of Aerosol-Photopolymerization: Nanoscale Polymer Particles. *Chem. Eng. Sci.* **101**, pp. 248-252. [DOI: 10.1016/j.ces.2013.06.010].

Akgün E., Hubbuch J. and Wörner M. (2014). Perspective of Aerosol-Photopolymerization: Organic-Inorganic Hybrid Nanoparticles. *Colloidal and Polymer Science* **292**, pp. 1241-1247. [DOI: 10.1007/s00396-014-3175-2].

Akgün E., Hubbuch J. and Wörner M. (2014). Perspective of Aerosol-Photopolymerization: Nanostructured Polymeric Particles. *Macromolecular Materials and Engineering* **299** (11), pp. 1316-1328. [DOI: 10.1002/mame.201400032].

Akgün E., Muntean A., Hubbuch J., Woerner M. and Sangermano M. (2015). Cationic Aerosol Photopolymerization. *Macromolecular Material Engineering* **300**, pp. 136-139. [DOI: 10.1002/mame.201400211].

Ananikov V. (2019). Organic-Inorganic Hybrid Nanomaterials. *Nanomaterials* **9** (9), pp. 1197-1209. [DOI: 10.3390/nano9091197].

Bazzano M. (2017). Development of UV-based polymerization techniques for the production of drug delivery devices. Ph.D. Dissertation. Politecnico di Torino, Italia.

Bazzano M., Latorre D., Pisano R., Sangermano M. and Wörner M. (2017). Nano-structured polymeric microparticles produced via cationic aerosol photopolymerization. *Journal of Photochemistry and Photobiology A: Chemistry* **346**, pp. 364-371. [DOI: 10.1016/j.photovhem.2017.06.009].

Biskos G., Vons V. Yurteri C. U. and Schmidt-Ott A. (2008). Generation and Sizing of Particles for Aerosol-Based Nanotechnology. *Powder and Particle Journal* **26**, pp. 13-35. [DOI: 10.14356/kona.26.2008006].

Calzoni E., Cesaretti A., Polchi A., Di Michele A., Tancini B. and Emiliani C. (2019). Biocompatible Polymer Nanoparticles for Drug Delivery Applications in Cancer and Neurodegenerative Disorder Therapies. *Journal of Funcional Biomaterials* **10** (4), pp. 1-15. [DOI: 10.3390/jfb10010004].

Colson Y. L. and Grinstaff M. W. (2012). Biologically Responsive Polymeric Nanoparticles for Drug Delivery. *Advanced Materials* **24**, pp. 3878-3886. [DOI: 10.1002/adma.201200420].

Cramer N. B. and Bowman C. N. (2001). Kinetics of Thiol-Ene and Thiol-Acrylate Photopolymerization with Real-Time Fourier Transform Infrared. *Journal of Polymer Science*

Part A: Polymer Chemistry **39** (19), pp. 3311-3319. [DOI: 10.1002/pola.1314].

Deng S., Gigliobianco M. R., Censi R. and Di Martino P. (2020). Polymeric Nanocapsules as Nanotechnological Alternative for Drug Delivery System: Current Status, Challenges and Opportunities. *Nanomaterials* **10** (5), pp. 1-36. [DOI: 10.3390/nano10050847].

Esen C. and Schweiger G. (1996). Preparation of Monodisperse Polymer Particles by Photopolymerization. *Journal of Colloid and Interface Science* **179** (1), pp. 276-280. [DOI: 10.1006/jcis.1996.0214].

Faraji A. H. and Wipf P. (2009). Nanoparticles in Cellular Drug Delivery. *Bioorganic and medicinal chemistry* **17**, pp. 2950-2962. [DOI: 10.1016/j.bmc.2009.02.043].

Farokhzad O. C. and Langer R. (2009). Impact of Nanotechnology on Drug Delivery. *ACS NANO* **3** (1), pp. 16-20. [DOI: 10.1021/nn900002m].

Fontaine S. D., Reid R., Robinson L., Ashley G. W. and Santi D. V. (2014). Long-Term Stabilization of Maleimide-Thiol Conjugates. *Bioconjugate Chemistry* **26** (1), pp. 145-152. [DOI: 10.1021/bc5005262].

Gao Z., Grulke E. A. and Ray A. K. (2007). Synthesis of monodisperse polymer microspheres by photopolymerization of microdroplets. *Colloid & Polymer Science* **285**, pp. 847-854. [DOI: 10.1007/s0036-006-1625-1].

Geest M. and Lolkema J. (2000). Membrane Topology and Insertion of Membrane Proteins: Search for Topogenic Signals. *Microbiology and Molecular Biology Review* **64** (1), pp. 13-33. [DOI: 10.1128/mmbr.64.1.13-33.2000].

Jain P., Huang X., El-Sayed I. and El-Sayed M. A. (2008). Noble Metals on the Nanoscale: Optical and Photothermal Properties and Some Applications in Imaging, Sensing, Biology, and Medicine. *Accounts of Chemical Research* **41** (12), pp. 1578-1586. [DOI: 10.1021/ar7002804].

Jasinski F., Zetterlund P. B., Braun A. M. and Chemtob A. (2018). Photopolymerization in Dispersed System. *Progress in Polymer Science* **84**, pp. 47-88. [DOI: 10.1016/j.progpolymsci.2018.06.006].

Lee J. C., Donahue N. D., Mao A. S., Karim A., Komarneni, Thomas E. E., Francek E. R., Yang W. and Wilhelm S. (2020). Exploring Maleimide-Based Nanoparticles Surface Engineering to Control Cellular Interactions. *ACS Applied Nano Materials* **3** (3), pp. 2421-2429. [DOI: 10.1021/acsanm.9b02541].

Longo D. (2019). Chain-growth versus step-growth polymerization in an aerosol photo-induced process. Tesi di Laurea Magistrale, Politecnico di Torino.

Lowe A. B. (2010). Thiol-ene "click" reactions and recent applications in polymer and materials synthesis. *Polymer Chemistry* **1** (1), pp. 17-36. [DOI: 10.1039/b9py00216b].

Nakamura K., Partch R. E. and Matijevic E. (1984). Preparation of Polymer Colloids by chemical Reactions in Aerosols. *Journal of Colloid and Interface Science* **99** (1), pp. 118-127. [DOI: 10.1016/0021-9797(84)90091-2].

Nieri P., Carpi S., Fogli S., Polini B., Breschi M. C. and Podestà A. (2017). Cholinesterase-like organocatalysis by imidazole and imidazole-bearing molecules. *Scientific Reports* **7** (1). [DOI: 10.1038/srep45760].

Northrop B. H. and Coffey R. N. (2012). Thiol-Ene Click Chemistry: Computational and Kinetic Analysis of the Influence of Alkene Functionality. *Journal of the American Chemical Society* **134** (33), pp. 13804-13817. [DOI: 10.1021/ja305441d].

Partch R., Nakamura K., Wolfe K. J. And Matijevic E. (1985). Preparation of polymer colloids by chemical reactions in aerosols. III. Polyurea and mixed polyurea-metal oxide particles. *Journal of Colloid and Interface Science* **105** (2), pp. 560-569. [DOI: 10.1016/0021-9797(85)90331-5].

Raula J., Eerikäinen H. and Kauppinen E. I. (2004). Influence of the solvent on the aerosol synthesis of pharmaceutical polymer nanoparticles. *International Journal of Pharmaceutics* **284** (1-2), pp. 13-21. [DOI: 10.1016/j.ijpharm.2004.07.003].

Reddy S. K., Okay O. and Bowman C. N. (2006). Network Development in Mixed Step-Chain Growth Thiol-Vinyl Photopolymerization. *Macromolecules* **39** (25), pp. 8832-8843. [DOI: 10.1021/ma060249m].

Sailor M. J. And Park J. (2012). Hybrid Nanoparticles for Detection and Treatment of Cancer. *Advanced Materials* **24** (28), pp. 1-24. [DOI: 10.1002/adma.201200653].

Salinas C. and Anseth K. S. (2008). Mixed Mode Thiol-Acrylate Photopolymerization for the Synthesis of PEG-Peptide Hydrogels. *Macromolecules* **41** (16), pp. 6019-6026. [DOI: 10.1021/ma800621h].

Sherrington D. C. (1998). Preparation, structure and morphology of polymer supports. *Chemical Communications* (21), pp. 2275-2286. [DOI: 10.1039/a803757d].

Shin D., Oh E. and Kim S. (1996). Preparation of Polymer Particles in Aerosol-Phase Reaction. *Aerosol Science Technology* **24** (4), pp. 243-254. [DOI: 10.1080/02786829608965369].

Sigmund S., Akgün E., Meyer J., Hubbuch J. Wörner M. and Kasper G. (2014). Defined Polymer Shells on Nanoparticles via Continuous Aerosol-Based Process. *Journal of Nanoparticle Research* **16** (8), pp. 2533-2544. [DOI: 10.1007/s11051-014-2533-9].

Singh A. P., Biswas A., Shukla A. and Maiti P. (2019). Targeted therapy in chronic diseases using nanomaterial-based drug delivery vehicles. *Signal Transduction and Targeted Therapy* **4** (1), pp. 2-21. [DOI: 10.1038/s41392-019-0068-3].

Sperling R. A. and Parak W. J. (2010). Surface modification, functionalization and bioconjugation of colloidal inorganic nanoparticles. *Philosophical Transactions of the Royal Society A: Mathematical, Phydical and Engineering Sciences* **368** (1915), pp. 1333-1383. [DOI: 10.1098/rsta.2009.0273].

Thiol-ene polymerization. Polymer Properties Database. Accessed 01 March 2021 from http://polymerdatabase.com/

Wang X., Yang L., Chen Z. and Shin D. M. (2008). Application of Nanotechnology in

Cancer Therapy and Imaging. *CA: A Cancer Journal for Clinicians* **58** (2), pp. 97-110. [DOI: 10.3322/CA.2007.0003].

Widmann J. F. and Davis E. J. (1996). Photochemical initiated photopolymerization of single microdroplets. *Colloid & Polymer Science* **274** (6), pp. 525-531. [DOI: 10.1007/bf00655227].

Zappitelli M. (2017). Production of micro-particles by photo-polymerization in aerosol through cationic and radical mechanism. Tesi di Laurea Magistrale, Politecnico di Torino.

Acknowledgements

My most sincere gratitude goes to Prof. Michael Wörner for his guidance and assistance during my stay in Karlsruhe. He always showed himself patient and encouraging and gave me valuable advice and constant support that helped me greatly with my lab work.

Vorrei ringraziare il Prof. Marco Sangermano per avermi dato l'opportunità di lavorare a questo progetto che mi ha consentito di crescere sia in ambito professionale che personale.

Infine ringrazio la mia famiglia, senza il cui supporto tutto questo non sarebbe stato possibile.